

國立交通大學
光電工程研究所

碩士論文

高頻光射頻頻譜分析儀



High Bandwidth
Optical RF Spectrum Analyzer

研究生： 林峰生

指導教授： 祁甦 教授

陳智弘 助理教授

中華民國九十三年六月

高頻光射頻頻譜分析儀

High Bandwidth Optical RF Spectrum Analyzer

研究生：林峰生

Student: Feng-Sheng Lin

指導教授：祁甦 教授

Advisor: Prof. Sien Chi

陳智弘 助理教授

Assist. Prof. Zhi-Hong Chen



A Thesis

Submitted to Institute of Electro-Optical Engineering
College of Electrical Engineering and Computer Science

National Chiao Tung University

In Partial Fulfillment of the Requirements

For the Degree of

Master

In

Institute of Electro-Optical Engineering

June 2004

Hsinchu, Taiwan, Republic of China

中華民國九十三年六月

致謝

ACKNOWLEDGEMENTS

碩士班的日子像眨眼般，不覺中即將結束了。一直覺得自己運氣非常地好，身邊總是圍繞著良師與益友。首先，非常感謝祁甦老師提供了我一個這麼設備完善的研究環境，祁老師的寬宏大度的處世態度也是令我們非常感佩的，而我也才能順利完成這篇論文。

還有陳智弘老師，能遇到老師，接受老師的指導，我的運氣真的很好。老師除了在實驗上盡心盡力地給予我們指導之外，在處世態度上也給予我們很多的啟發與示範。真的很少遇到像老師這麼平易近人且為學生著想的老師，老師謝謝您。碩士班這段日子真的學到了蠻多東西的，謝謝您們，兩位老師。

此外，還有實驗室的學長姐們—林玉明博士，彭朋群學長，彭煒仁學長，明芳學姊...，謝謝你們不吝惜分享你們的經驗給我，讓我能更快地進入狀況。

以及實驗室裡，一起努力的同學們—家健，宥燁，建宏，偉至，馥宇，盈傑，嘉和，至洋...謝謝你們在這段期間給我的幫助，與我一起討論。

最後，謝謝我的家人們以及許多陪伴我度過壓力最大的那段日子的朋友們。

峰生 2004.5.24

高頻光射頻頻譜分析儀

學生：林峰生

指導教授：祁牲 教授

陳智弘 助理教授

國立交通大學光電工程研究所碩士班



隨著光通訊系統的傳輸速率的增加，傳統量測光通訊信號的方法漸漸地顯得局促了。由於這些傳統的方法是將光通訊訊號先轉為電信號，再由電的分析儀器來分析，所以，受到了光轉電以及分析儀器電子電路頻寬的限制。

其中，信號的射頻頻譜是一個很重要且基本的量測。一般電的射頻頻譜分析儀，其頻寬限制約在 50GHz，對於 40Gbps 的光通訊信號而言，以顯不足。為此，Dorrer 博士和 Maywar 博士在 2003 年提出了一個全光量測光信號射頻頻譜的方法。這是一個簡單而且對於往後高傳輸速率的光通訊系統深具潛力的射頻頻譜量測方法。我們對它非常感興趣，因此依循 Dorrer 博士和 Maywar 博士的方法，架設了如此一個光射頻頻譜分析儀。

並且，仔細討論了它的工作原理以及相關的理論，包括模擬量測的頻譜，以之與實驗的結果比較，並預測此方法因為信號光能量過大造成的誤差，找出較適合的操作。

除此之外，我們以實驗以及理論模擬預測了所架的光射頻頻譜分析儀其具有的頻寬。在不考慮頻譜展開以及信號重疊的情況下，它具有約 750GHz 的頻寬，比電的射頻頻譜分析儀高出了一個數量級。

最後，我們討論了此種全光光射頻頻譜分析儀的主要缺點—測量解析度的問題，並建議了幾種改進的方法。



High Bandwidth Optical RF Spectrum Analyzer

Student: Feng-Shen Lin

Advisors: Prof. Sien Chi

Assistant Prof. Zhi-Hong Chen

Institute of Electro-Optical Engineering

National Chiao Tung University



The conventional approach for measuring the optical communication signals is too restricted when the higher optical communication systems come. These conventional approaches are to convert the optical signal into electrical signal first and then do analysis by electrical instruments, so they are restricted by the optical-to-electrical conversion and electrical circuits in bandwidth.

One of important and basic measurements for communication signals is to measure its RF spectrum. The largest bandwidth for general electrical RF spectrum analyzer is around 50GHz, which is insufficient for the measurement of 40Gbps optical communication signals. Therefore Dr. Dorrer and Dr. Maywar proposed an all optical approach for measuring the RF spectrum of optical signals in 2003. It is a simple method and has large potential for high bit rate optical communication

systems. We have great interest in this all optical approach, so we set build up an optical RF spectrum analyzer based on the approach proposed by Dr. Dorrer and Dr. Maywar.

Furthermore we discuss its working principle and the related theories including simulating the spectrum that we prepare to measure and compare it with the practical measured results. And predict the distortion due to too large signal power in this approach and find a suitable signal power in operation.

Beside those, we still predict the achievable bandwidth of the optical RF spectrum analyzer with experiment and simulation. It has the largest bandwidth around 750GHz in the case without considering spectral extending and signal overlapping.

Finally we discuss the major drawback of this approach—bad measuring resolution and suggest several possible methods for enhancing the measuring resolution.



Contents

Acknowledgements	i
Chinese Abstract	ii
English Abstract	iv
Contents	vi
Lists of Figures	viii
List of Tables	xi
Chapter 1: Introduction	1
Chapter 2: Design of the optical RF spectrum analyzer	4
2-1: Working principle of the “optical RF spectrum analyzer”— Nonlinear intensity to field conversion (NLIFC)	4
2-2: Simulation of the optical spectrum of the reference wave after NLIFC— Estimate the maximum signal power without distorting the RF spectrum	10
Chapter 3: Setup of the optical RF spectrum analyzer	27
3-1: Required highly nonlinear fiber (HNLF)	27
3-1-1: The measurement of its high nonlinear coefficient, γ	28
3-1-2: The measurement of its dispersion properties	40
3-1-3: Control and estimate the loss	43
3-2: Measurement results of 10Gbps RZ signal and 40GHz sinusoidal signal	46
3-2-1: 10Gbps RZ signal	46
3-2-2: 40GHz sinusoidal signal	52
3-3: Simulation for the measurement with OSA	56

Chapter 4: The performance of the optical RF spectrum analyzer	64
4-1: The bandwidth performance and optimization	64
4-1-1: The model considering the group delay between signal and reference waves	65
4-1-2: The model considering the group delay inside the signal wave	72
4-2: The resolution consideration and enhancement	85
4-2-1: Enhancement with a mathematical deconvolution	85
4-2-2: Enhancement with a coherent heterodyne detection	87
Chapter 5: Conclusion	90
Reference	92



List of figures

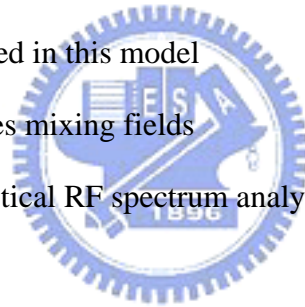
- Fig 1** Illustration of the working principle of optical RF spectrum analyzer
- Fig 2** Illustration of the simulation of generation of optical spectrum of reference light after HNLF
- Fig 3** Pattern and eye diagram of the simulated 10Gbps signal under test ($P_{av}=12.39\text{mW}$)
- Fig 4** Optical spectrum of the signal light passing through the HNLF
- Fig 5** RF spectrum of the signal under test
- Fig 6** Difference between RF spectrum signals and the optical spectrum of the reference light
- Fig 7** Compare the two optical spectrums ($P_{av}=12.39\text{mW}$)
- Fig 8** Distortion in the case of 10Gbps signal with 12.39 mW input power
- Fig 9** The optical spectrums and distortion in the case of 10Gbps signal with $P_{av}=4.2\text{mW}$
- Fig 10** The relation between the signal power and the 3-dB bandwidth
- Fig 11** Pattern and eye diagram of the 40Gbps signal under test ($P_{av}=12.39\text{mW}$)
- Fig 12** Resulting spectrums for 40Gbps signal with $P_{av}=12.39\text{mW}$
- Fig 13** Difference between the RF spectrum and optical spectrum and distortion caused by the key approximation for 40Gbps signal
- Fig 14** Spectrums of term1 and term2 in eq.2-12
- Fig 15** Simulated MI gain coefficient (input laser with power=16dBm, $\lambda =1559\text{nm}$)
- Fig 16** Simulated MI gain spectrum (input laser with power=16dBm, $\lambda =1559\text{nm}$)

- Fig 17** Experiment setup of the observation of the MI gain spectrum
- Fig 18** MI gain spectrum (PI=16dBm, $\lambda = 1559\text{nm}$)
- Fig 19** The MI gain spectrums
- Fig 20** Left: The linear relation between g_{max} and PI
Right: The linear relation between Δf^2 and PI
- Fig 21** The value of γ , $|\beta_2|$ (D) and λ_0
- Fig 22** Dispersion properties of Corning HNLF measured by ADVANTEST Q7760 optical network analyzer
- Fig 23** Dispersion properties of Corning HNLF
- Fig 24** Setup of measuring the intrinsic loss of HNLF and splicing loss
- Fig 25** A sketch of the optical RF spectrum analyzer
- Fig 26** Experimental setup of the RF spectrum of 10Gbps signal
- Fig 27** Eye of the signal under test before amplification
- Fig 28** Eye of the signal under test after amplification and adjusting the DL
- Fig 29** Measurement result of 10G signal power at 14.7dBm
- Fig 30** Measurement result of 10G signal power at 10dBm
- Fig 31** Measurement result of 10G signal power at 5dBm
- Fig 32** Experimental setup of the RF spectrum of 40Gbps signal
- Fig 33** 40GHz sinusoidal signal before amplification
- Fig 34** 40GHz sinusoidal signal after amplification
- Fig 35** Measurement result of 40G signal power at 19.1dBm
- Fig 36** Measurement result of 40G signal at 15dBm
- Fig 37** Measurement result of 40G signal at 10dBm
- Fig 38** Measurement result of 40G signal at 5dBm
- Fig 39** Simplified block diagram of OSA (extracted from [5])

- Fig 40** The assumed filter with bandwidth=1GHz and dynamic range=60dB
- Fig 41** Optical spectrums of reference light for 10Gbps RZ signal with signal input power of 14.7dBm
- Fig 42** Dynamic range of OSA
- Fig 43** Optical spectrums of reference light for 40GHz sinusoidal signal with signal input power of 14.7dBm
- Fig 44** Sketch map of phase mismatching
- Fig 45** Bandwidth reduction function
- Fig 46** β_1 and β_2 of the Corning HNLF
- Fig 47** 3dB bandwidth versus the separation
- Fig 48** Sketch map of the model considering the phase mismatching inside signal
- Fig 49** The simulated bandwidth reduction operated at best arrangement based on the modified model
- Fig 50** 3dB-bandwidth versus the separation between signal and reference lights
- Fig 51** The explanation of additional fields generation and the spectral extending
- Fig 52** The simulated bandwidth reduction operated involving condition-1 and condition2
- Fig 53** 3dB-bandwidth versus the separation at various conditions
- Fig 54** The experiment setup for measuring the bandwidth of the optical RF spectrum analyzer
- Fig 55** Measured bandwidth reduction
- Fig 56** The measured 3dB-bandwidth versus the separation
- Fig 57** Simulated deconvolution result
- Fig 58** Filter shape
- Fig 59** Deconvolution result
- Fig 60** Explanation of the heterodyne approach

List of tables

- Table 1** Simulation parameters for 10Gbps signal
- Table 2** Simulation parameters for 40Gbps signal
- Table 3** Corning Highly Non-linear, Zero Dispersion @ 1550 Specialty Fiber
- Table 4** Compression of measured results from MI gain spectrum and Q7760
- Table 5** The best fusion conditions of for fusing the HNLF and SMF
- Table 6** Experimental conditions for 10Gbps signal
- Table 7** Comparison of some characteristics of signal before and amplification
- Table 8** Experimental conditions for 40Gbps signal
- Table 9** Parameters in the simulation of OSA measurement process
- Table 10** Some symbols used in this model
- Table 11** The six four-waves mixing fields
- Table 12** Features of the optical RF spectrum analyzer



Chapter One Introduction

Motivation

The bit rate of optical communication system is increasing. Now 40 Gbps long haul systems are commercially available, and higher bit rate system will come in the future. Thus there will be a trouble coming with these high bit rate communication systems—the lack of high speed diagnostics.

One of useful diagnostics is to measure the **RF spectrum** of the signal under test, which is the power spectrum of the signal intensity. It is measured through a fast photo detector and an electrical super-heterodyne RF spectrum analyzer in optical communications. This kind of approach has limited bandwidth (~50GHz) due to the bandwidth limitations of the photo detector and the electronics in RF spectrum analyzer. Thus even for the 40Gbps system, the commercial electrical spectrum analyzer is inefficient in bandwidth for observing the second harmonics of the 40Gbps signal.

Fortunately, there is an interesting approach for measuring the RF spectrum of the high bit rate optical signal proposed by C. Dorrer and D.N. Maywar in 2003 [1, 2, and 3]. And, this new method is an all optical approach, so it avoids the bandwidth limitation from the optical-to-electrical conversion and electronics and has an amazing large bandwidth (~750GHz).

Outline

In the thesis, an all optical RF analyzer followed the approach of C. Dorrer and

D.N. Maywar is repeated and the related theories, simulations and discussions are also involved. Further, we suggest some methods to overcome the biggest drawback of this approach—bad measuring resolution. Although this new all optical approach for measuring the RF spectrum of an optical communication signal has a very larger bandwidth than the conventional electrical RF spectrum analyzer, its measurement resolution is still too bad, which depends on the light frequency resolving instruments. In the setup of Dr. Dorrer and Dr. D.N. and ours, an OSA is used to resolve the reference light after nonlinear interaction, so the resolution is determine by the OSA and around 1GHz. There are several methods for improving the resolution are discussed in this thesis.

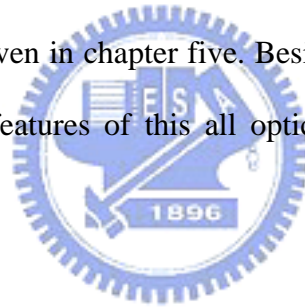
In chapter two, we state the basics of the optical RF spectrum analyzer including the derivation of its working principle—the nonlinear intensity to field conversion (NLIFC) and simulating the optical spectrum of the reference wave after NLIFC that is useful for further discussions. Because this approach is based on the nonlinear intensity to field conversion, which is formed by cross phase modulation (XPM), the theories of XPM and how the NLIFC realizes our desire will be considered in section 2-1. And in section 2-2, we explain how a simulated optical spectrum of a reference wave after NLIFC is produced and show that it is similar to the RF spectrum of the original signal under test. Further, we will consider the distortion originated from the key approximation of this approach.

In chapter three, we will build up the optical RF spectrum analyzer. Some important parameters will be measured including the nonlinear coefficient of the HNLF and its dispersion properties and loss, which are in section 3-1. And, the section 3-2 describes the practical measurements of the RF spectrum of signals. Then, we will do the simulation of OSA measurement in section 3-3. We will find that the simulated and experimental results are similar.

In chapter four, we discuss the performance of the optical RF spectrum analyzer. The performance of the optical RF spectrum analyzer includes the bandwidth performance that is discussed in section 4-1, and the resolution performance that is contained in section 4-2. In section 4-1, we will discuss the reasons causing the bandwidth degradation of the NLIFC and our optical RF spectrum analyzer based on NLIFC. We will have some analytical models to predict the bandwidth degradation and the best operation condition (to have largest measuring bandwidth).

Because the major drawback of this new approach for measuring the RF spectrum of an optical signal is that the measurement resolution of this approach is much lower than that of the conventional electrical RF spectrum analyzer, we discuss some possible methods for improving the resolution in section 4-2.

Finally, a conclusion is given in chapter five. Besides conclude the works that we done, we also compare the features of this all optical approach for measuring RF spectrum of a signal.



Chapter Two Design of the Optical RF Spectrum Analyzer

2-1 Working principle of the “optical RF spectrum analyzer”—

Nonlinear intensity to field conversion (NLIFC)

This section explains the working principle of the optical RF spectrum analyzer with mathematical derivation.

“RF spectrum” and “Optical spectrum”

Before investigating how the “optical RF spectrum analyzer” works, we have to know the meanings and their differences between RF spectrum and optical spectrum. The “RF spectrum” of a communication signal is the power spectrum of the temporal intensity of the signal, $I(t)$:

$$I_{\text{RF}}(f) \equiv \left| \int I(t) \exp^{i2\pi ft} dt \right|^2 \dots \text{eq. (2-1)}$$

It is the most popular measurement for investigating the communication signal in frequency domain with respect to the eye diagram in the time domain. It is very basic in the field of communication including optical communication and communication with other carriers. It is achieved through an electrical RF spectrum analyzer. And, we have to transfer the optical signal into electrical form by a fast photo detector.

The measurement of an optical spectrum is to measure the power spectrum of the electric field of a light, $E(t)$:

$$I_{\text{optical}}(f) \equiv \left| \int E(t) \exp^{i2\pi ft} dt \right|^2 \dots \text{eq. (2-2)}$$

It is a physical parameter and obtained by an optical spectrum analyzer (OSA).

Nonlinear intensity to field conversion (NLIFC)

In one word, this new approach uses a nonlinear interaction between signal light and reference light transferring the RF spectrum of the signal under test to the optical spectrum of the reference light observed.

In fact, this nonlinear interaction that we use is a cross phase modulation (XPM) between signal and reference inside a high nonlinear fiber (HNLF). Through a proper choice of signal power and nonlinear coefficient— γ , we can transfer the nonlinear phase term containing the intensity information of signal light into the amplitude of the electric field of the reference light with a approximation. Thus, Dr. Dorrer and Dr. Maywar named the nonlinear interaction used in the new approach as “nonlinear intensity to field conversion (NLIFC)”.

Following is a theoretical discussion about the NLIFC starting from XPM in a fiber. As to the related knowledge of the XPM in a fiber, it is introduced in [4].

Consider two lights propagating inside a fiber and suffering 3rd order nonlinear effect including XPM and SPM (self phase modulation). Because of the intensity dependent nonlinear refractive index— n_2 or n_2 , we can found that each of the two lights will obtain a nonlinear phase term dependent on the intensities of itself or the other co-propagating light after passing through the fiber. And, the nonlinear phase term can be represented as the eq. (2-3):

$$\phi_j^{NL} = \left(\frac{2\pi f_{0j} z}{c} n_{2j} \right) \left\{ |\overline{E}_j|^2 + 2|\overline{E}_{3-j}|^2 \right\} \dots \text{eq. (2-3)}$$

The index j varying from 1 to 2 represents each light inside the fiber, \overline{E}_j is the amplitude of electric field of each light and n_{2j} is the nonlinear refractive index with unit of reciprocal of $|\overline{E}_j|^2$, m^2/V^2 . We can see that the nonlinear phase term is composed by SPM and XPM.

For explaining the NLIFC, we rewrite the eq. (2-3) by replacing $|\overline{E}_j|^2$ with intensity, I.

$$\begin{aligned} \phi_0^{NL} = \frac{2\pi f_0 z}{c} n_2^I (I_0 + 2I(t)) &= \frac{2\pi f_0 z}{c} n_2^I I_0 + 2 \times \frac{2\pi f_0 z}{c} n_2^I I(t) \\ &\quad \underbrace{\hspace{1.5cm}}_{SPM} \quad \underbrace{\hspace{1.5cm}}_{XPM} \quad \dots \text{ eq. (2-4)} \\ &= \phi_0^{NL}_{SPM} \quad = \phi_0^{NL}_{XPM} \end{aligned}$$

In this equation, ϕ_0^{NL} is the nonlinear phase term suffered by the reference light after passing through the fiber, f_0 is the frequency of the reference light, I_0 is the intensity of the reference laser, and $I(t)$ is the temporal intensity of the signal under test. As to n_2^I , it is calculated around the frequency of reference light and related with n_2 by following equation.

$$n_2^I = \frac{2n_2}{\epsilon_0 c n_L} \dots \text{ eq. (2-5)}$$

, which is due to the unit conversion between $|\overline{E}|^2$ and I, and derived by following relation between $|\overline{E}|^2$ and I.

$$I = \frac{1}{2} \epsilon_0 c n_L |\overline{E}|^2 \quad \therefore |\overline{E}|^2 = \left(\frac{2}{\epsilon_0 c n_L} \right) I$$

And, the unit of n_2 is m^2/V^2 , but that of n_2^I is m^2/W .

There is one thing needed to be discussed: the nonlinear intensity phase term suffered by reference is composed of two contributions. One is due to the XPM from the signal light— $\phi_0^{NL}_{XPM}$ and the other is originated from the SPM of reference light itself— $\phi_0^{NL}_{SPM}$. The former is what we need; but the latter is just interference for our measurement. But it can be neglected fortunately, if we use a monochromatic laser as our reference light, because the field caused by SPM has a very narrow spectrum (a delta function in ideal) centered at f_0 , and the spectrum of the field caused by XPM

can be preserved outside f_0 . It will be more specific in the discussion about the spectral extent. The SPM and XPM are all viewed as one kind of four wave mixing process (SPM: $f = f_0 + f_0 - f_0$; XPM: $f = f_0 + f_s - f_s$), and the spectrum of the fields after various nonlinear interactions will be shown in the discussion of spectral extent.

Now for simplifying the following analysis, let's neglect the contribution from SPM. Thus, the eq. (2-4) is approximated as:

$$i\phi_0^{NL} \approx i\phi_0^{NL}_{XPM} = i2 \times \frac{2\pi f_0 z}{c} n'_2 I(t) \dots \text{eq. (2-6)}$$

If the length of high nonlinearity fiber equals to L, the optical field of the reference wave after HNLF, $E'_0(t)$ can be derived as:

$$E'_0(t) = A \exp^{-i2\pi f_0 t} \times \exp\left(i\left(2 \times \frac{2\pi f_0 L}{c} n'_2\right) I(t)\right) \dots \text{eq. (2-7)}$$

, where 'A': the amplitude of $E'_0(t)$ in unit of V/m.

Define $m = i\left(2 \times \frac{2\pi f_0 L}{c} n'_2\right)$, and the eq. (2-7) can be rewritten as:

$$E'_0(t) = A \exp^{-i2\pi f_0 t} \times \exp^{mI(t)}$$

If the product of ' $mI(t)$ ' $\ll 1$, then we can approximate $\exp^{mI(t)} \approx 1 + mI(t)$. And we have the following representation of the electric field of reference light after HNLF.

$$E'_0(t) \approx A \exp^{-i2\pi f_0 t} \times [1 + mI(t)] \dots \text{eq. (2-8)}$$

, where $m = i\frac{2\omega_0 L}{c} n'_2$ is a complex in unit of $\frac{m^2}{W}$. And we will estimate its value in our experiment later.

Optical spectrum of the reference light after HNLF

With the eq. (2-8) we can investigate the optical spectrum of the reference light after HNLF, and we will find that the RF spectrum of signal under test is hidden in the optical spectrum of the reference light. Substitute the eq. (2-8) into the definition of the optical spectrum—eq. (2-2). Then we have:

$$\begin{aligned}
I'_{optical}(f) &= \left| \int E'_0(t) \exp^{i2\pi ft} dt \right|^2 \\
&= A^2 \left| \int \left(\exp^{-i2\pi f_0 t} \times [1 + mI(t)] \right) \exp^{i2\pi ft} dt \right|^2 \\
&= A^2 \left| \int [1 + mI(t)] \exp^{i2\pi(f-f_0)t} dt \right|^2 \\
&= A^2 \left| \int \exp^{i2\pi(f-f_0)t} dt + m \int I(t) \exp^{i2\pi(f-f_0)t} dt \right|^2
\end{aligned}$$

Then expand the square in the equation:

$$\begin{aligned}
&I'_{optical}(f) \\
&\propto \left[\delta(f - f_0) + m \int I(t) \exp^{i2\pi(f-f_0)t} dt \right] \times \left[\delta(f - f_0) + m \int I(t) \exp^{i2\pi(f-f_0)t} dt \right]^* \\
&= \left[\delta(f - f_0) + m \int I(t) \exp^{i2\pi(f-f_0)t} dt \right] \times \left[\delta(f - f_0) + m^* \left(\int I(t) \exp^{i2\pi(f-f_0)t} dt \right)^* \right] \\
&= \delta(f - f_0) + |m|^2 \left| \int I(t) \exp^{i2\pi(f-f_0)t} dt \right|^2 + \\
&\quad \delta(f - f_0) \times m^* \left(\int I(t) \exp^{i2\pi(f-f_0)t} dt \right)^* + \delta(f - f_0) \times m \int I(t) \exp^{i2\pi(f-f_0)t} dt
\end{aligned}$$

, in which:

- (1) The term $\left| \int I(t) \exp^{i2\pi(f-f_0)t} dt \right|^2$ is RF spectrum of the signal under test, but its frequency is translated to the frequency of the reference light, f_0 .
- (2) $\delta(f - f_0) \times m^* \left(\int I(t) \exp^{i2\pi(f-f_0)t} dt \right)^* = \delta(f - f_0) \times m \int I(t) \exp^{i2\pi(f-f_0)t} dt = \delta(f - f_0)$

Thus, the optical spectrum of the reference light after HNLF is in the form:

$$I'_{optical}(f) \propto \delta(f - f_0) + |m|^2 \left| \int I(t) \exp^{i2\pi(f-f_0)t} dt \right|^2 = \delta(f - f_0) + |m|^2 \times (I_{RF}(f)) \Big|_{f_0}$$

... eq. (2-9)

The RF spectrum is involved in the optical spectrum in the optical spectrum of the reference light after HNLF, but reduced by the square of the efficiency of NLIFC, m . And, there will be an additional delta function around f_0 .

Fortunately, these can be overcome or improved. To overcome the reduction from 'm²', we can choose a reference light with suitable power and resolve its optical spectrum after HNLF by an optical spectrum resolving devices with sufficient dynamic range as grating based OSA (optical spectrum analyzer) that has best dynamic performance in various types of OSA. [5]

At the end of the section, let's show the diagram to explain how the NLIFC accomplished, and the RF spectrum is copied to the optical spectrum of the reference light.

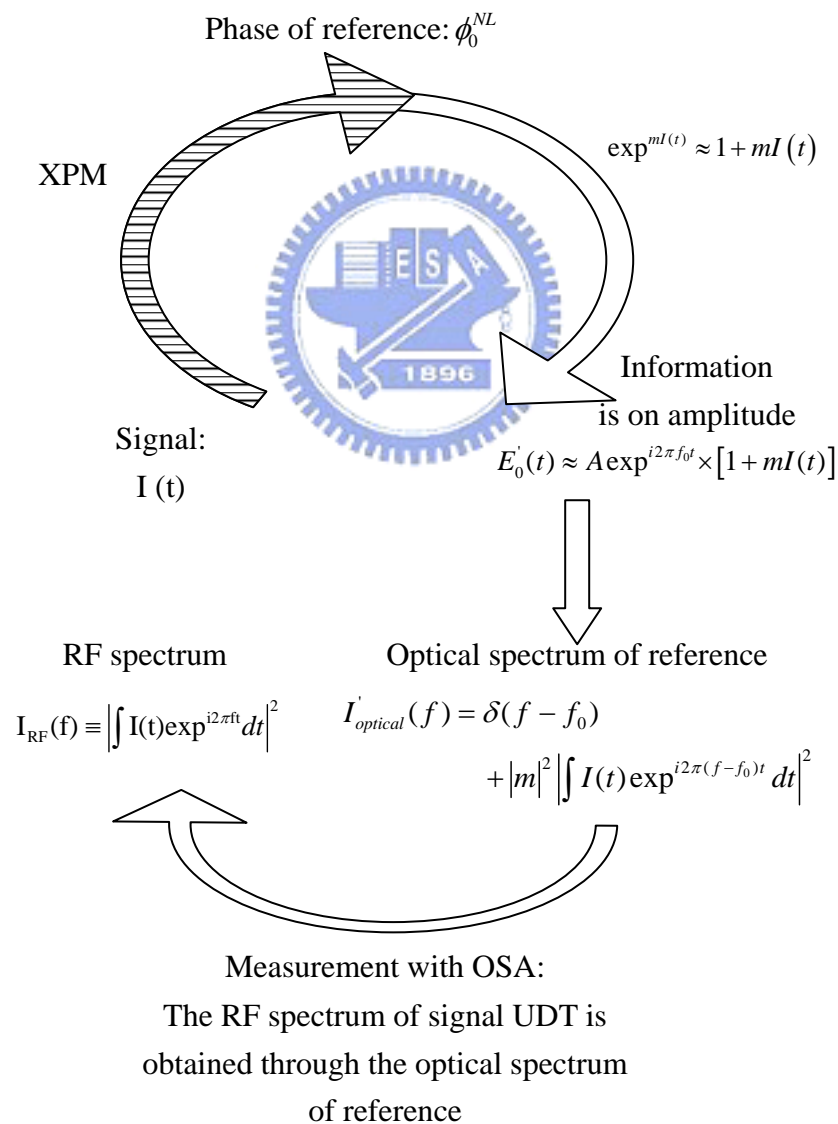


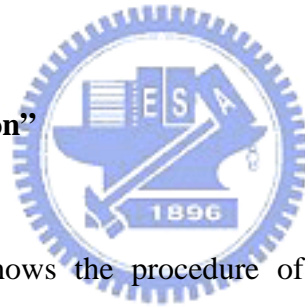
Fig 1 Illustration of the working principle of optical RF spectrum analyzer

2-2 Simulation of the optical spectrum of reference wave after NLIFC—

Estimate the maximum signal power without
distorting the RF spectrum

In this section, the optical spectrum of the reference light passing through the HNLF is simulated with matlab according to the working principle of the optical RF spectrum analyzer described in section 2-1. The simulated result not only gives us a specific shape of the spectrum that we discussed but also helps us to do some prediction and discussion. For example, we can know the suitable signal power without distortion and see the difference between the optical spectrum of reference light after HNLF and the RF spectrum of signal that we want to measure.

“Illustration of the simulation”



The following picture shows the procedure of the simulation of the optical spectrum of the reference light passing through the HNLF. In the beginning, we create a time slot –‘t’ and generate the RZ ones train with supper Gaussian form:

$$y(t) = \exp \left[-0.5 \times \left(\frac{2(t-t_D)}{T} \right)^{2m} \right] \dots \text{eq. (2-10)}$$

, in which:

- (1) ‘ t_D ’ adjusts the delay of the Gaussian pulse train. In our simulation, it is set as the half of the separation of each bit. For 10Gbps signal the bit separation is 0.1ns, so t_D is chosen as 0.05ns.
- (2) ‘T’ is the width of each Gaussian pulse.
- (3) ‘m’ is the supper Gaussian factor. The larger the value of ‘m’, the shape of the pulse train is closer to a square wave.

Then use an n-bits “linear feedback shift register (LFSR)” to generate a PRBS (pseudo random binary sequence) with length of 2^n-1 bits.

Then calculate the $E'_0(t)$ based on the eq. (2-8) but neglect the fast sinusoidal varying from $\exp^{i\omega t}$ for reducing the load of computer. This approximation just leads the resulting spectrum to shift from the frequency of reference light, f_0 to 0 and is not to matter much for us.

Finally, after doing a Fourier transform and a square on $E'_0(t)$, we will obtain the optical spectrum of reference light after HNLF, $I'_{optical}(f)$.

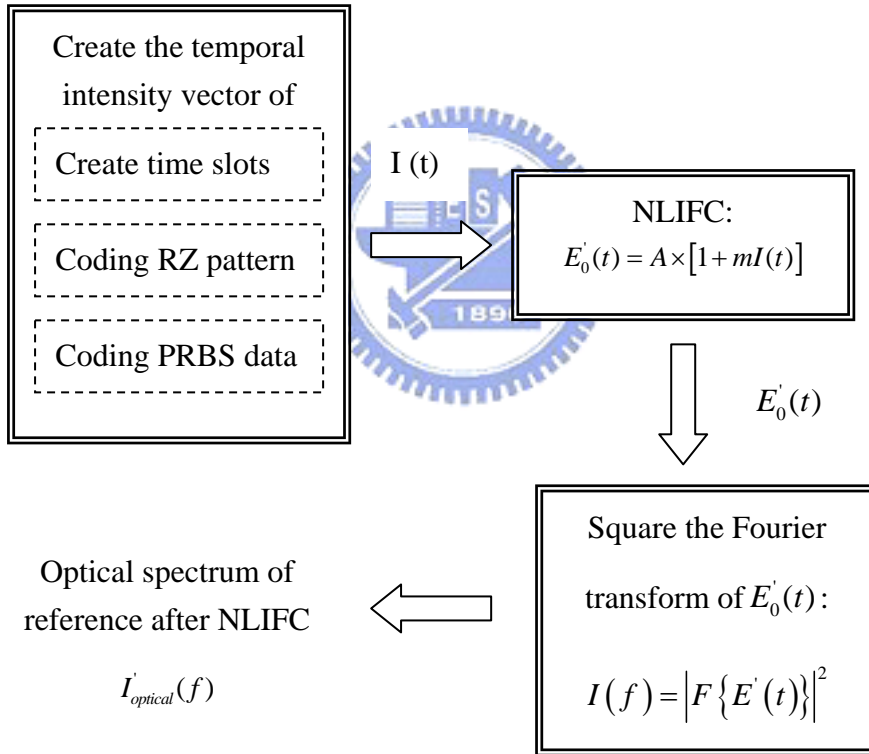


Fig 2 Illustration of the simulation of generation of optical spectrum of reference light after HNLF

The simulation result

Following table describes the needed parameters that are according to practical experiment conditions.

Measurement Parameters		Sampling slots interval	Fiber Properties		
t _i (initial time)	t _f (Stop time)		Length	A _{eff}	$\gamma^{-1} / (\text{km} \cdot \text{W})$
0 ns	100 ns	0.01 ns	1 km	14.5 μm^2	11.1
Signal light properties					
f	width	Temporal bias	Gaussian parameter	Average Power PI	PRBS length 2 ⁿ -1
10GHz	0.03ns	0.05 ns	1	12.39/4.2mW	n=10
Reference light properties					
Power					
0.5mW					

Table 1 Simulation parameters for 10Gbps signal

Note:

1. The effective area, $A_{\text{eff}}=14.5\mu\text{m}^2$ is determine by referring to the data sheet of Corning HNLF [Appendix C].
2. The value of nonlinear coefficient, γ is around $11.1 \frac{1}{\text{Km} \times \text{W}}$ that is estimated by observing the modulation instability (MI) gain spectrum of the HNLF.
3. The average power is according to the experiment condition. The signal power before entering the fiber 3-dB coupler is around 14.7dBm, the loss of the coupler is 3.12dB and the connection loss between SMF and HNLF is 0.65dB. Thus the power entering the HNLF is $14.7-3.12-0.65=10.93\text{dBm}=12.39\text{mW}$.

4. The simulated Eye diagram of signal matches that of experiment by adjusting the Gaussian parameter and the pulse width as the following diagrams:

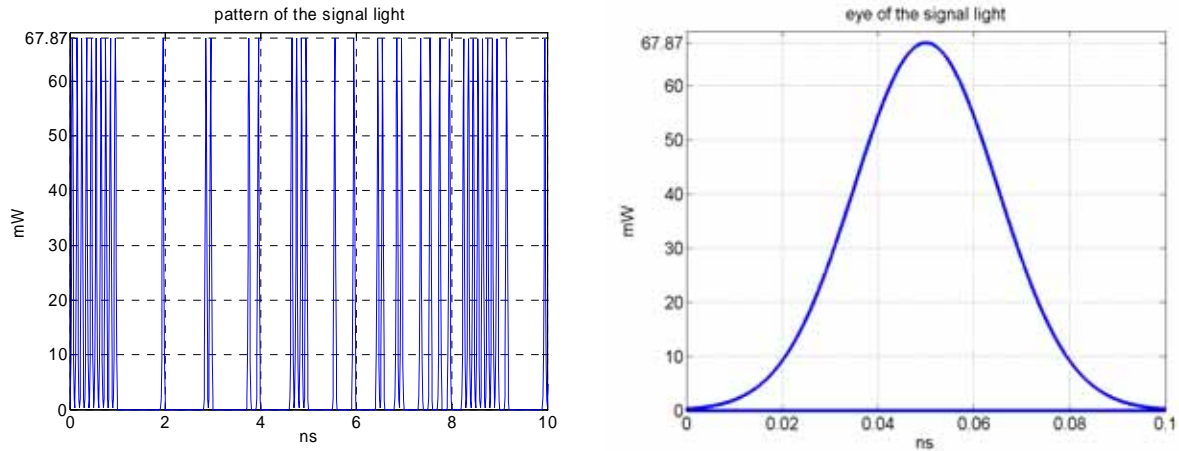


Fig 3 Pattern and eye diagram of the simulated 10Gbps signal under test

$$(P_{av}=12.39mW)$$

5. There is a relation between the amplitude of the signal (P_{amp}) and the average power of the signal (P_{av}):

$$P_{amp} = P_{av} \times \frac{\max(I) \times N}{\text{sum}(I)} \dots \text{eq. (2-11)}$$

, so $P_{av} = 67.87mW$, when $P_{av} = 12.39mW$.

Then the following picture is the simulated resulting optical spectrum of the reference light passing through the HNLF. We can see the 10GHz harmonic peaks in the spectrum as our expectation. It is off course that we can't measure an optical spectrum with so sharp peaks by general OSA, which has measurement resolution around 1GHz (0.01nm). The resolution of the spectrum in this simulation is assumed as the reciprocal of the duration of measurement ($t_f - t_i$), so in this case of $t_f - t_i = 100ns$, the resolution of this spectrum is $\frac{1}{t_f - t_i} = \frac{1}{100ns} = 0.01GHz$. And, we take it as the real

spectrum before the distortion of the OSA measurement. We will also simulate the result after OSA measurement based on the spectrum in the next section, and it is

more similar to the experiment result.

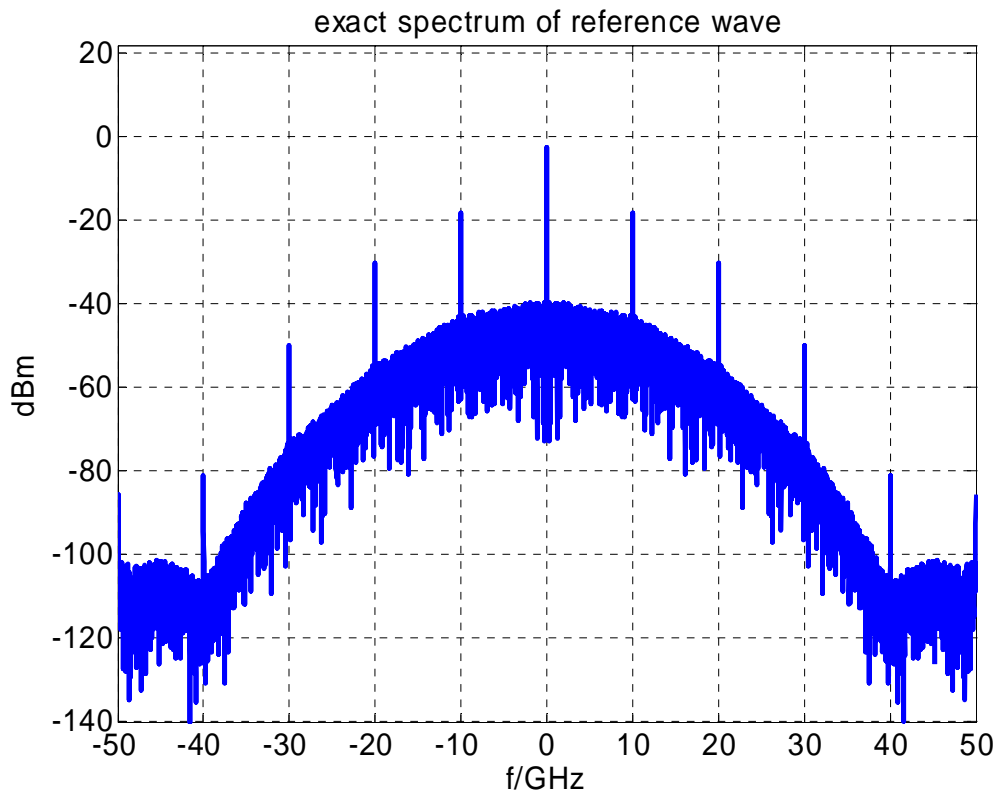


Fig 4 optical spectrum of the signal light passing through the HNLF

Before doing that work, let's show that the optical spectrum of the reference light after HNLF is almost the same with the RF spectrum of the signal light. Thus we simulate the RF spectrum of the signal under test according to the definition of RF spectrum—eq. (2-1) that is show in the figure 5.

By comparing figure 4 and figure 5, we can find that the optical spectrum of the reference light is almost the same with the RF spectrum of the signal except that there is a down shift of figure 4 around 36.6dB that is originated from the square of 'm' in eq. (2-9) and an additional delta function causing a 8dB error in the center of figure 4.

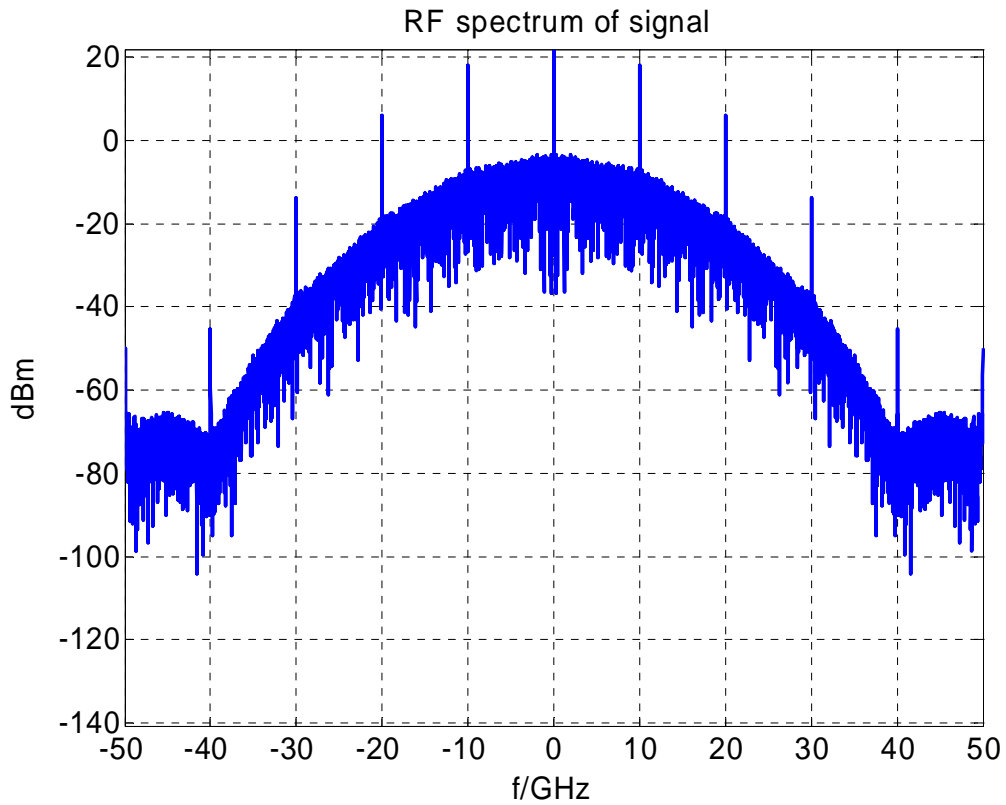


Fig 5 RF spectrum of the signal under test



We can see these discussions in the following picture showing their difference.

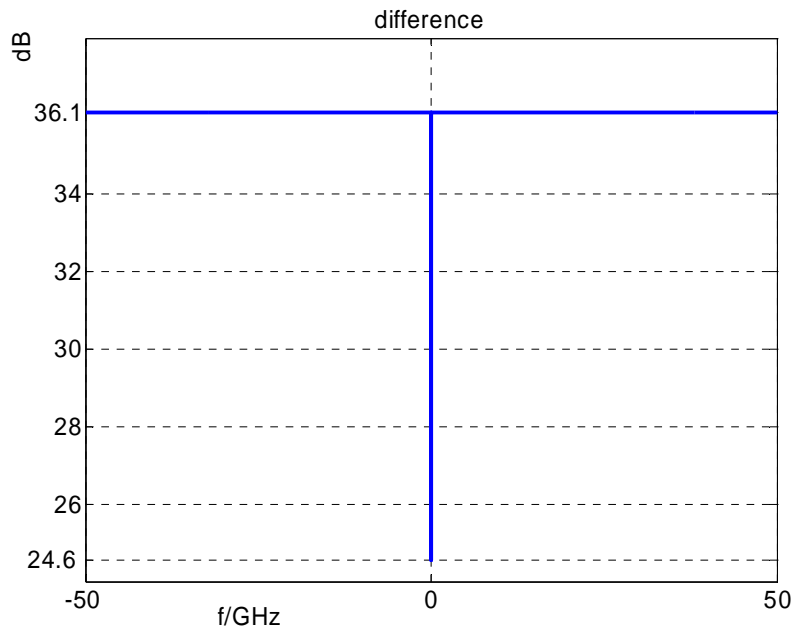


Fig 6 Difference between RF spectrum signals and the optical spectrum of the reference light

Furthermore, the constant difference between the optical spectrum of the reference light and the RF spectrum of the signal shown in figure 6 proves that there is no distortion when we measure the RF spectrum of the signal by observing the optical spectrum of the reference light. All of these discussions can be justified in eq. (2-9). But it is needed to be declared that these conclusions are right based on the existence of the approximation: $\exp^{mI(t)} \approx 1 + mI(t)$

Following let's to have some discussions about the influences of the key approximation

Distortion from the approximation— $\exp^{mI(t)} \approx 1 + mI(t)$

Although there is almost no distortion between the target RF spectrum of the signal (Fig 5) and the optical spectrum of the reference light calculated from eq. (2-8), the optical spectrum of the reference light calculated from eq. (2-8) is not the real one that be measured. In fact the optical spectrum of the reference light passing through the HNLF should be calculated based on the equation $E_0'(t) = A \exp^{mI(t)}$. Following picture plots the optical spectrums of the reference light after HNLF in two cases: one is based on eq. (2-8) and another is based on $E_0'(t) = A \exp^{mI(t)}$.

We will find that there exists a specific difference between the two spectrums. Thus when we measure the RF spectrum of signal by observing the optical spectrum of the reference light, there will be a specific distortion that is originated from the approximation— $\exp^{mI(t)} \approx 1 + mI(t)$ and is the difference between the two spectrums in figure 7. In figure 7, we can also observe that the region without distortion is in the center of the spectrum with bandwidth around 20GHz (+20GHz~-20GHz).

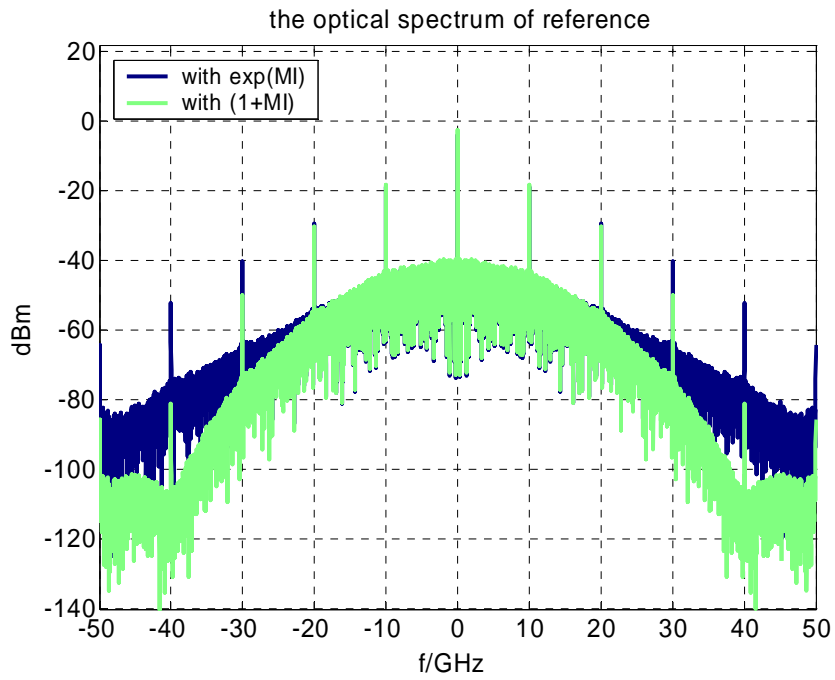


Fig 7 Compare the two optical spectrums (PI=12.39mW)

It is more specific in the following picture.

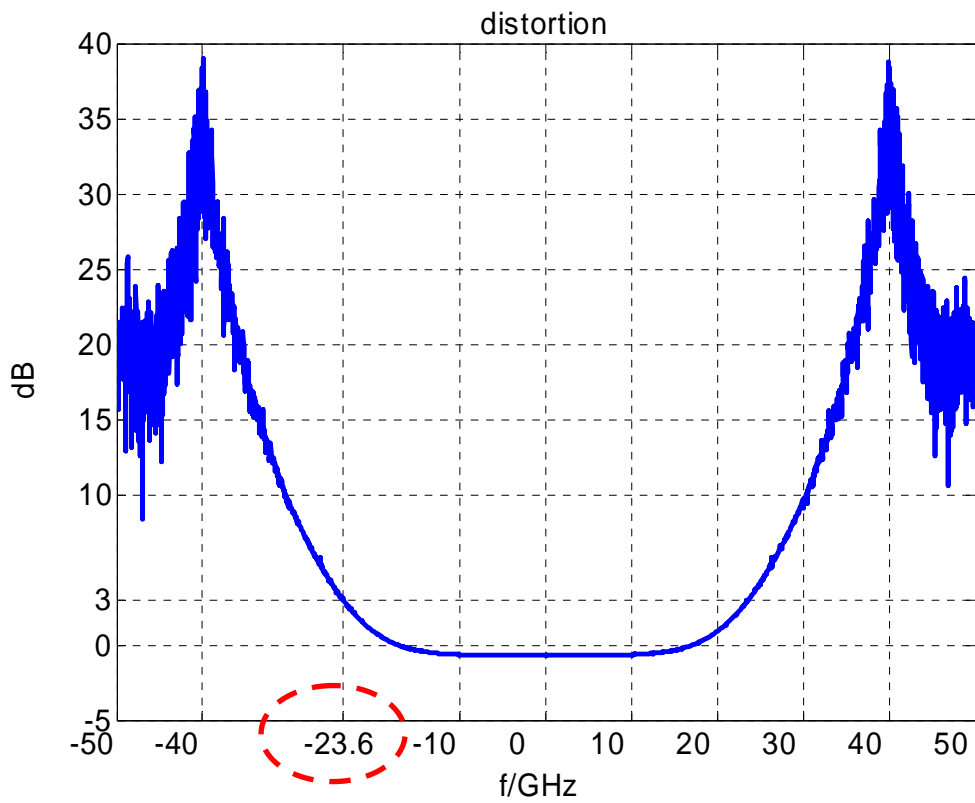


Fig 8 distortion in the case of 10Gbps signal with 12.39 mW input power

It plots the difference between the two spectrums in dB scale in figure 8.

We can see that the 3-dB bandwidth is only around 23.6 GHz ($\pm 23.9\text{GHz}$), so the correct measurement is restricted within the second harmonics for the 10Gbps signal, but fortunately the bandwidth can be increased by decreasing signal power, which can be predicted from the condition of the approximation— $\exp^{mI(t)} \approx 1 + mI(t)$:

$$|mI(t)| \ll 1$$

Following picture shows the simulation corresponding to figure 7 and figure 8 in the case of $PI=4.2\text{mW}$ that corresponds to the experiment with average signal power before entering 3-dB coupler around 10dBm.

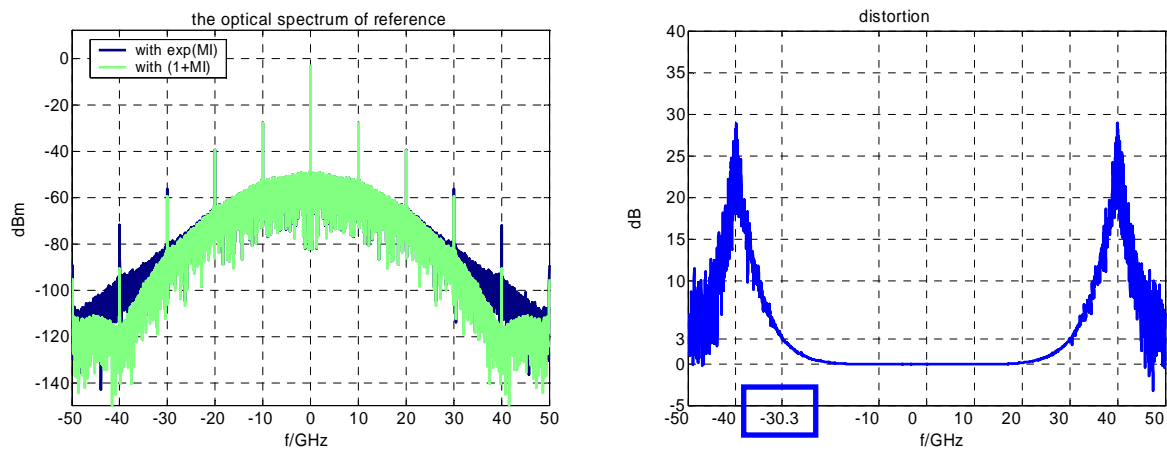


Fig 9 the optical spectrums and distortion in the case of 10Gbps signal with $PI=4.2\text{mW}$

It is indeed that the region without distortion is broadened.

Following picture is the relation between the signal power and the corresponding 3-dB bandwidth of region without distortion:

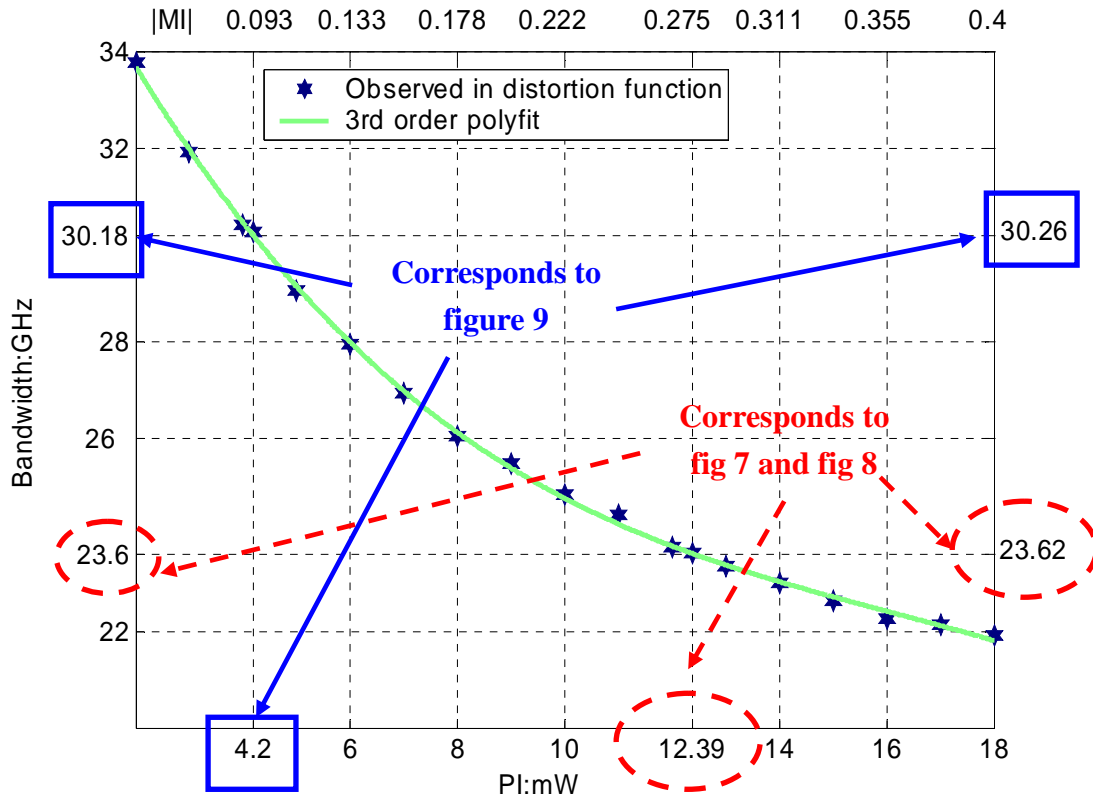


Fig 10 The relation between the signal power and the 3-dB bandwidth

Although we know that the bandwidth increases with the decreasing of PI in figure 10, there is still a trade off in choosing the signal power, PI. Because the optical RF spectrum analyzer utilizes the nonlinear interaction in a HNLF—XPM, it is power sensitive and needs sufficient power to have obvious interaction. And, the OSA or other optical frequency resolving devices have a finite dynamic range or a finite noise floor, so the spectrum to be measured should be above the noise floor; otherwise the components under the noise floor will be buried.

Thus we have to choose a suitable signal power to have widest range without distortion and above the noise floor of resolving devices. For example, if the noise floor is -80dBm, the PI=4.2mW (corresponding to Fig 9) is a better choice that has the bandwidth of the measurement range without distortion and above noise floor around 30 GHz for 10Gbps signal, so we can observe the complete and correct spectrum up

to the third harmonic. As to the case of $PI=12.39\text{mW}$, the spectrum has distortion larger than 3dB outside $\pm 23.6\text{GHz}$, although it has larger range above -80dBm. But, if the noise floor is around -60dBm that is more reasonable for our practical experiment, although we can observe the peak of the third harmonic, some part between it and the peak of second harmonic is buried. However, a correct measurement range up to the second harmonic peak is guaranteed. These discussions will be justified later in the simulation involving the OSA measurement and practical experiment.

Simulation for 40Gbps signal

Now we have to think about an important problem: the region without distortion only has bandwidth around 20~35GHz that is discussed in the simulation for 10Gbps signal in last subsection, but what we want to design is an optical RF spectrum analyzer with ultra-wide bandwidth relative to conventional electrical RF spectrum analyzer that has very restricted bandwidth. Thus, the bandwidth caused by the distortion of the deviation of the key approximation almost destroys the plan.

But, it is very fortunately that this kind of distortion has a special feature—the distortion depends on the RF signal under test itself. More specifically the bandwidth of region without distortion increases with the increasing of the repetition rate of the RF signal. It can be seen in the following simulation for 40Gbps signal. And the mathematical explanation is described in the next section.

The setting parameters in the simulation program for 40Gbps signal are shown in the table 2. Most of them are the same with those for 10Gbps signal except “sampling slots interval”, “pulse width” and “the number of shifter register” (n). Because the bit rate is increased by 4 times, it is off course that the pulse width and the sampling slots interval should be quartered to maintain the same resolution of the resulting simulated

spectrum. And, the length of PRBS also should be increased by 4 times in the case without coding the PRBS twice.

Measurement Parameters		Sampling	Fiber Properties		
t_i (initial time)	t_f (Stop time)		slots interval	Length	A_{eff}
0 ns	100 ns	0.0025 ns	1 km	14.5 μm^2	11.1
Signal light properties					
f	width	Temporal bias	Gaussian parameter	Average Power PI	PRBS length 2^{n-1}
40GHz	0.0075ns	0.05 ns	1	12.39 mW	n=12
Reference light properties					
Power					
0.5mW					

Table 2 Simulation parameters for 40Gbps signal

(The parameters with boldface mean that they are different comparing with the case of 10Gbps signals.)

The results are shown in following pictures.

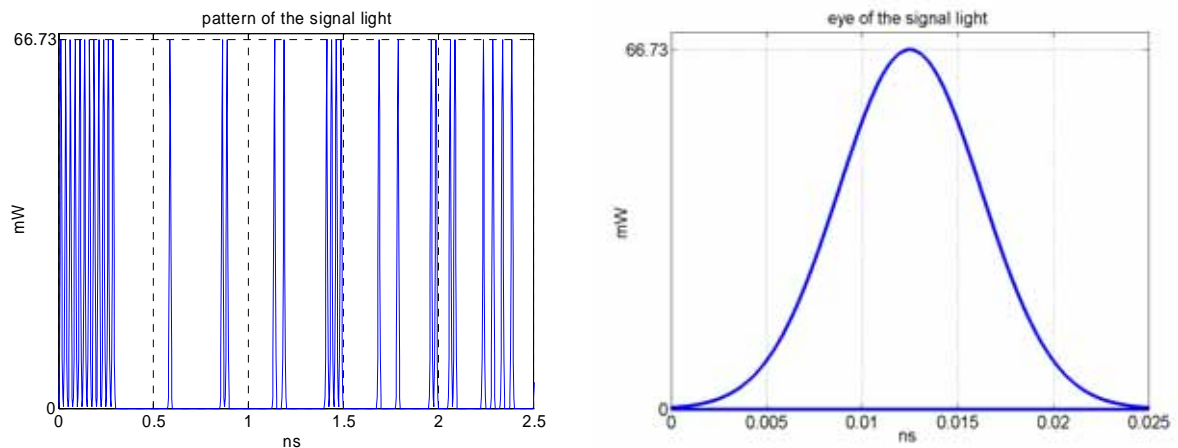


Fig 11 Pattern and eye diagram of the 40Gbps signal under test ($P_{av}=12.39mW$)

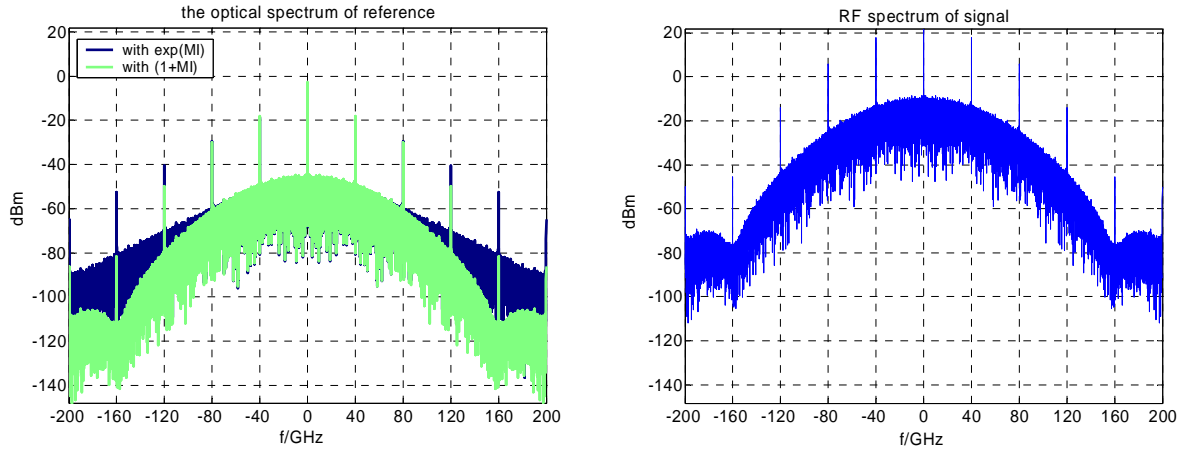


Fig 12 Resulting spectrums for 40Gbps signal with $PI=12.39mW$

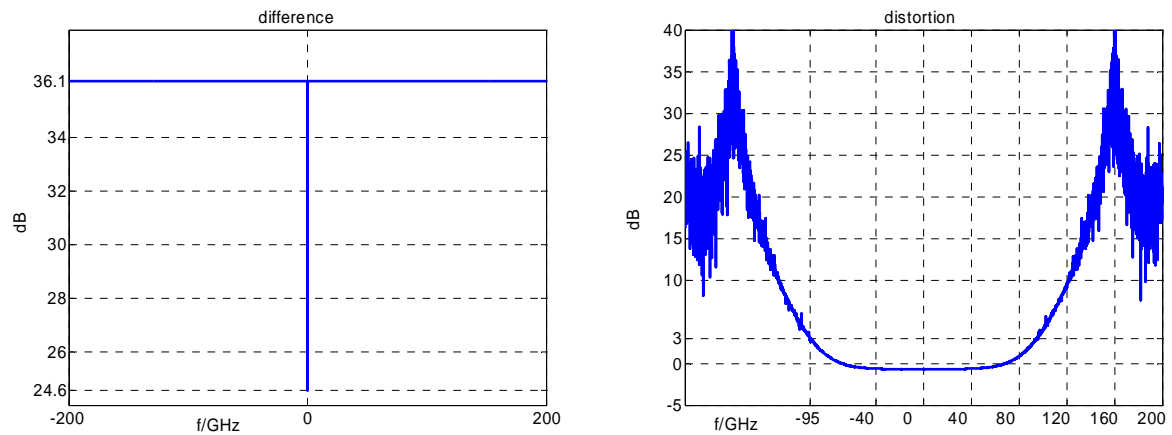


Fig 13 Difference between the RF spectrum and optical spectrum and distortion caused by the key approximation for 40Gbps signal

From figure 11, we can see that the pulse shape of 40Gbps signal is almost with that of 10Gbps signal shown in figure 3, and figure 12 enable us to compare the RF spectrum of signal under test and the optical spectrums of reference light with and without the key approximation. We can find that the difference between RF spectrum and the optical spectrum of reference light in 40Gbps is the same with the case of 10GBps. Then let's see the distortion caused by the deviation of the key approximation. It is shown by comparing the cases of 10G and 40G that the

bandwidth of the region without distortion is increased by four times as the bit rate of signal under test.

Thus the optical RF spectrum analyzer can also guarantee a correct measurement range up to the second harmonic peak for 40Gbps or higher bit rate signals at least. And, if the dynamic range of the OSA or other optical frequency resolving devices can have a little improvement, the correct measurement range can be broadened up to the third harmonic peak.

As to the explanation of the lucky feature, we need to have a deeper understanding for the origin of distortion that will be discussed in next subsection.

Power expanding of $E_o'(t) = A \exp^{-2\pi f_0 t} \exp^{mI(t)}$

In section 2-1, we obtain eq. (2-9) $I_{optical}(f) = \delta(f - f_0) + |m|^2 \times (I_{RF}(f))|_{f_0}$ by the approximation: $E_o'(t) = A \exp^{-2\pi f_0 t} \exp^{mI(t)} \approx A \exp^{-2\pi f_0 t} [1 + mI(t)]$, but in fact there is still a lot of higher order terms neglected, which causes the distortion in the last subsection. In this subsection, we try to think about two questions:

1. Why does the distortion perform serious seriously in the edges of the spectrum?
2. Why does the region without distortion increase with the increasing of bit rate of signal under test?

We still start from the electrical field of the reference light passing through HNLF.

$$E_o'(t) = A \exp^{-2\pi f_0 t} \exp^{mI(t)}$$

$$= A \exp^{-2\pi f_0 t} \left[1 + mI(t) + \frac{(mI(t))^2}{2} + \frac{(mI(t))^3}{6} + \dots \right] \approx A \exp^{-2\pi f_0 t} [1 + mI(t)]$$

If we calculate the optical spectrum with the last equation as the produce in the last section, we will have:

$$\begin{aligned}
I'_{optical}(f) &= \left| \int E'_0(t) \exp^{i2\pi ft} dt \right|^2 \\
&= A^2 \left| \int \left(\exp^{-i2\pi f_0 t} \times \left[1 + mI(t) + \frac{(mI(t))^2}{2} + \dots \right] \right) \exp^{i2\pi ft} dt \right|^2 \\
&= A^2 \left| \int \left[1 + mI(t) + \frac{(mI(t))^2}{2} + \dots \right] \exp^{i2\pi(f-f_0)t} dt \right|^2 \\
&= A^2 \left| \int \exp^{i2\pi(f-f_0)t} dt + \int (mI(t)) \exp^{i2\pi(f-f_0)t} dt + \int \left(\frac{(mI(t))^2}{2} \right) \exp^{i2\pi(f-f_0)t} dt + \dots \right|^2
\end{aligned}$$

If we only consider the first three terms and expand the last equation:

$$\begin{aligned}
I'_{optical}(f) &= A^2 \left| \int \exp^{i2\pi(f-f_0)t} dt + \int (mI(t)) \exp^{i2\pi(f-f_0)t} dt + \int \left(\frac{(mI(t))^2}{2} \right) \exp^{i2\pi(f-f_0)t} dt \right|^2 \\
&= A^2 \left[\int \exp^{i2\pi(f-f_0)t} dt + \int (mI(t)) \exp^{i2\pi(f-f_0)t} dt + \int \left(\frac{(mI(t))^2}{2} \right) \exp^{i2\pi(f-f_0)t} dt \right] \\
&\quad \times \left[\int \exp^{i2\pi(f-f_0)t} dt + \int (mI(t)) \exp^{i2\pi(f-f_0)t} dt + \int \left(\frac{(mI(t))^2}{2} \right) \exp^{i2\pi(f-f_0)t} dt \right]^* \\
&= A^2 \left[\delta(f-f_0) + \int (mI(t)) \exp^{i2\pi(f-f_0)t} dt + \int \left(\frac{(mI(t))^2}{2} \right) \exp^{i2\pi(f-f_0)t} dt \right] \\
&\quad \times \left[\delta(f-f_0) + \left(\int (mI(t)) \exp^{i2\pi(f-f_0)t} dt \right)^* + \left(\int \left(\frac{(mI(t))^2}{2} \right) \exp^{i2\pi(f-f_0)t} dt \right)^* \right]
\end{aligned}$$

Follow the derivation in section 2-1, we have:

$$\begin{aligned}
I'_{optical}(f) &\propto \left[\delta(f-f_0) + \int (mI(t)) \exp^{i2\pi(f-f_0)t} dt + \int \left(\frac{(mI(t))^2}{2} \right) \exp^{i2\pi(f-f_0)t} dt \right] \\
&\quad \times \left[\delta(f-f_0) + \left(\int (mI(t)) \exp^{i2\pi(f-f_0)t} dt \right)^* + \left(\int \left(\frac{(mI(t))^2}{2} \right) \exp^{i2\pi(f-f_0)t} dt \right)^* \right]
\end{aligned}$$

In the figure 14, we find that the spectrum of $\frac{(MI)^2}{2}$ (the term 2) has larger high frequency components than that of (MI) (the term 1), which is due to the operation of square. And, the spectrum of $\frac{(MI)^3}{6}$, $\frac{(MI)^4}{24}$ and other higher order terms will have larger components in high frequency, but these higher order terms are all neglected in eq. (2-8) and eq. (2-9), so it is obvious that there are larger distortion in the edge.

As to the question2, because the distortion originates from the higher order terms of signal under test, it is off course that the region without distortion will broaden with the broadening of the spectrum of signal under test or the narrowing of its pulse width. In the simulation, the pulse width is decreased in the same ration when the bit rate increase from 10Gbps to 40Gbps. Thus the region without distortion also broadens by 4 times.

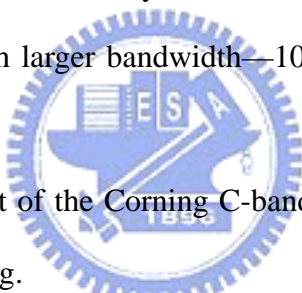


Chapter Three Setup of the optical RF spectrum analyzer

3-1 Required highly nonlinear fiber (HNLF)

The key of the optical RF spectrum analyzer is the highly nonlinear fiber that performs the XPM between the signal light and reference light. Although there is still other component able to perform the XPM between two lights, for example— SOA (semiconductor optical amplifier) that is popular in the application of wavelength conversion, the HNLF is still the better choice in this application—constructing the high bandwidth optical RF spectrum analyzer. It is because that the applied nonlinear interaction in HNLF has much larger bandwidth—10THz [3]. Thus, we also choose the HNLF in our experiment.

Following is the data sheet of the Corning C-band highly nonlinear fiber that we use. It is obtained from Corning.



Item	Specification	Unit
Operating Wavelength	1550	nm
Attenuation @ 1550 nm	~ 0.5	dB/km
Attenuation @ 1380 nm	~ 2	dB/km
Cutoff	~1150	nm
Effective Area	14-15	μm^2
Zero Dispersion Wavelength	1550 +/- 20	nm
Dispersion Slope @ 1550 nm	~0.04	ps/nm ² /km

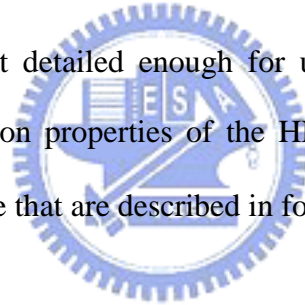
Table 3 Corning Highly Non-linear, Zero Dispersion @ 1550 Specialty Fiber

Item	Specification	Unit
Dispersion @ 1525 nm	~ -1.0 to -1.7	ps/nm ² /km
Dispersion @ 1550 nm	- 0.08 to -0.6	ps/nm ² /km
Dispersion @ 1575 nm	0.98 to 0.31	ps/nm ² /km
Cladding Outside Diameter	125 +/- 2	μm
Coating Outside Diameter	245 +/- 15	μm
Coating	Dual UV-curable acrylate	

Table 3 Corning Highly Non-linear, Zero Dispersion @ 1550 Specialty Fiber

(continued)

But, the data sheet is not detailed enough for us. We still need the nonlinear coefficient, γ and the dispersion properties of the HNLF. Thus we do some simple measurements to know it more that are described in following paragraphs.



3-1-1: The measurement of its high nonlinear coefficient

We have assumed the nonlinear coefficient, γ around $11.1 \frac{1}{(km \times W)}$ in the previous simulation in section 2-2. It is the result of estimation in the following experiment— observation of the MI (modulation instability) gain spectrum of a light passing through the HNLF. There are several different approaches for measuring the nonlinear coefficient [6], which are classified by two types: interferometric methods and non-interferometric methods. What we adopt is based on the modulation instability that belongs to the non-interferometric methods, because of its simplicity. [7][8] Before entering the measurement of nonlinear coefficient by modulation

instability, we have a brief introduction about the phenomenon—modulation instability. [4]

Generation of modulation instability—

Linear stability analysis of nonlinear Schrodinger equation

Modulation instability originates from the interplay between nonlinear and dispersive effects. It only occurs in the anomalous dispersive region ($D>0$ or $\beta_2<0$). These can be explained from the “linear stability analysis of nonlinear Schrodinger equation” stated as below.

Equation (3-1) is the nonlinear Schrodinger equation neglecting the loss term.

$$i \frac{\partial A}{\partial z} = \frac{1}{2} \beta_2 \frac{\partial^2 A}{\partial T^2} - \gamma |A|^2 A \dots \text{eq. (3-1)}$$

, where $A(z, T)$ is the amplitude of the pulse envelope, β_2 is the GVD parameter and γ is the nonlinear coefficient.

In the case of CW, radiation at the input end of the fiber, i.e. $A(0, T) = \text{constant}$: If there is no any noise or perturbation inside the fiber in the propagation process, we will have a steady-state solution by assuming that the A is independent of time (, so

solve the equation: $i \frac{\partial \bar{A}}{\partial z} = -\gamma |\bar{A}|^2 \bar{A}$):

$$\bar{A} = \sqrt{P_0} e^{i\Phi_{NL}},$$

$$\Phi_{NL} = \gamma P_0 z$$

This solution means that the amplitude of incident light is unchanged except acquiring a power-dependent phase shift.

But, there is always some noise or perturbation in the fiber, so let's discuss whether the steady-state solution is stable for a small perturbation: Let's assume

$$A(z, T) = \left(\sqrt{P_0} + a(z, T) \right) e^{i\Phi_{NL}} \dots \text{eq. (3-2)}$$

Substitute eq. (3-2) into eq. (3-1), then we have:

$$i \frac{\partial a}{\partial z} = \frac{1}{2} \beta_2 \frac{\partial^2 a}{\partial T^2} - \gamma P_0 (a + a^*) \dots \text{eq. (3-3)}$$

If we assume a general solution of the form:

$$a(z, T) = a_1 \cos(Kz - \Omega T) + ia_2 \sin(Kz - \Omega T) \dots \text{eq. (3-4)}$$

, the eq. (3-3) will provide a set of two equations for a_1 and a_2 . And, from the representation of a_1 and a_2 , we will obtain the relation between the K and Ω :

$$K = \pm \frac{1}{2} |\beta_2| \Omega \left[\Omega^2 + \text{sgn}(\beta_2) \Omega_c^2 \right]^{1/2} \dots \text{eq. (3-5)}$$

$$\Omega_c^2 = \frac{4\gamma P_0}{|\beta_2|} \dots \text{eq. (3-6)}$$

(Derivation)

$$\text{With eq. (3-3): } i \frac{\partial a}{\partial z} = \frac{1}{2} \beta_2 \frac{\partial^2 a}{\partial T^2} - \gamma P_0 (a + a^*)$$

$$\text{Because } a(z, T) = a_1 \cos(Kz - \Omega T) + ia_2 \sin(Kz - \Omega T)$$

$$\frac{\partial a}{\partial z} = -a_1 K \sin(Kz - \Omega T) + ia_2 K \cos(Kz - \Omega T)$$

$$\frac{\partial^2 a}{\partial T^2} = -a_1 \Omega^2 \cos(Kz - \Omega T) - ia_2 \Omega^2 \sin(Kz - \Omega T),$$

$$a + a^* = 2a_1 \cos(Kz - \Omega T)$$

Thus, we have the following two equations:

$$a_2 K = \frac{\beta_2 a_1 \Omega^2}{2} + 2\gamma a_1 P_0$$

$$a_1 K = \frac{\beta_2 a_2 \Omega^2}{2}$$

Then, we can eliminate the a_1 :

$$a_2 K = \frac{\beta_2 \Omega^2}{2} \left(\frac{\beta_2 a_2 \Omega^2}{2K} \right) + 2\gamma P_0 \left(\frac{\beta_2 a_2 \Omega^2}{2K} \right)$$

$$K^2 = \frac{\beta_2^2 \Omega^4}{4} + \gamma \beta_2 \Omega^2 P_0 = \frac{\beta_2^2 \Omega^4 + 4\gamma \beta_2 \Omega^2 P_0}{4}$$

$$K^2 = \frac{\beta_2^2 \Omega^4 + \frac{\text{sgn}(\beta_2)}{|\beta_2|} 4\gamma \beta_2^2 \Omega^2 P_0}{4}$$

$$K = \pm \frac{|\beta_2|}{2} \Omega \left[\Omega^2 + \text{sgn}(\beta_2) \left(\frac{4\gamma P_0}{|\beta_2|} \right) \right]^{1/2}$$

$$K = \pm \frac{|\beta_2|}{2} \Omega \left[\Omega^2 + \text{sgn}(\beta_2) \Omega_c^2 \right]^{1/2},$$

$$\text{where } \Omega_c^2 = \frac{4\gamma P_0}{|\beta_2|}$$

The eq. (3-5) shows that the stability of the steady-state depends on whether light experiences normal or anomalous dispersion. In the case of normal dispersion ($D < 0$, $\beta_2 > 0$), the K is always real for all Ω , so the steady state is stable for small perturbation. But, in the case of anomalous dispersion ($D > 0$, $\beta_2 < 0$), the K is imaginary for $\Omega < \Omega_c$, so the perturbation will grow exponentially with z and the steady state solution is unstable, so a MI gain spectrum exists around the input laser that can be calculated by eq. (3-5). Thus there are side lobes in the optical spectrum of the laser after MI interaction, and the CW input laser is broken into a train of ultra-short pulses.

MI gain spectrum

Because our measurement of the nonlinear coefficient utilizes the observation of the MI gain spectrum, we discuss the relation between the MI gain coefficient and the nonlinear coefficient that we want to measure here. Besides the nonlinear coefficient, the experiment can also give us the dispersion parameter, D and zero dispersion wavelength, λ_0 .

When the pump laser is operated at anomalous GVD and $\Omega < \Omega_c$, the perturbation will grow exponentially with z , so we will have a gain spectrum in $\omega_0 \pm \Omega$.

$$a(z) \sim e^{jKz} = e^{i\text{Re}\{K\}z} e^{-\text{Im}\{K\}z},$$

$$|a(z)|^2 = e^{-2\text{Im}\{K\}z} = e^{g(\Omega)z},$$

Substitute the equation $K = \pm \frac{1}{2} |\beta_2| \Omega \left[\Omega^2 + \text{sgn}(\beta_2) \Omega_c^2 \right]^{1/2}$, and then we have:

$$g(\Omega) = -2 \text{Im}\{K\} = |\beta_2| \Omega \left(\Omega_c^2 - \Omega^2 \right)^{1/2} \dots \text{eq. (3-7)}$$

$$\Omega_{\max} = \frac{\Omega_c}{\sqrt{2}}; g_{\max} = \frac{1}{2} |\beta_2| \Omega_c^2 \dots \text{eq. (3-8)}$$

, where g is the gain coefficient in unit of 1/km.

The eq. (3-7) and eq. (3-8) are the simple mathematical describing for the MI gain spectrum. Then let's rewrite them by some physical parameters with the relation— $\Omega_c^2 = \frac{4\gamma P_0}{|\beta_2|}$:

$$g(\Omega) = |\beta_2| \Omega \left(\frac{4\gamma P_0}{|\beta_2|} - \Omega^2 \right)^{1/2} \dots \text{eq. (3-9)}$$

$$\Omega_{\max} = \left(\frac{2\gamma P_0}{|\beta_2|} \right)^{1/2} ; g_{\max} = 2\gamma P_0 \dots \text{eq. (3-10)}$$

The following figures show the simulated MI gain coefficient and gain spectrum corresponding to the experiment with 1559nm input laser. The needed parameters are set as: $\beta_2 = -0.38 \text{ ps}^2 / \text{km}$, $\gamma = 11.1 \frac{1}{\text{W} \cdot \text{km}}$, input power=16dBm(around 0.0398W) and fiber length=1Km.

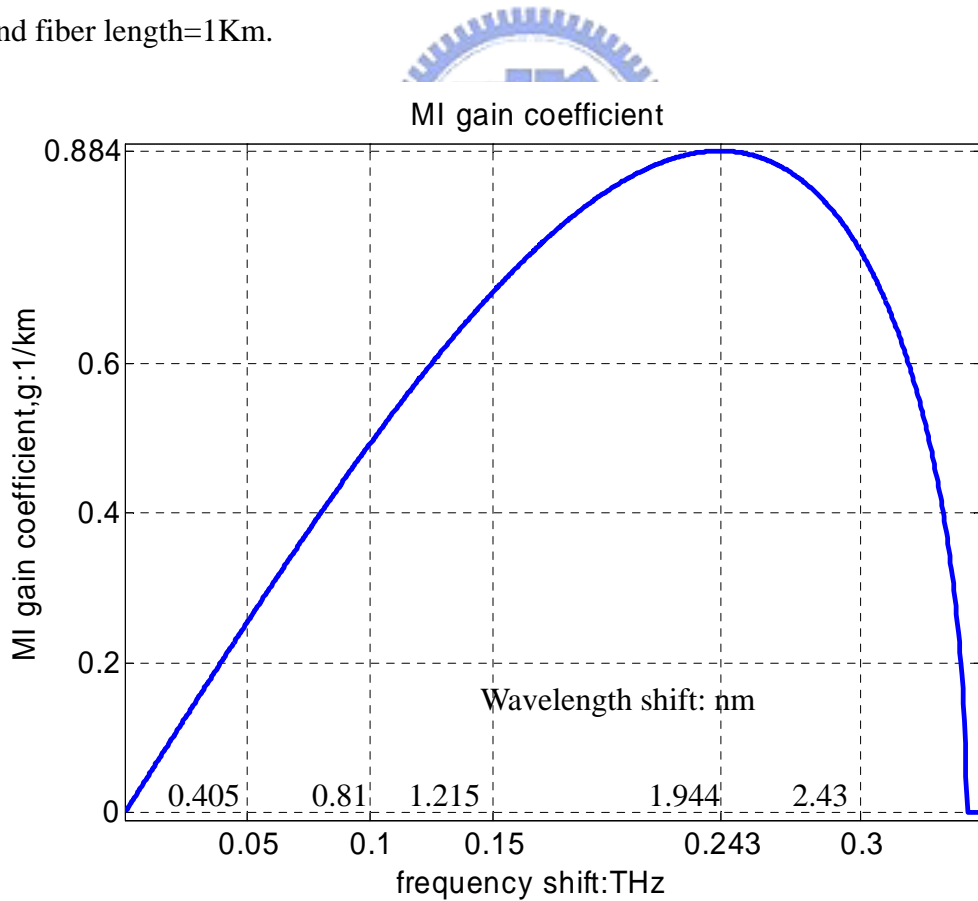


Fig. 15 simulated MI gain coefficient (input laser with power=16dBm, $\lambda = 1559\text{nm}$)

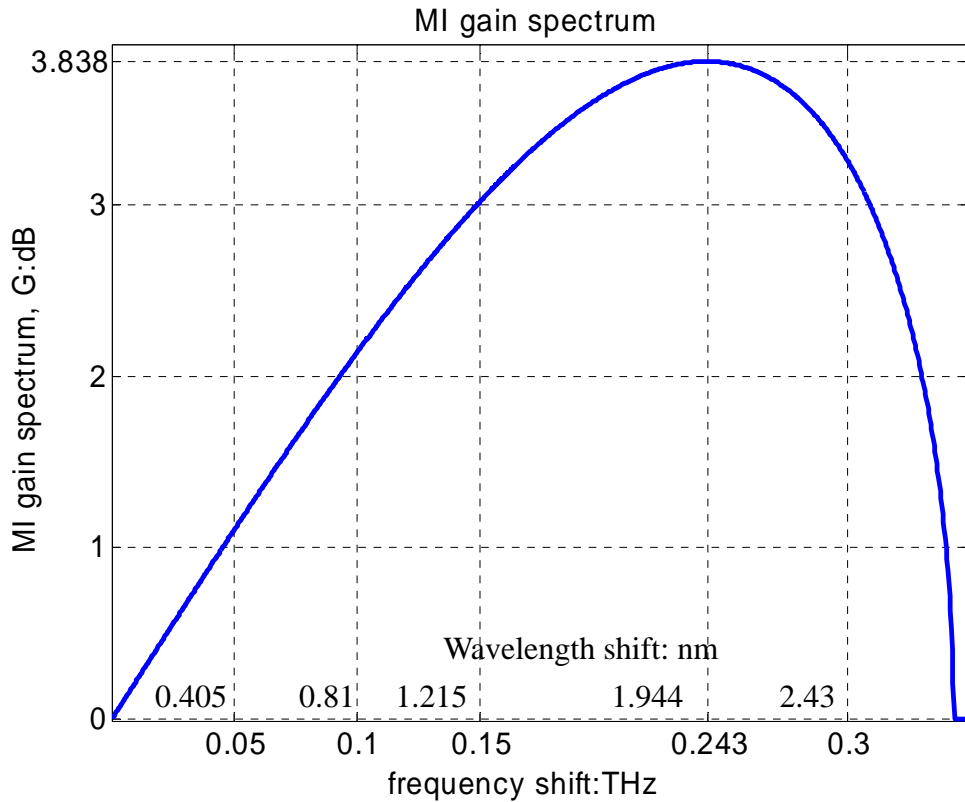
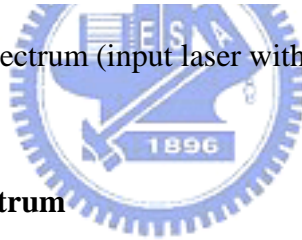


Fig. 16 simulated MI gain spectrum (input laser with power=16dBm, $\lambda = 1559\text{nm}$)



Observation of MI gain spectrum

Before explaining how to estimate γ , D and λ_0 from the MI gain spectrum, let's explain the experiment setup and the observed MI gain spectrum first. The experiment setup for observing the MI gain spectrum is very simple and shown in the following figure.

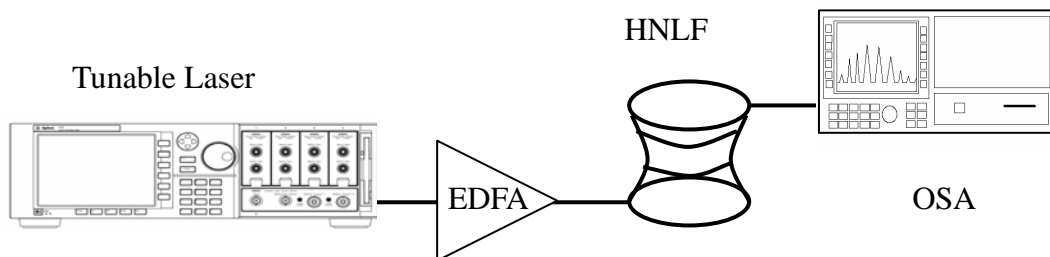


Fig 17 Experiment setup of the observation of the MI gain spectrum

We measure the MI gain spectrum produced by our HNLF in various input powers and wavelengths. Following figure shows one of these results that the input power is around 16dBm and its wavelength is at 1559nm.

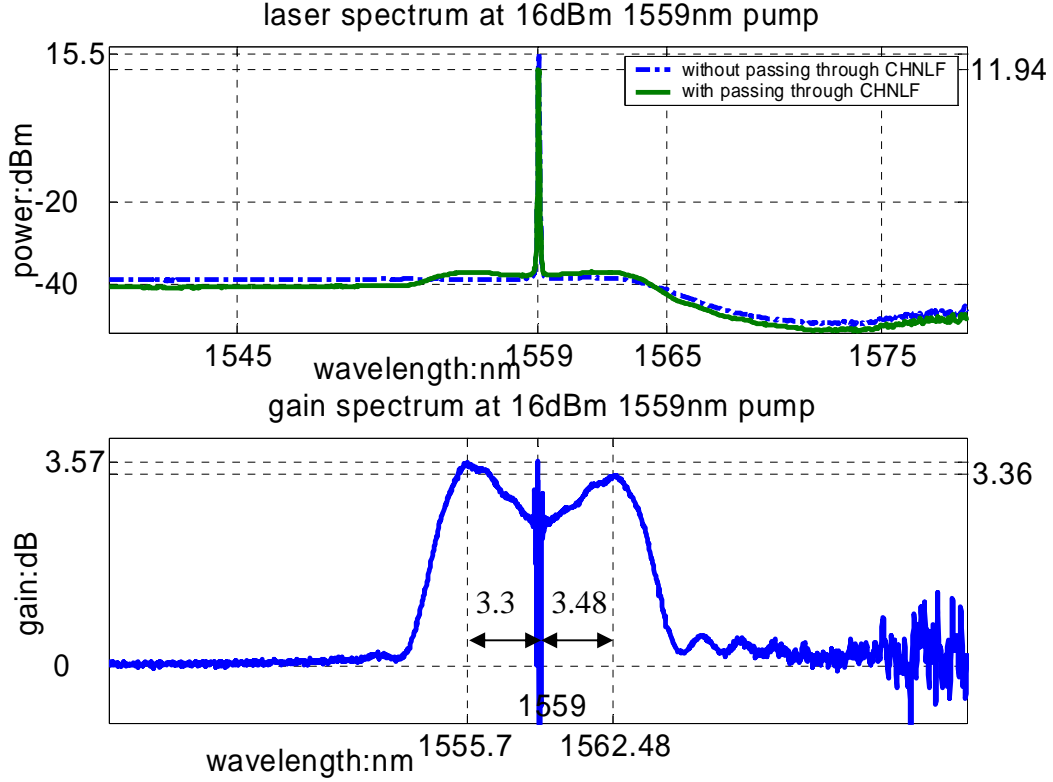


Fig 18 MI gain spectrum (PI=16dBm, $\lambda = 1559\text{nm}$)

In the figure16 and figure 18, we notice two important indexes—the max value of the MI gain spectrum, G_{\max} and the frequency shift, Δf , in which the max gain occurs ($\Delta f = \frac{\Omega_{\max}}{2\pi}$). The measured value of G_{\max} is close to that in the simulation, but the measured value of Δf has larger difference with that in the simulation. I think it is because that value of $\gamma (=11.1 \frac{1}{(\text{km} \times W)})$ is determined by this experiment but that of β_2 is by the measurement of an optical network analyzer.

From eq. (3-11) we can know that $G_{\max} (= \exp(g_{\max} L))$ is determined by γ , but

$\Omega_{\max} = \left(\frac{2\gamma P_0}{|\beta_2|} \right)^{1/2}$ is inverse proportional to $(|\beta_2|)^{1/2}$, which can be justified by the comparison between the experimental and simulated results.

Estimation of γ , β_2 (D) and λ_0

From the eq. 3-10, we can know that the maximum gain coefficient, g_{\max} and the square of the frequency shift, Δf^2 are proportional to the input laser power, so we can have the following results and use the slopes— $m_{(g_{\max}, P_0)}$ and $m_{((\Delta f)^2, P_0)}$ to estimate γ , β_2 and λ_0 . $m_{(g_{\max}, P_0)}$ is the slope of the relation between g_{\max} and input laser power, and $m_{((\Delta f)^2, P_0)}$ is that between Δf and input laser power.

(1) Calculate the nonlinear coefficient, γ

$$g_{\max} = 2\gamma P_0,$$

$$\frac{g_{\max}}{P_0} = m_{(g_{\max}, P_0)},$$

$$\gamma = \frac{m_{(g_{\max}, P_0)}}{2} \dots \text{eq. (3-11)}$$

(2) Calculate the absolute value of β_2

$$2\pi \times \Delta f = \left(\frac{2\gamma P_0}{|\beta_2|} \right)^{1/2} \dots \text{eq. (3-12)}$$

$$(4\pi^2) \times \frac{(\Delta f)^2}{P_0} = \frac{2\gamma}{|\beta_2|}$$

$$m_{((\Delta f)^2, P_0)} = \frac{(\Delta f)^2}{P_0}$$

$$|\beta_2| = \frac{2\gamma}{(4\pi^2) \times m_{((\Delta f)^2, P_0)}} \dots \text{eq. (3-13)}$$

Following picture shows the MI gain spectrum measured at input laser at various conditions.

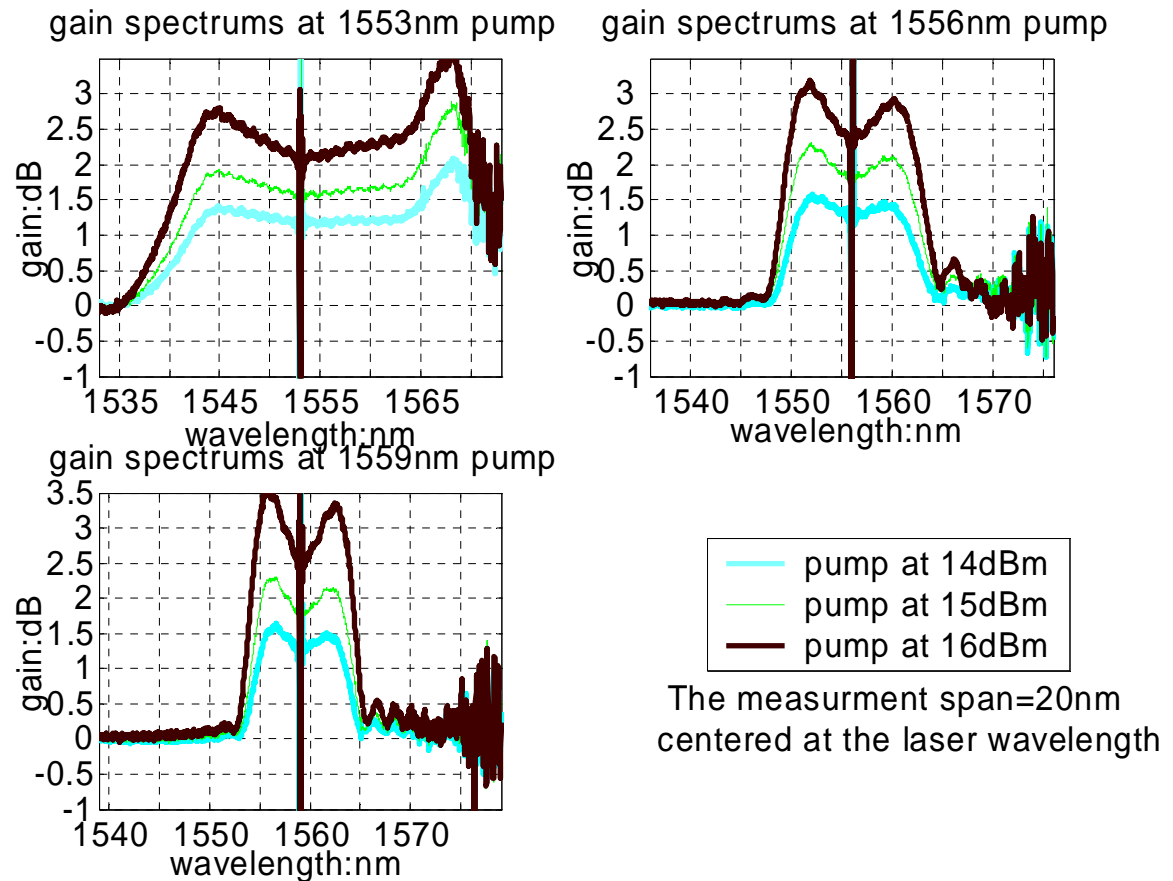


Fig 19 The MI gain spectrums

There are some things that can be found in figure 19:

1. The shorter the laser wavelength, the larger the span of MI gain spectrum. It is because that the absolute value of β_2 is smaller in shorter wavelengths after λ_0 . And it can be explained by eq. (3-12).
2. The MI gain spectrum corresponding to the laser wavelength at 1553nm is different with the MI gain spectrum corresponding to the laser wavelengths at

1556nm and 1559nm—the gain peak at longer wavelength is higher than that at shorter wavelength. And, we will see the following results corresponding to 1553nm laser wavelength have larger deviation. It should be because the MI occurs in the anomalous dispersive region and the λ_0 of our HNLF is in 1552nm.

Then, the following figure shows the linear relation between g_{\max} and PI and that between Δf^2 and PI.

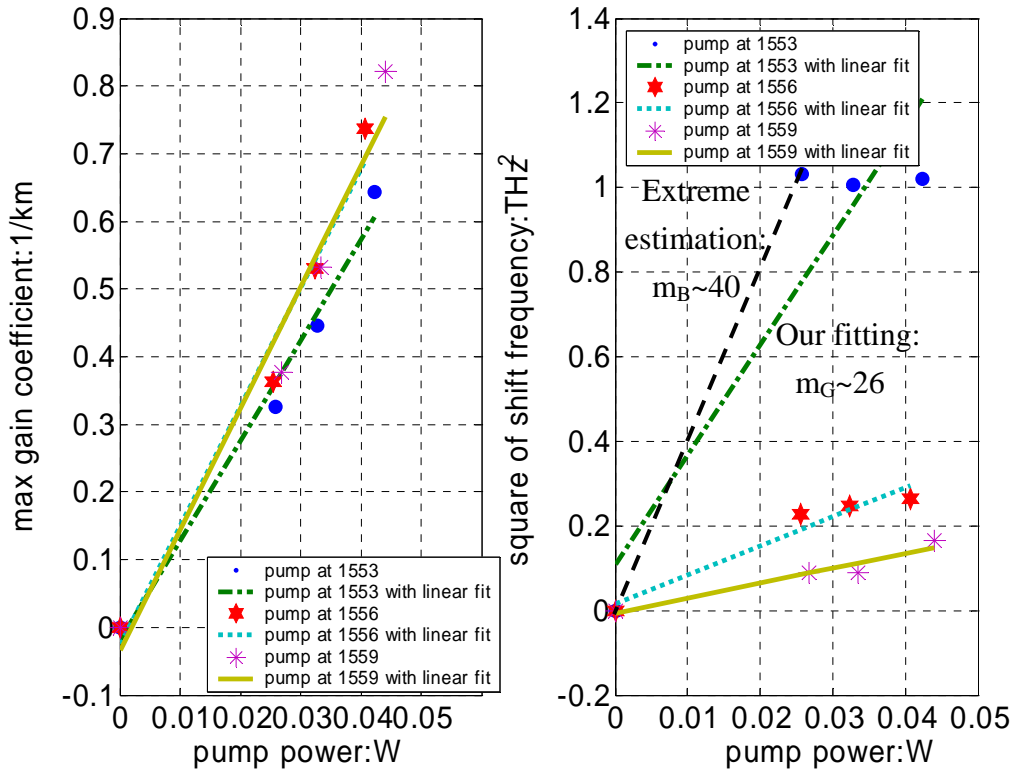


Fig 20 Left: The linear relation between g_{\max} and PI

Right: The linear relation between Δf^2 and PI

In figure 20, the dots are measured data and the lines are linear fittings. We can obtain the slopes that we desired from the fitting lines.

We can utilize the slopes of the three fitting lines in the left figure to calculate the γ corresponding to the three wavelengths. And, the absolute values of β_2 at the three wavelengths are obtained by the slopes of the three lines in the right figures.

Furthermore, we know the sign of β_2 are negative, because the MI occurs only in the anomalous dispersive region. Then we can derive D from β_2 with the following equation— $D = \frac{-2\pi c}{\lambda^2} \beta_2$. These are show in the following figure.

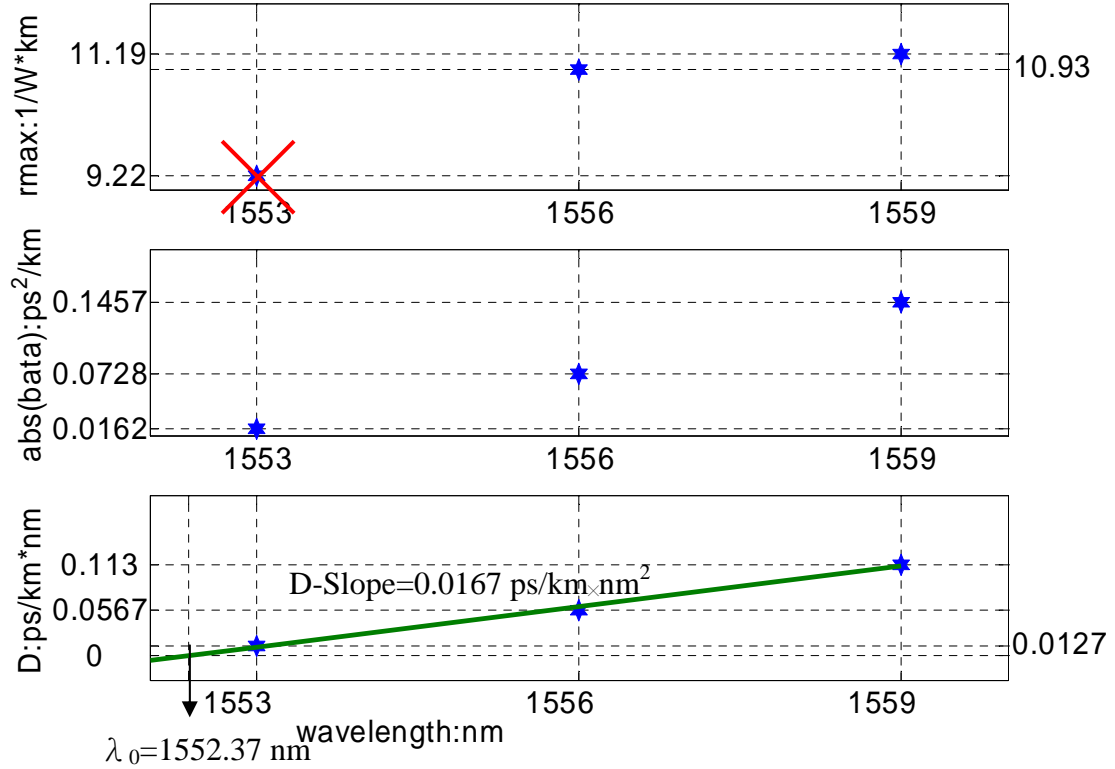


Fig 21 The values of γ , $|\beta_2|$ (D) and λ_0

Finally, λ_0 is obtained by stretching the fitting line of the D to the intersection point with zero.

We can obtain some conclusions and have some discussions in figure 20 and figure 21:

1. The value of γ of this HNLFF is around $11.1 \frac{1}{km \times W}$, which is obtained by averaging the value of γ measured in 1556 nm and 1559 nm. We neglect the value at 1553 nm, because we think that it is incorrect.
2. The value of γ shown in figure 21 is not direct calculated from eq. (3-11),

because the calculation directly from eq. (3-11) and the measured slope of the relation between g_{\max} and PI actually refers to random polarization. That referring to linear polarization and marked in the figure 21 needs an additional transforming factor— $\frac{9}{8}$. [8] Besides that, we need to modify the reduction of the fiber loss.

[4] Thus the value of γ marked in figure 21 is calculate by following equation.

$$\gamma = \frac{m_{(g_{\max}, P_0)}}{2} \times \frac{9}{8} \times (Loss)^{-1} \dots \text{eq. (3-14)}$$

And, the equation (3-15) is also modified as:

$$|\beta_2| = \frac{2\gamma}{(4\pi^2) \times m_{((\Delta f)^2, P_0)} \times (Loss)^{-1}} \dots \text{eq. (3-15)}$$

, so we know that the absolute value of β_2 is independent with the fiber loss.

3. Note the right figure in Fig. 20. There are a large difference between the measured data (dots) and the fitting line, which is because we force $\Delta f (PI=0) = 0$ that is according to eq. (3-12); or the slope will be greatly underestimated, and $|\beta_2|$ and D will be overestimated.

4. Following discussion is the error of $m_{((\Delta f)^2, P_0)}$ and the resulting error of $|\beta_2|$ at 1553 nm laser wavelength. In the right figure of Fig.20, we seem to underestimate $m_{((\Delta f)^2, P_0)} \big|_{1553\text{nm}}$, but we will show that its influence is very limited in following results— $|\beta_2|$ at 1553 nm and λ_0 . In our measurement, the maximum $m_{((\Delta f)^2, P_0)}$ at 1553 nm is around $40 \text{ THz}^2/\text{W}$ belonging to the black line.

Then we assume the relative error of $m_{((\Delta f)^2, P_0)} \big|_{1553\text{nm}}$ as:

$$\text{Error} \big|_{m_{((\Delta f)^2, P_0)}} = \frac{m_G - m_B}{m_G} = \frac{26 - 40}{26} = -53.8\% \dots \text{eq. (3-16)}$$

, and that of $|\beta_2|$ at 1553 nm as:

$$Error|_{\beta_2,1553nm} = \frac{|\beta_2|_G - |\beta_2|_B}{|\beta_2|_G} \dots \text{eq. (3-17)}$$

And, with eq. (3-15), we can express eq. (3-17) as m_G and m_B .

$$\begin{aligned} Error|_{\beta_2,1553nm} &= \frac{|\beta_2|_G - |\beta_2|_B}{|\beta_2|_G} \\ &= \frac{m_B - m_G}{m_B} \quad ; \\ &= \frac{40 - 26}{40} = 35\% \end{aligned}$$

Furthermore, we know that the relative error of D equals to that of $|\beta_2|$ from the relation between D and β_2 .

$$Error|_{D,1553nm} = \frac{D_G - D_B}{D_G} = 35\%$$

Thus the difference between $|\beta_2|_G$ and $|\beta_2|_B$ (or D_G and D_B) at 1553nm is very small, because it is near λ_0 of the fiber.

$$\begin{aligned} \Delta|_{\beta_2} &= |\beta_2|_G - |\beta_2|_B \quad \Delta|_D = D_G - D_B \\ &= |\beta_2|_G \times Error|_{\beta_2,1553nm} = D_G \times Error|_{D,1553nm} \\ &= 0.0162 \text{ ps}^2/\text{km} \times 35\% = 0.0127 \text{ ps}^2/\text{km} \times 35\% \\ &= 0.0057 \text{ ps}^2/\text{km} = 0.0044 \text{ ps}^2/\text{km} \end{aligned}$$

So the measurement of β_2 and D has nice linear dependence and well prediction of $\lambda_0=1552.37$ nm.

3-1-2: The measurement of its dispersion properties

Although the MI gain spectrum also tells us the dispersion properties of HNLF, we also make a more detailed measurement of the dispersion properties of the HNLF with the ADVANTEST Q7760 optical network analyzer. The obtained result not only

gives us a comparison with that obtained by MI gain spectrum but also lets us able to do the prediction of the bandwidth of our optical RF spectrum analyzer based on the measured dispersion data in chapter 4.

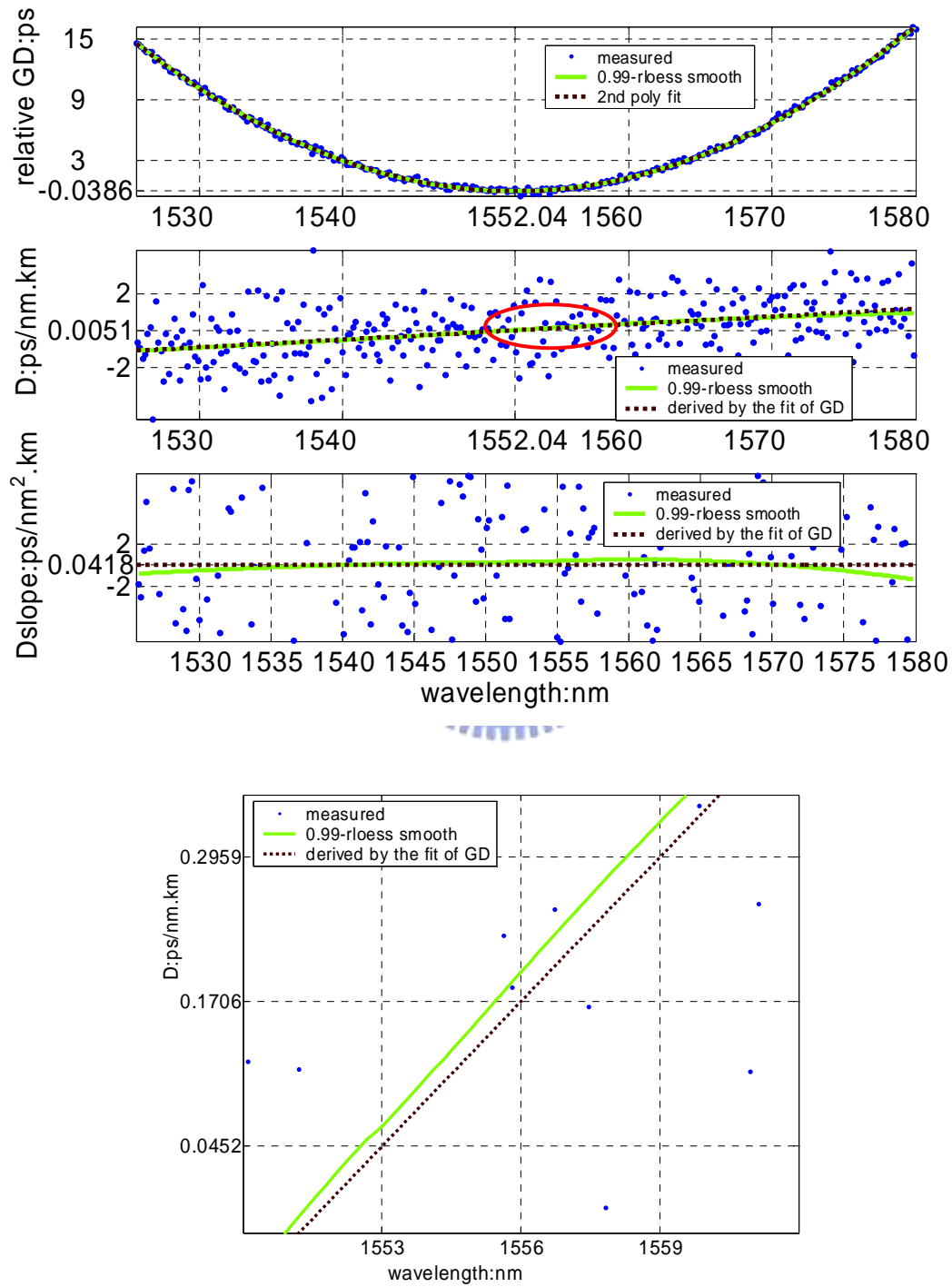


Fig 22 Dispersion properties of Corning HNLF

measured by ADVANTEST Q7760 optical network analyzer

In figure 22, the blue dots are the initial measured data from Q7760 and the green solid lines are that after smoothing. Furthermore, we also use the 2nd order polynomial fitting to describe the relative GD (group delay)—the coffee dot line in first figure, and we can obtain the function describing D (dispersion) and D-slope utilizing the 2nd order polynomial GD by differentiation—the coffee dot line in second and third figures.

For the completeness, we calculate relative β_1 and β_2 utilizing the fitting function of D in figure 22.

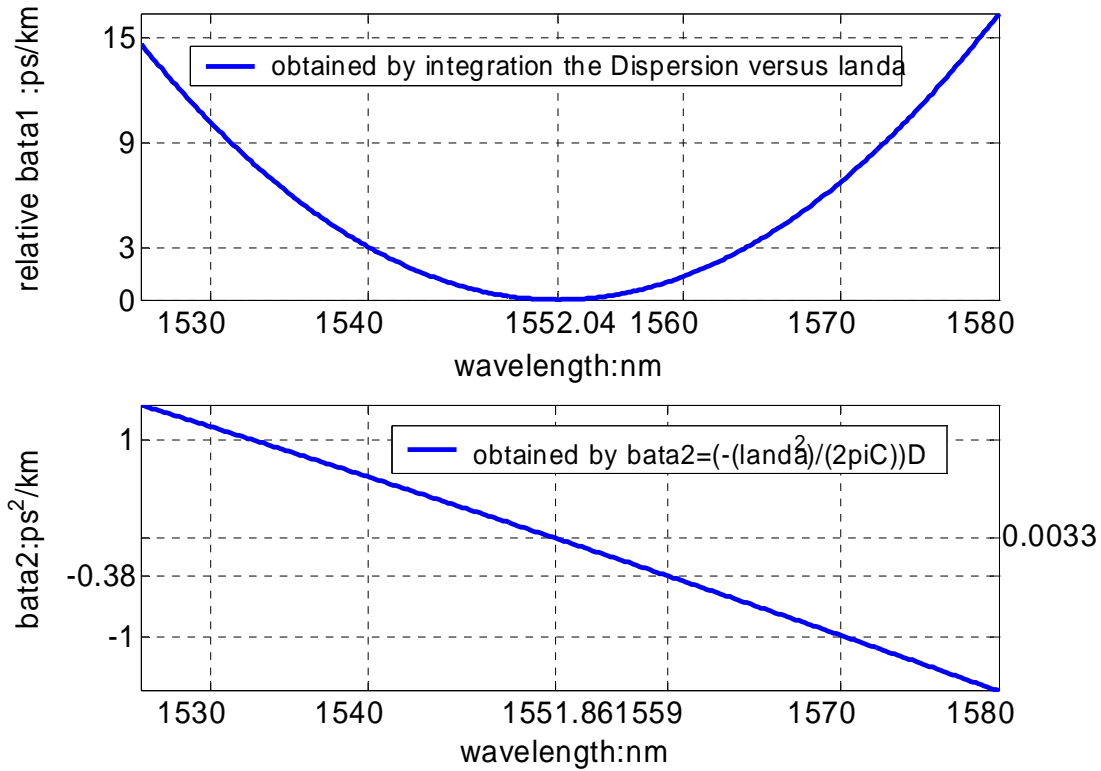


Fig 23 dispersion properties of Corning HNLF

The relative β_1 and β_2 are calculated by following equations.

$$D = \frac{d\beta_1}{d\lambda} \quad \therefore \Delta\beta_1 = \int \beta_1 d\lambda \dots \text{eq. (3-18)}$$

$$D = \frac{-2\pi c}{\lambda^2} \beta_2 \quad \therefore \beta_2 = -\frac{\lambda^2}{2\pi c} D \dots \text{eq. (3-19)}$$

In following table, we have a simple compression about some parameters from the measurement of MI gain spectrum and Q7760.

Parameters		MI	Q7760
λ_0		1552.37 nm	1552.04 nm
D-slope		0.0167 ps/km.nm ²	0.0418 ps/km.nm ²
D	1553 nm	0.0127 ps/km.nm	0.0452 ps/km.nm
	1556 nm	0.0567 ps/km.nm	0.1706 ps/km.nm
	1559 nm	0.113 ps/km.nm	0.2959 ps/km.nm
β_2	1553 nm	-0.0162 ps ² /km	-0.0579 ps ² /km
	1556 nm	-0.0728 ps ² /km	-0.2191 ps ² /km
	1559 nm	-0.1457 ps ² /km	-0.38 ps ² /km

Table 4 Compression of measured results from MI gain spectrum and Q7760

Although there are some differences existing between the values obtained from these two approaches, the trends and orders still agree with each other.

3-1-3: Control and estimate the loss

Reduction the fusion loss between HNLF and SMF

The HNLF has a much smaller core than general SMF, so there is a larger splicing loss when they are fused together. But, we can reduce the spicing loss through adjusting the fusion parameters including the discharging duration, discharging intensity and push moment. The fiber is fused by the fiber splicer— “Sumitomo Electric type 36”. The best fusion condition is described in the following table and

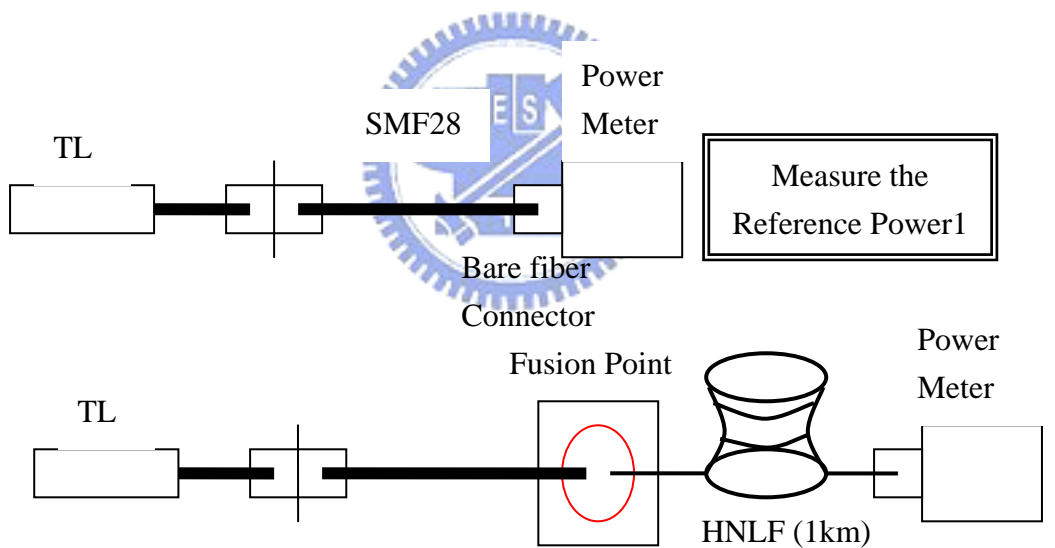
saved in “Sumitomo Electric type 36”.

Parameters	Best setting	Standard(SMF)	Units
Discharging duration	13	1.05	second
Discharging intensity	17	9	step
Push moment	10	15	um

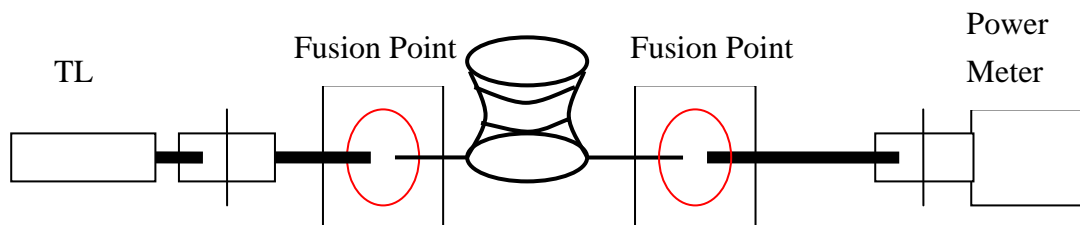
Table 5 The best fusion conditions of for fusing the HNLf and SMF

At this condition the splicing loss is around 0.6~0.7 dB.

Estimate the splicing loss and the intrinsic loss of HNLf



Splicing Loss in Er-other2 mode, $L_1=L(\text{HNLf}) +L(\text{splice}, 1) =1.1 \text{ dB}$



$L_2=L(\text{HNLf}) +L(\text{splice},1)+L(\text{splice},2)-V=1.5 \text{ dB}$

Fig 24 Setup of measuring the intrinsic loss of HNLf and splicing loss

In figure 24, 'V' is the loss decreasing caused by instating the bare fiber connector with a PC connector and is measured as 0.25dB in previous experiment. With 'V', 'L1' and 'L2', we can estimate the intrinsic loss of HNLF and the splicing loss:

$$L (\text{HNLF}) = 0.45 \text{ dB}$$

$$L (\text{splice, 1}) = L (\text{splice, 2}) = 0.65 \text{ dB}$$

, which agree with the previous data.



3-2 Measurement results of 10Gbps and 40Gbps signal

In this section, our optical RF spectrum analyzer will be shown. Following figure is a sketch of the optical RF spectrum analyzer. It is so simple that we need only a HNLF and an OSA to measure the RF spectrum of the signal under test.

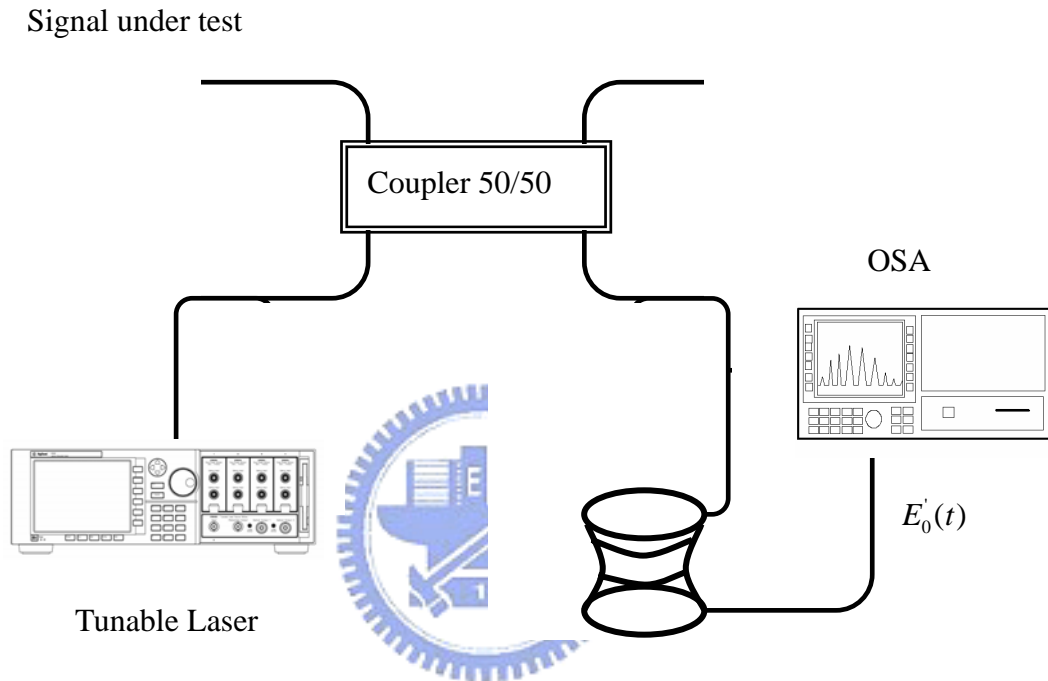


Fig 25 A sketch of the optical RF spectrum analyzer

And, for demonstrating its high bandwidth performance, we use it to measure the RF spectrum of two signals: one is 10GBps RZ signal with/without coding ($2^{10}-1$) PRBS; the other is 40GBps RZ ones train.

3-2-1: 10GBps signal

In this subsection, the measurement of RF spectrum of 10GBps signals by this new all optical approach is demonstrated. The following picture is the detailed experiment setup and the table describes the experimental conditions.

Experiment setup and conditions

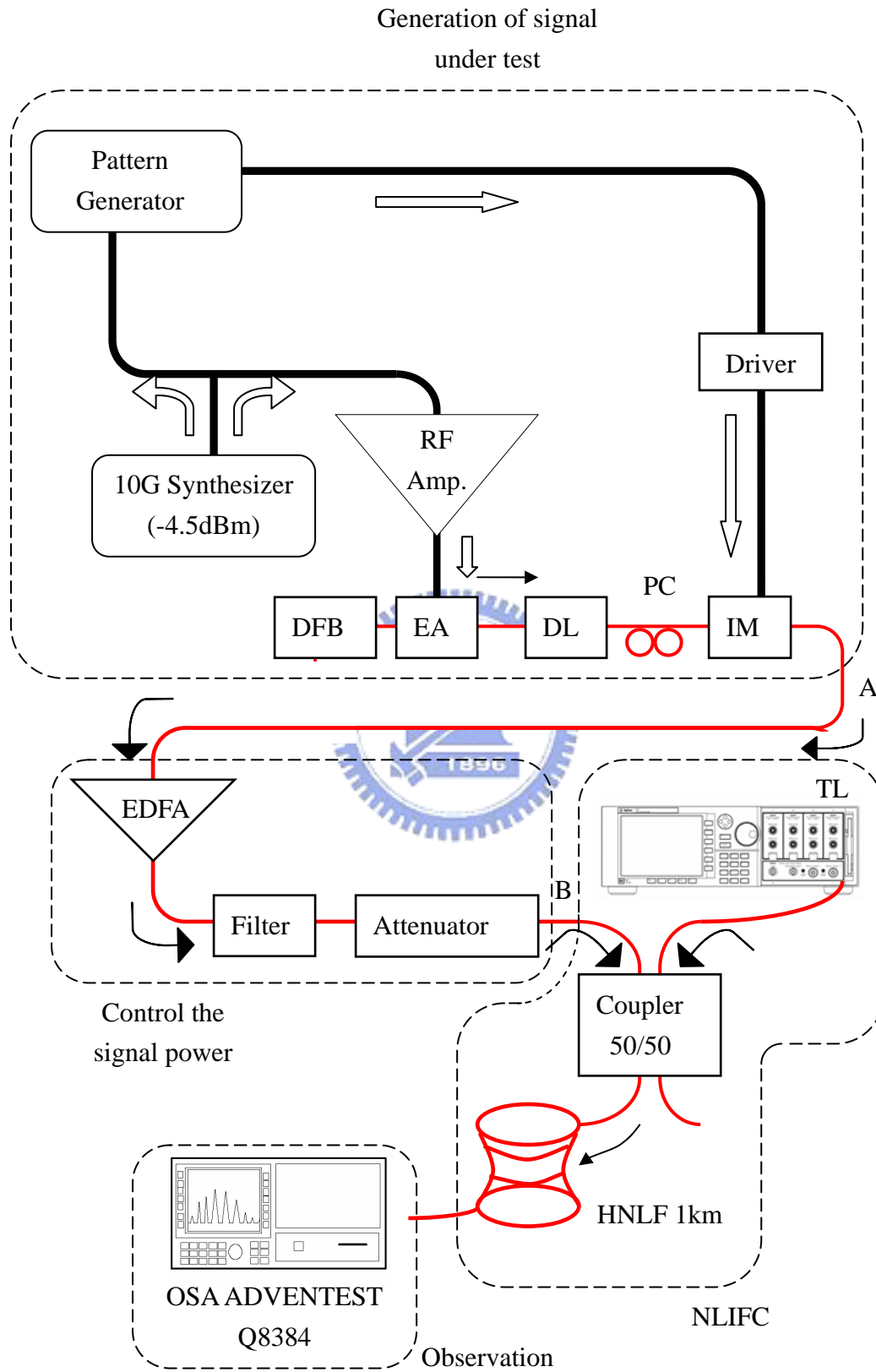


Fig 26 Experimental setup of the RF spectrum of 10Gbps signal

Physical condition							
RZ train coding				PRBS coding		TL	
I_F	T_C	EA_{BIAS}	RF power	V_{BIAS}	V_{GC}	Power	λ
84.8mA	16.7°C	-1.22V	-4.5dBm	+1.22V	-6V	3.5dBm	1554nm
Measurement Instrument							
OSA				Sampling Scope			
Resolution		Sampling points		Scale		Offset	
0.01nm		1001		500uW/div		300uW	

Table 6 experimental conditions for 10Gbps signal

In figure 26, the thick lines represent the path of electrical RF signal (RF cable); and thin lines represent that of optical signal (fiber). The setup is divided into four parts: generation of signal under test, controlling the signal power, NLIFC and observation, which are all marked in the figure 26.

First we have to generate an optical signal under test. In this part, we choose to generate a 10GBps RZ signal. The 10GHz sinusoidal signal is generated from the “**Agilent 83624B signal generator**”. It is split into two parts: one is used to trigger the “**Anritsu pulse pattern generator**” that generates a PRBS data and the other enters the “**Agilent 83017A microwave system amplifier**”. The amplified 10GHz sinusoidal signal is sent into the EA (electrical absorption) modulator, and the continuous light from DFB laser is modulated as a RZ ones train.

Then the optical RZ ones train passes through a DL (delay line) that is used to synchronize the RZ ones train and the PRBS coding. The PRBS coding is performed by the “**JDSU 10GBps Lithium Niobate AM modulator**” and the “**Picosecond Pulse Lab model 5865 modulator driver**”. Now the optical signal under test as that in figure 3 is generated. We observe it at ‘A’ with Agilent sampling scope. The result is shown in figure 27.

Then the optical signal is amplified by an EDFA and an optical filter that suppress the ASE from EDFA. Following the filter we insert an optical attenuator to adjust the power of the signal under test. We also utilize the sampling scope to see the eye of the signal under test after amplification at 'B', which are shown in figure 28. But, note that the power of signal passing through the attenuator is adjusted to 0dBm for protecting the sampling scope.

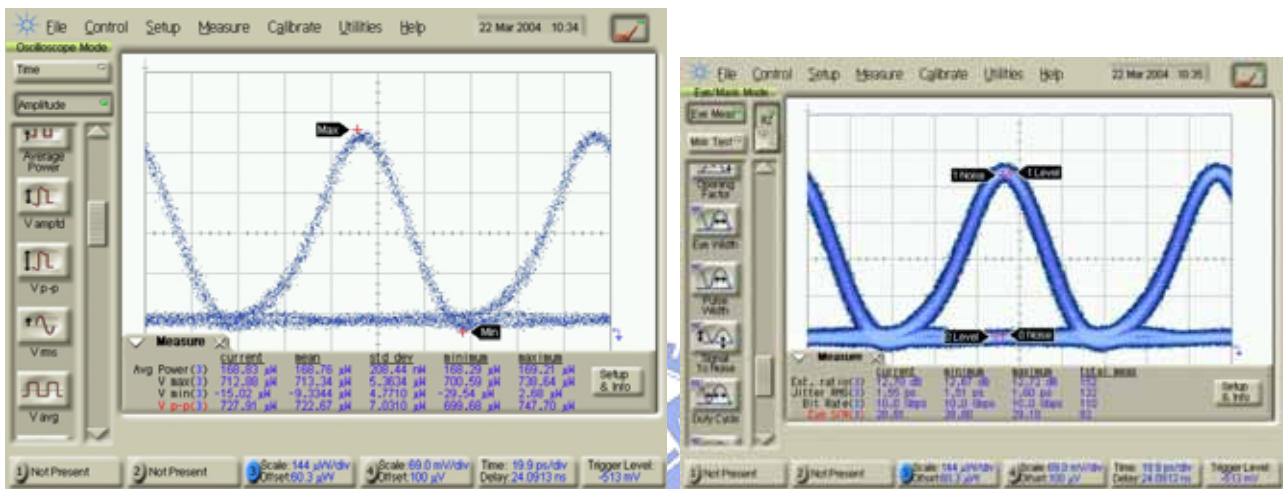


Fig 27 Eye of the signal under test before amplification

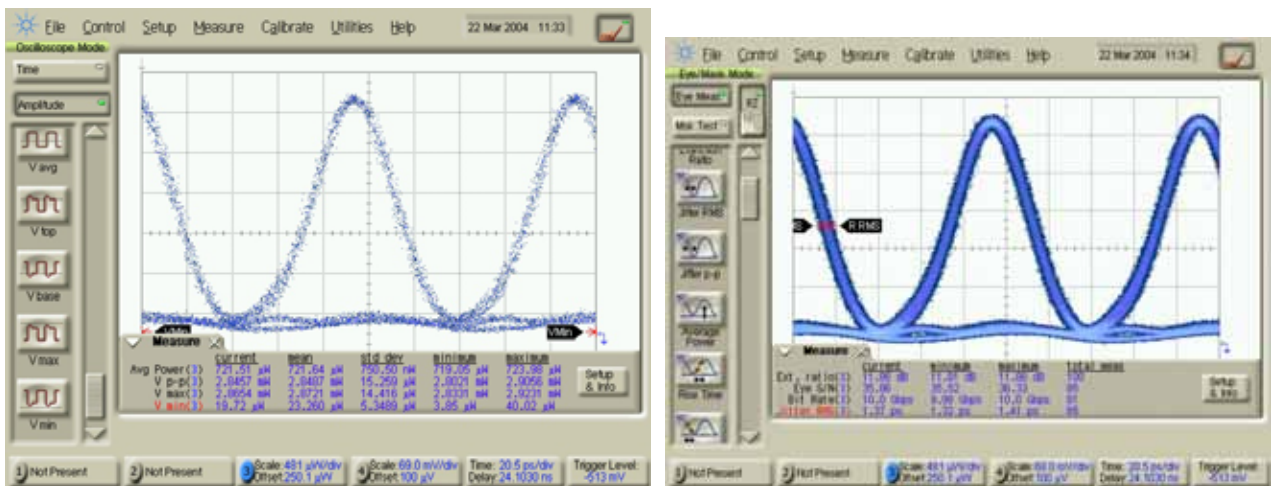


Fig 28 Eye of the signal under test after amplification and adjusting the DL

Following table compares some important characteristics of the optical signal

under test. We can find that the amplification of signal reduces the extinction ratio of signal but seems to improve the signal jitter.

Parameters	Average Power	One's Level	Zero's Level	Extinction ratio	Jitter RMS	Eye S/N
Before Amplification	168.83 uW	712.88 uW	-15.02 uW	12.7 dB	1.55 ps	28.21
After Amplification	739.38 uW	2.9641 mW	10.58 uW	11.86 dB	1.4 ps	37.32

Table 7 Comparison of some characteristics of signal before and amplification

Finally, the optical signal under test and the reference laser are combined by 50/50 fiber coupler and sent into the 1km-HNLF. The nonlinear interaction between the signal and the reference laser that we expect is performed in the HNLF, and we can measure the RF spectrum of the signal under test through measuring the optical spectrum of the reference laser after HNLF by a general OSA according to the previous discussion.

The measured results

Following pictures are the measured results by the “**ADVENTEST Q8384 Optical Spectrum Analyzer**”. We do the measurement at four signal powers: 14.7dBm (Fig 29), 10dBm (Fig 30) and 5dBm (Fig 31). We will see that the more clear-cut spectrum is obtained at larger signal power. Furthermore, note the eq. (2-9): there is an additional delta function at the center of the spectrum that we measured,

$$I'_{optical}(f) \propto \delta(f - f_0) + |m|^2 \times (I_{RF}(f))|_{f_0}$$

, so we measure the optical spectrum of the reference laser without the signal light, $I_0'(f)$. Then take it as the additional delta function and we can remove its influence by $I_{0'optical}(f) - I_0'(f)$. In figure 29, the left one is directly measured by OSA and the right one is that after removing the delta function.

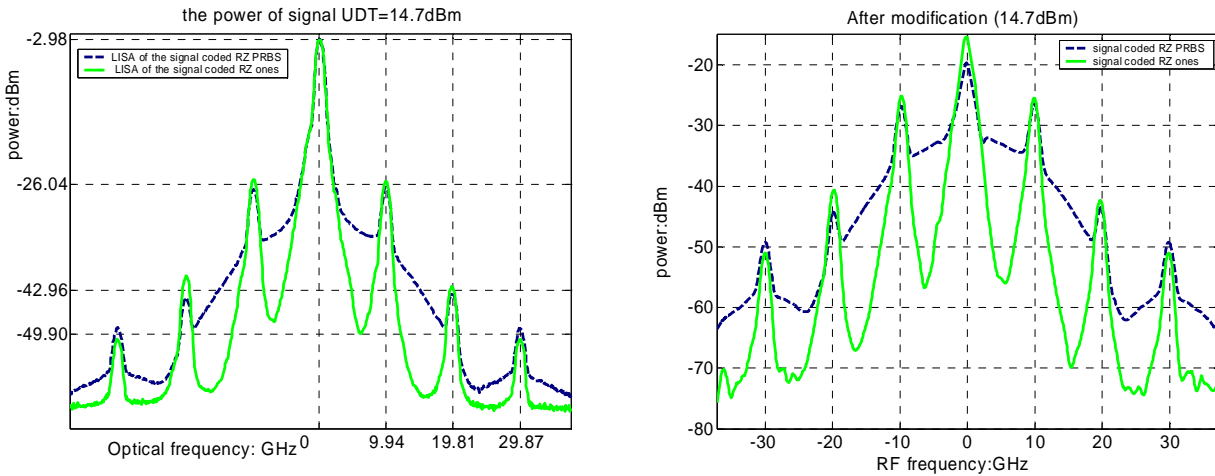


Fig 29 Measurement result of 10G signal power at 14.7dBm

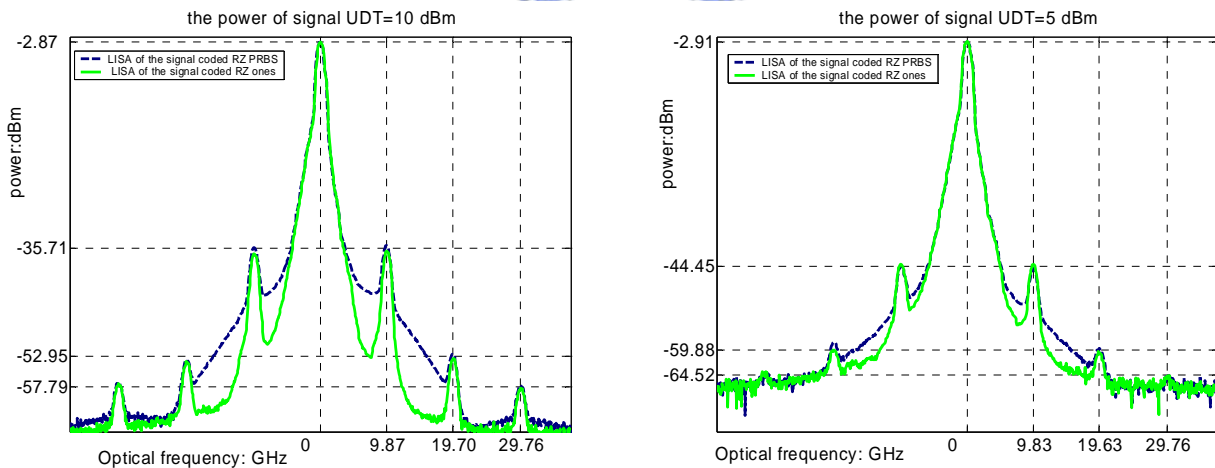


Fig 30 Measurement result of 10G
signal power at 10dBm

Fig 31 Measurement result of 10G
signal power at 5dBm

In these figures, the dashed lines represent the spectrum with PRBS coding and that of solid lines are spectrum of RZ ones train.

3-2-2: 40Gbps signal

This subsection states the observation of the RF spectrum of the 40Gbps RZ ones train with the optical RF spectrum analyzer to show its high bandwidth performance.

Experiment setup and conditions

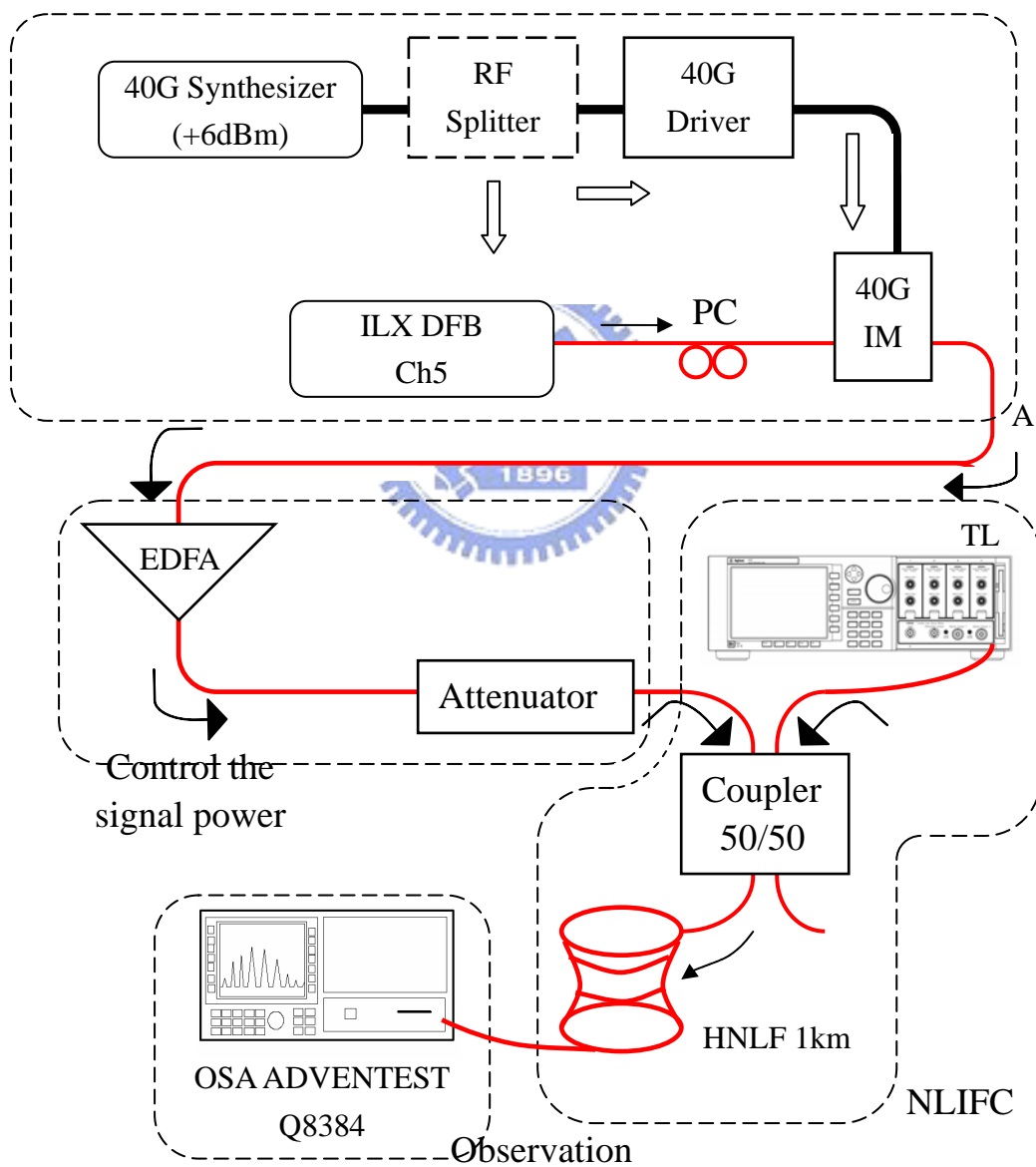


Fig 32 Experimental setup of the RF spectrum of 40Gbps signal

Physical condition				
Signal under test			Reference laser (TL)	
RF power	Laser power	Laser λ	Power	λ
+6dBm	+6dBm	1549.42nm	+4.5dBm	1554.58nm

Table 8 experimental conditions for 40Gbps signal

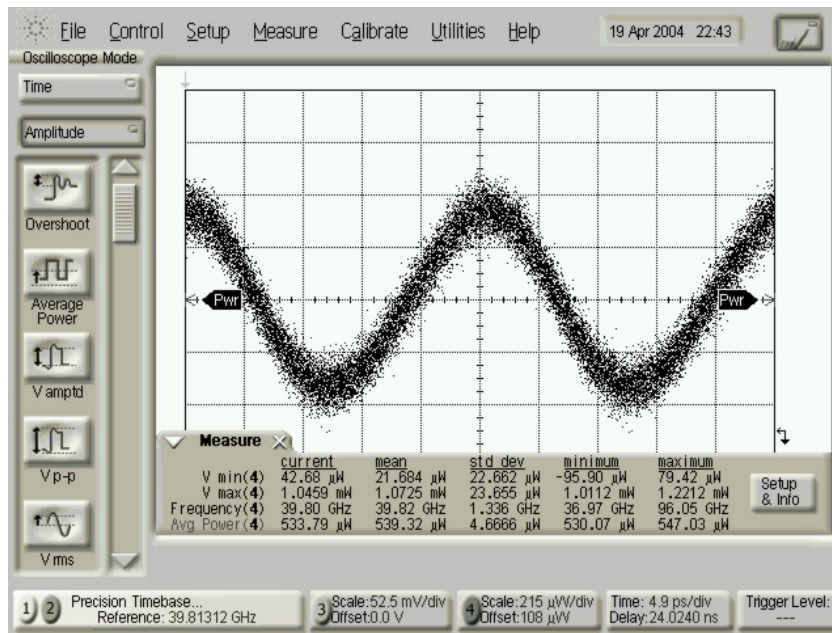


Fig 33
40GHz sinusoidal
signal before
amplification

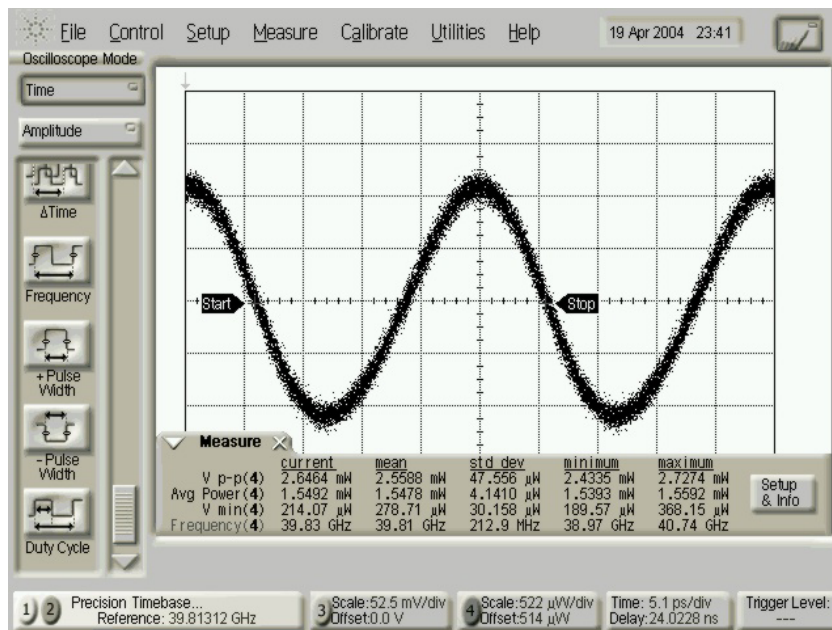


Fig 34
40GHz sinusoidal
signal after
amplification

As the observation for 10Gbps signal, a 40GHz sinusoidal signal is generated by the “**ROHDE&SCHWARZ signal generator**”. Then after amplification of the “**SHF 806E modulator driver**”, the RF signal enters the “**EOspace LiNbO3 modulator**” and the CW laser from “**ILX DFB laser**” is modulated as a RZ ones train. Till now the optical RZ ones train is formed, we can observe it with the “**Agilent 86116A sampling scope**” to observe the optical RZ ones train that is shown in figure 33.

Then the power of the RZ ones train is controlled by the combination of an EDFA and an optical attenuator similar to that used in 10Gbps case except that the filter is removed now. It is because that the filter without enough large bandwidth will distort our signal. The signal after amplification is in the figure 34.

And, the following setup is the same with the 10Gbps case.

The measurement results



Following pictures are the measurement results for 40GHz sinusoidal signal at various signal powers.

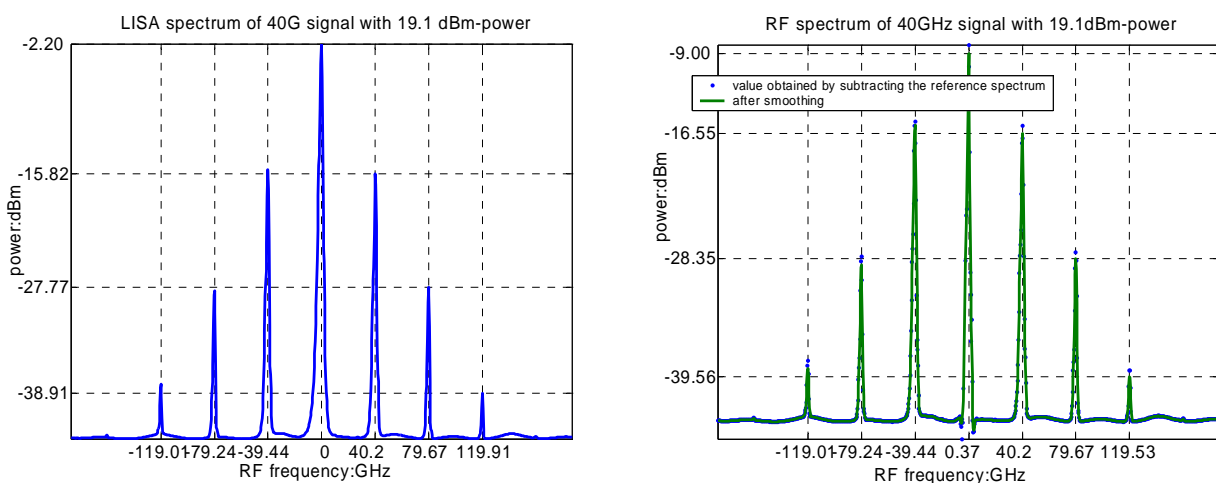


Fig 35 Measurement result of 40G signal power at 19.1dBm

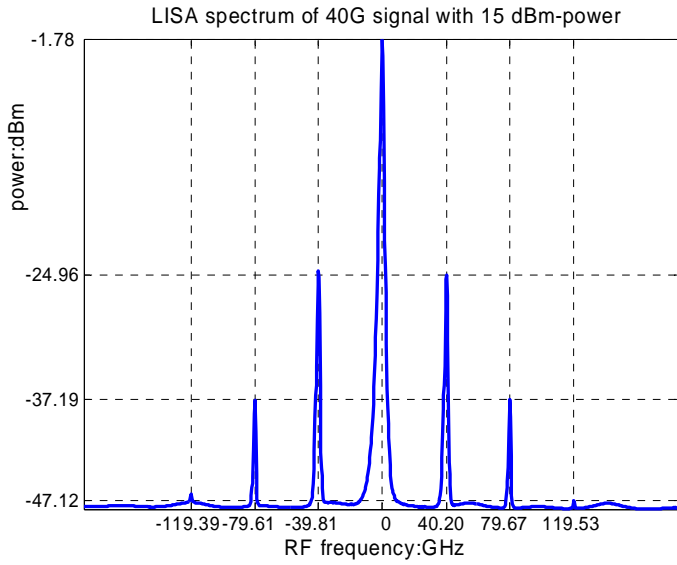


Fig 36
Measurement result
of 40G signal at
15dBm

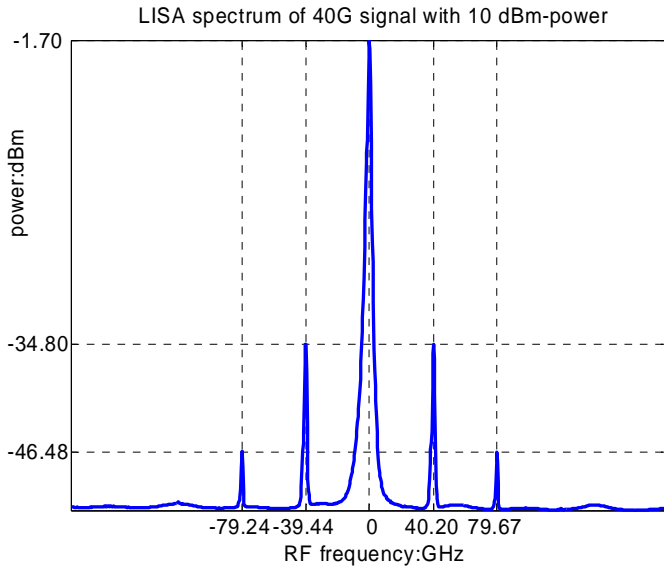


Fig 37
Measurement result
of 40G signal at
10dBm

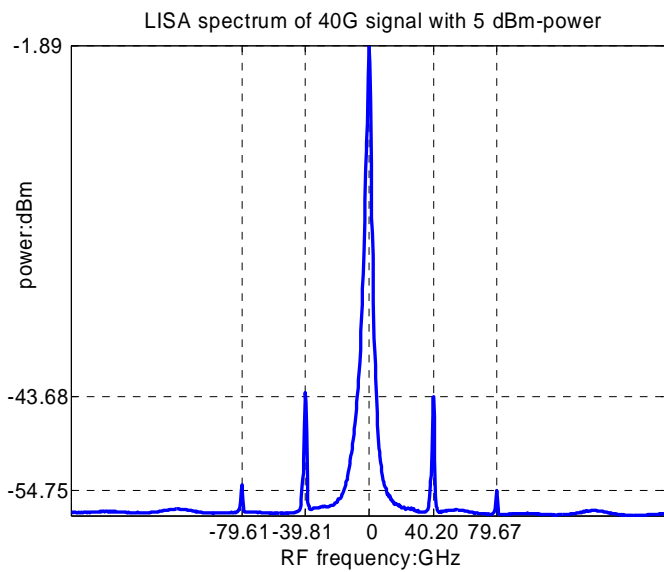
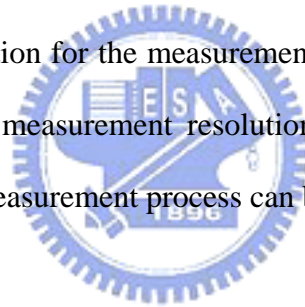


Fig 38
Measurement result
of 40G signal at
5dBm

3-3 Simulation for the measurement with OSA

Now we have simulated the optical spectrum of the reference light passing through the HNLF. With the simulation we can predict that a correct measurement range up to the second harmonic peak is guaranteed for 10Gbps and 40Gbps signal at least. But, these spectrums that we simulated in section 2-2 (Fig 4, Fig 7, Fig 9 and Fig 12) is still very unlike with that we observed with OSA in the practical experiment (Fig 29, Fig 30, Fig 31, Fig35, Fig 36, Fig 37, Fig 38). It is because of the OSA measurement and the limited resolution bandwidth of OSA.

Thus we try to simulate the measuring process of OSA in this section. And the simulated results are found to be quit similar to that observed in experiment in section 3-2. Furthermore, this simulation for the measurement process of OSA stimulates the discussion of enhancing the measurement resolution by applying the operation of deconvolution, because the measurement process can be viewed as a convolution.



Simplified block diagram of OSA

Although the structure of a commercial OSA is very complex and precise [5], we simplify its structure with the following diagram for building a model to simulate the OSA measurement process:

The input light passes through a tunable bandpass filter, which resolves an individual part of spectral component of the input light and is controlled by a ramp generator such that the central frequency of the filter sweeping through the spectral width of the light step by step. The photo-detector is used to measure the power of the light resolved by the filter. It transfers the photon energy of the light passing through the filter into electrical current.

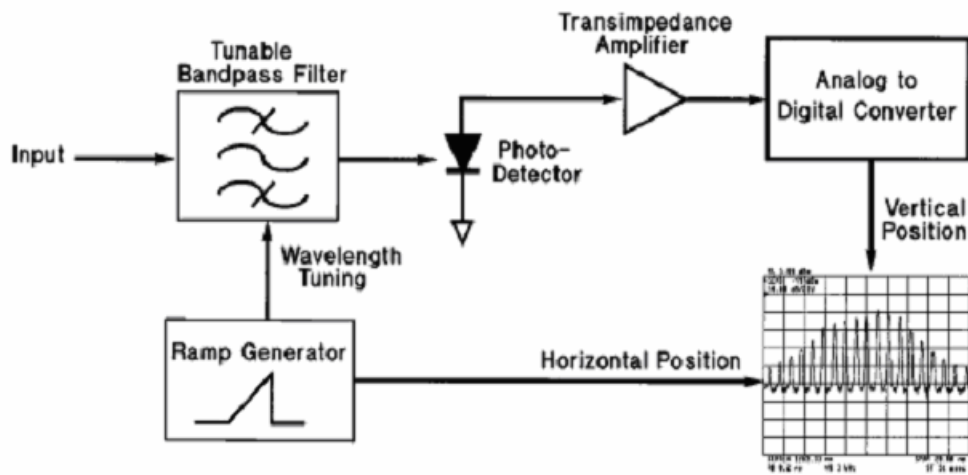


Fig 39 Simplified block diagram of OSA (extracted from [5])

Then the transimpedance amplifier converts the currents into voltages. In next steps, the voltage signal is digitalized, and the following signal processes are all performed digitally.

Finally, the voltage signal representing optical power at each frequency is displayed in the vertical axis, and the corresponding central frequency is displayed in the horizontal axis. Then the optical spectrum of the light is performed.

Convolution

From the simplified block diagram of OSA in figure 39, we can know that the measured spectrum of OSA can be viewed as a convolution between the spectrum of the input light and the shape of the filter as the following equation:

$$S'(f) = S(f) \otimes F(f) = \int S(f')F(f - f')df' \dots \text{eq. (3-20)}$$

, where $S(f)$: the spectrum of the input light

$F(f)$: shape of the OSA filter

$S'(f)$: measured spectrum of OSA

And, we know that $S'(f) \neq S(f)$ unless $F(f) = \delta(f)$, a delta function.

Furthermore, because the tunable filter is controlled by a ramp generator and scans step by step, the eq. (3-20) should be rewritten as:

$$S'(f = m\Delta f) = \int S(f')F(m\Delta f - f')df', m=0, 1, 2, \dots \dots \text{eq. (3-21)}$$

, where Δf : the step of the filter scanning

, but f' is continuous

Thus a sampling accompanies the OSA measurement, which prevents us from recovering the original signal by applying a simple deconvolution. This property is also considered in the simulation.

Define the filter of OSA



Although a practical OSA is very complex with various parameters and specifications including the resolution bandwidth, dynamic range, sensitivity and etc, we only consider the **resolution bandwidth** and **dynamic range**.

The term resolution bandwidth is often used to describe the width of the optical filter in an OSA, which determines the ability of an OSA to display two signals closely spaced in wavelength as two distinct responses.

As to the dynamic range of an OSA, it refers to the ability of the OSA to simultaneously look at large and small signals in the same sweep. The dynamic range of an OSA is primarily determined by the filter shape and stopband performance of the tunable filter.

Therefore we can control the two important specifications of an OSA by defining the filter of the OSA. Following figure shows the OSA filter that we assume in the simulation.

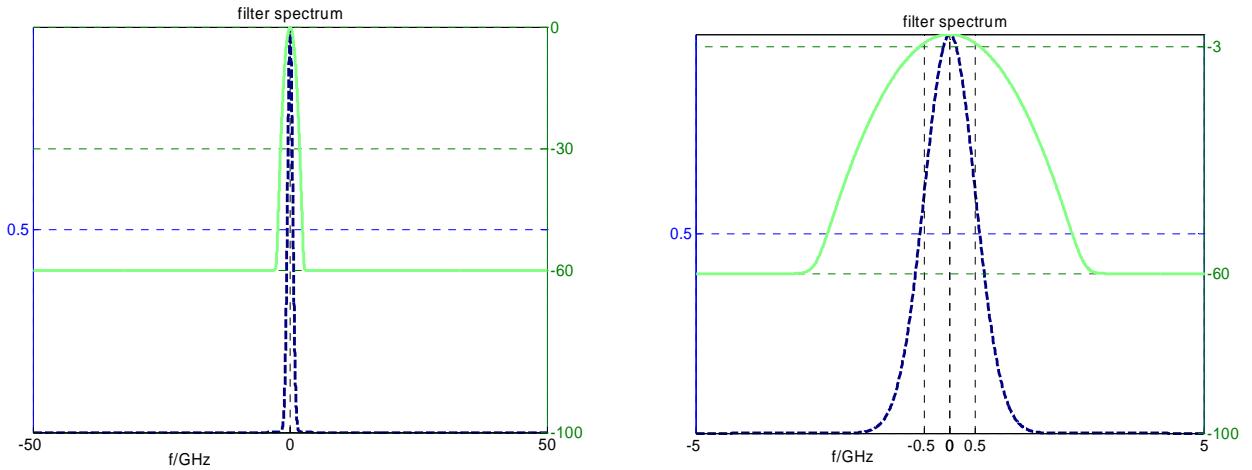


Fig 40 the assumed filter with bandwidth=1GHz and dynamic range=60dB

Its resolution bandwidth and dynamic range are assumed as 1GHz and 60dB. These values are referred to the OSA that we used in the experiment, “ADVENTEST Q8384”.

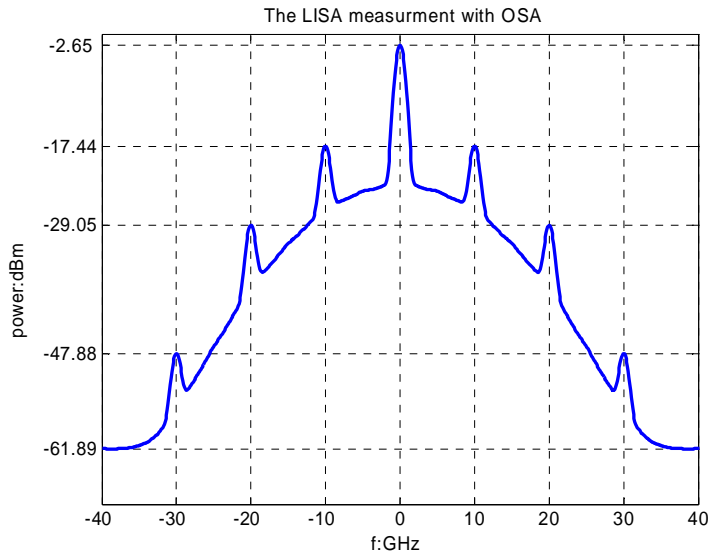
Following table states the related parameters used in this simulation.

Parameters	Resolution Bandwidth	Dynamic Range	Tuning Step	Filter Shape
value	1GHz	60dB	0.1GHz	Gaussian

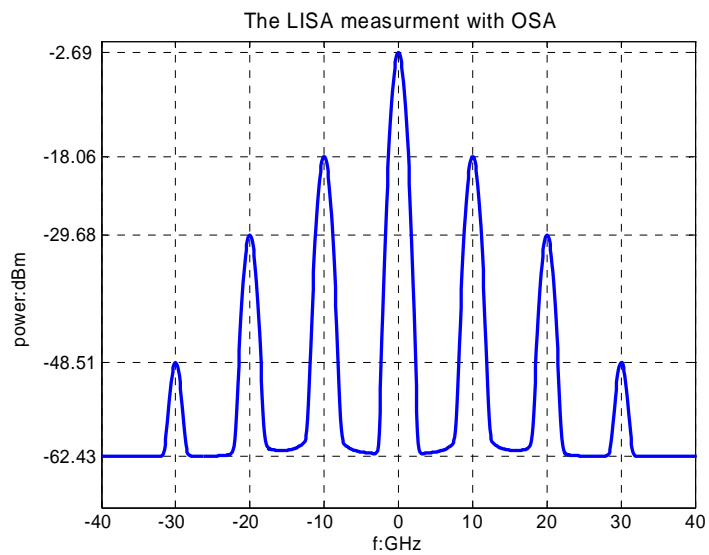
Table 9 Parameters in the simulation of OSA measurement process

The optical spectrum of the reference light

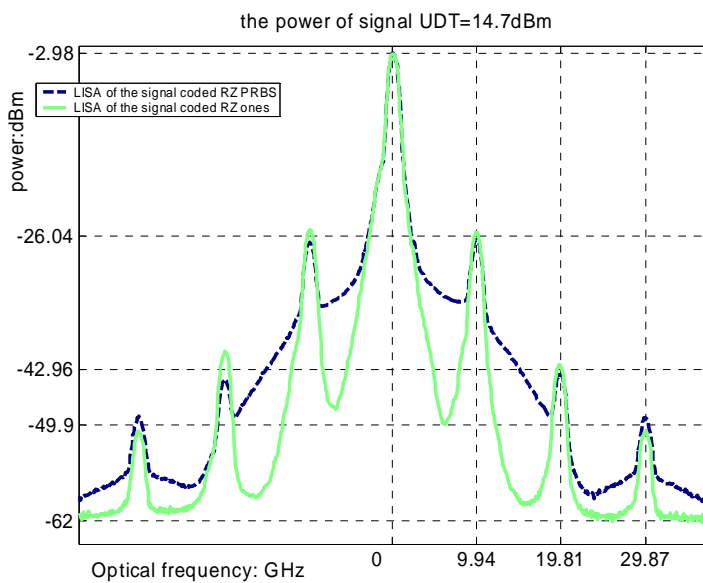
In section 3-2, we have stated the observations of RF spectrums of signal under test through the optical spectrums of the reference light for the 10Gbps RZ signal and 40GHZ sinusoidal signal. Now we compare them with the corresponding simulated results in the following figures.



A. Simulated result for 10Gbps RZ signal with PRBS coding



B. Simulated result for 10GHz RZ ones train



C. Experimental result for 10Gbps RZ signal

Fig 41
Optical spectrums of reference light for 10Gbps RZ signal with signal input power of 14.7dBm

We can find that the simulated optical spectrums of reference light are more similar to those from experiment, although they are still not exactly the same. This should be originated from following reasons:

1. The assumed signal under test in simulation is not exactly the same with that generating in practical experiment, although this difference (that can be seen by comparing Fig 3 with Fig 27 and Fig 28) should be small
2. There is a large difference between the effective filter shape of the OSA that we use in the experiment and that we assume in the simulation. The real shape of the effective filter of the OSA is not a simple Gaussian function. Following figure is extracted from the data sheet of the OSA that we use and used to explain the dynamic range performance of the OSA.

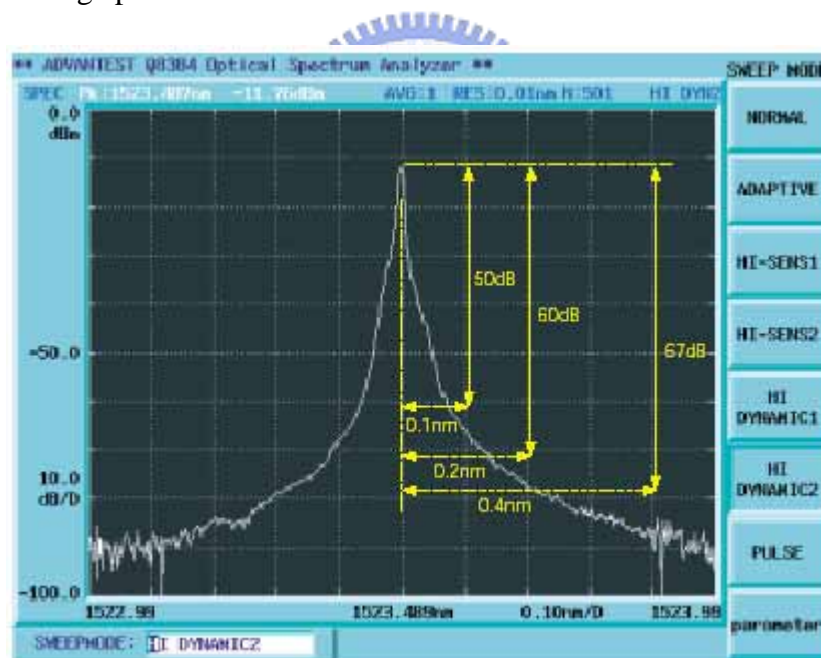


Fig 42 dynamic range of OSA

This figure tells us that the filter is not as sharp as our assumption. The 60dB dynamic range is achieved in the region outside the center of the filter around 0.2nm. Thus, we will find that the experimental result can not perform the sharp and deep valleys as that in simulation, which is performed in Fig 41. Furthermore,

we can expect that the difference between simulation and experiment will be greatly improved in the observation of 40GHz sinusoidal signal, because the wider intervals between the peaks in the spectrum (or valleys) reduce the requirement for sharp filter.

Then let's see the case of measurement of 40GHz sinusoidal:

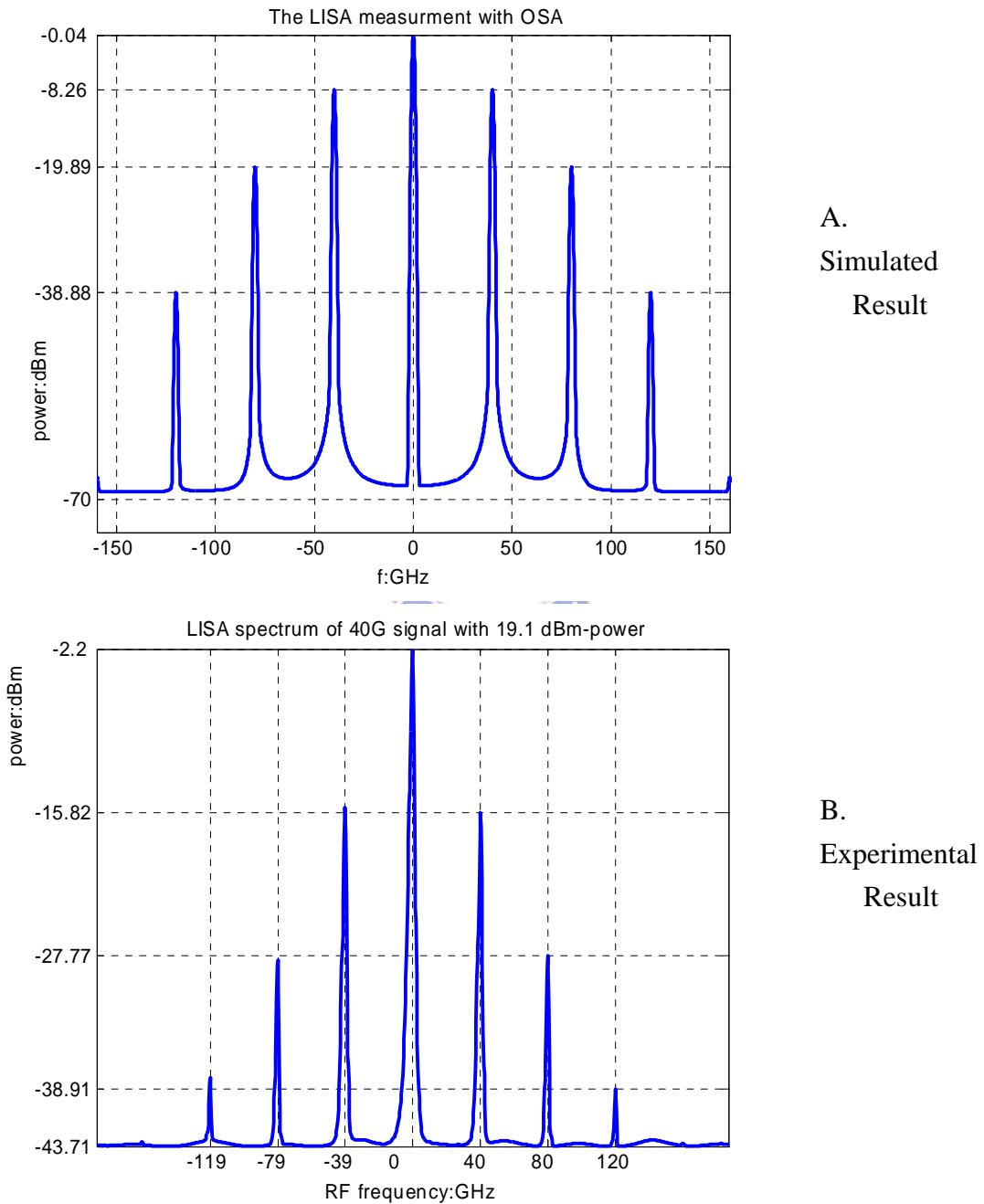


Fig 43 Optical spectrums of reference light for 40GHz sinusoidal signal with signal input power of 14.7dBm

It is as our expectation that the shape of simulated result is more similar to that of experimental result, but the bottom of the experimental result is higher than that of simulation, which should be originated from the removing of the filter in signal arm.



Chapter Four the performance of the optical RF spectrum analyzer

4-1 The bandwidth performance and optimization

There are two schemes that limit the bandwidth of the nonlinear intensity to field conversion (NLIFC) [3], so they also limit the bandwidth of the optical RF spectrum analyzer based on NLIFC that we performed: the response of the nonlinear interaction and the phase matching consideration.

1. Response of the nonlinear interaction

The nonlinear material and the nonlinear interaction used in the NLIFC limit the bandwidth of NLIFC, which is discussed by the Dr. C. Dorrer and Dr. D. N. Maywar. They take an example: if the NLIFC is based on the nonlinearity exhibited in the electronic transition between conduction and valance band in SOA, the NLIFC has bandwidth limitation about 10GHz due to the response time of the nonlinear interaction of SOA.

Fortunately, the NLIFC in our experiment is based on the intensity-dependent refractive index in nonlinear fiber, which has bandwidth larger than 10THz, so this factor is not dominated.

2. Phase matching consideration

Phase matching consideration is an important factor for utilizing the nonlinear optical effects. It is due to the different group velocities of waves at different frequency (dispersion). And, the efficiency of nonlinear interaction will decrease, when the phase mismatching between interacting waves get serious.

The phase matching is the dominate factor that limiting the bandwidth of our

optical RF spectrum analyzer.

Following we will consider how to achieve the maximum bandwidth through the arrangement of the wavelength of the source wave and reference wave and the maximum bandwidth of the optical RF spectrum analyzer.

4-1-1: The model considering the group delay between signal and reference waves

The analytical discussion of the effect of phase matching on the nonlinear intensity to field conversion follows the analysis of Dr. C. Dorrer and Dr. D. N. Maywar in 2004 [3]. Assume the group velocity of the source wave, the wave under test equals to V_s ; and that of the reference wave equals to V_0 . Because of the finite difference between V_s and V_0 , the source wave propagating at some position x in the fiber at time t no more modulates the reference wave propagating at (x, t) . The reference wave propagating at (x, t) is modulate by the source wave propagating at $(x, t - \frac{x}{V_s} - \frac{x}{V_0})$, as the following sketch map.

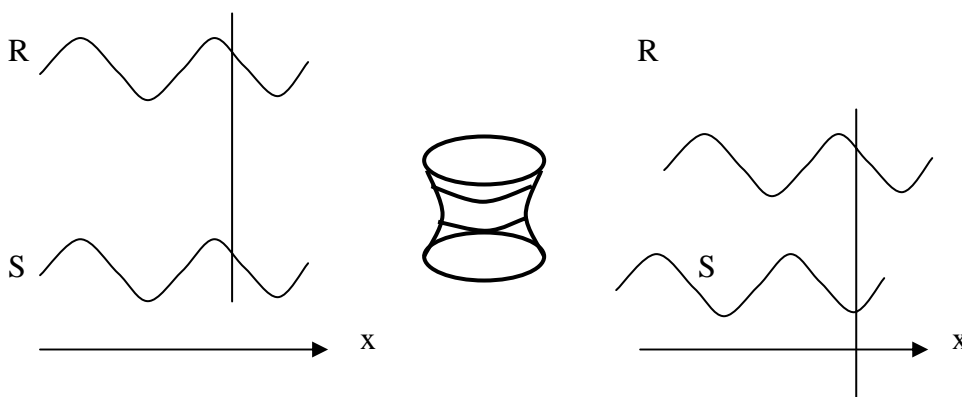


Fig 44 Sketch map of phase mismatching,

“R” represents the reference wave

“S” represents the signal waves

Therefore the original equation describing the field of the modulated reference light, eq. (2-7) is modified as:

$$E'(t) = A \exp[-i2\pi f_0 t] \bullet \exp\left[m \int_0^L I\left(t - \frac{x}{V_s} - \frac{x}{V_0}\right) \frac{dx}{L}\right]$$

$$E'(t) = A \exp[-i2\pi f_0 t] \bullet \exp\left[m \int_0^L I\left(t - \frac{x}{V}\right) \frac{dx}{L}\right] \dots \text{eq. (4-1)}$$

$$\text{, where } V = (1/V_s - 1/V_0)^{-1} \dots \text{eq. (4-2)}$$

From eq. (4-1) we can derive the optical spectrum of the modulated reference light:

$$I'_{optical}(f) \propto \delta(f - f_0) + |m|^2 S(f - f_0) \text{sinc}^2\left(\frac{L(f - f_0)}{V}\right) \dots \text{eq. (4-3)}$$

$$I'_{optical}(f) \propto \delta(f - f_0) + |m|^2 S(f - f_0) \text{sinc}^2(GD(f - f_0)) \dots \text{eq. (4-4)}$$

, where $GD = \frac{L}{V}$, the Group delays between the reference and source waves. Compare eq. (4-4) with eq. (2-9), we have an additional term that is the bandwidth reduction function due to the phase mismatching between the signal and reference waves:

$$R(f - f_0) = \text{sinc}^2(GD \bullet (f - f_0)) \dots \text{eq. (4-5)}$$

Then following is the derivation of the optical spectrum of the modulated reference light with reduction function.

(Derivation)

$$E'(t) = A e^{-i2\pi f_0 t} \times e^{m \int_0^L I\left(t - \frac{x}{V}\right) \frac{dx}{L}}$$

$$E'(t) \cong A e^{-i2\pi f_0 t} \times \left(1 + m \int_0^L I\left(t - \frac{x}{V}\right) \frac{dx}{L}\right)$$

$$I'(f) = \left| \int E'(t) e^{i2\pi f t} dt \right|^2 = A^2 \left| \int \left(1 + m \int_0^L I\left(t - \frac{x}{V}\right) \frac{dx}{L}\right) e^{i2\pi(f - f_0)t} dt \right|^2$$

$$I_{optical}(f) \propto \delta(f - f_0) + |m|^2 \left| F \left\{ \int_0^L I\left(t - \frac{x}{V}\right) \frac{dx}{L} \times e^{i2\pi(f-f_0)t} \right\} \right|^2$$

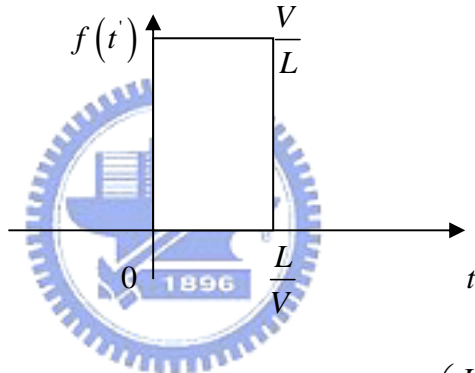
$$I_{optical}(f) \propto \delta(f - f_0) + |m|^2 \left| F \left\{ \int_0^L I\left(t - \frac{x}{V}\right) \frac{dx}{L} \right\} \otimes \delta(f - f_0) \right|^2$$

Let's calculate the Fourier transform of $\int_0^L I\left(t - \frac{x}{V}\right) \frac{dx}{L}$ first:

$$\int_0^L I\left(t - \frac{x}{V}\right) \frac{dx}{L} = \int_0^{\frac{L}{V}} I(t-t') \frac{V}{L} dt'$$

$$\text{, where } t' = \frac{x}{V}$$

Define $f(t')$ as:



The Fourier transform of $f(t')$: $F\{f(t')\} = \text{sinc}\left(\frac{L}{V}f\right) e^{i\left(-\frac{L}{2V}2\pi f\right)}$

$$\text{Thus } \int_0^L I\left(t - \frac{x}{V}\right) \frac{dx}{L} = \int_0^{\frac{L}{V}} I(t-t') \frac{V}{L} dt' = \int_{-\infty}^{\infty} I(t-t') f(t') dt'$$

Using the theorem: $F\left\{ \int_{-\infty}^{\infty} x_1(t-t') x_2(t') dt' \right\} = X_1(f) X_2(f)$

$$\text{Thus } F\left\{ \int_0^L I\left(t - \frac{x}{V}\right) \frac{dx}{L} \right\} = F\left\{ \int_{-\infty}^{\infty} I(t-t') f(t') dt' \right\} = I(f) \text{sinc}\left(\frac{L}{V}f\right) e^{i\left(-\frac{L}{2V}2\pi f\right)}$$

$$\text{So, } I_{optical}(f) \propto \delta(f - f_0) + |m|^2 \left| I(f - f_0) \text{sinc}\left(\frac{L}{V}(f - f_0)\right) e^{i\left(-\frac{L}{2V}2\pi(f-f_0)\right)} \right|^2$$

$$I_{optical}(f) \propto \delta(f - f_0) + |m|^2 S(f - f_0) \sin^2 \left(\frac{L(f - f_0)}{V} \right)$$

, where $S(f - f_0) = I_{RF}(f)|_{f_0}$ in eq. (2-9) is the RF spectrum of the signal under test.

We can have some discussions about the bandwidth reduction with on this simple model—eq. (4-4) and eq. (4-5), which assumes that:

1. The signal and reference light are both monochromatic.
2. Therefore the phase matching is caused by the relative group delay (GD) between signal and reference lights only, and the GD is constant throughout the range of measurement.

Following figure shows the bandwidth reduction function due to the phase mismatching at various GD values. Note that the wavelength of reference light is assumed at 1554 nm.

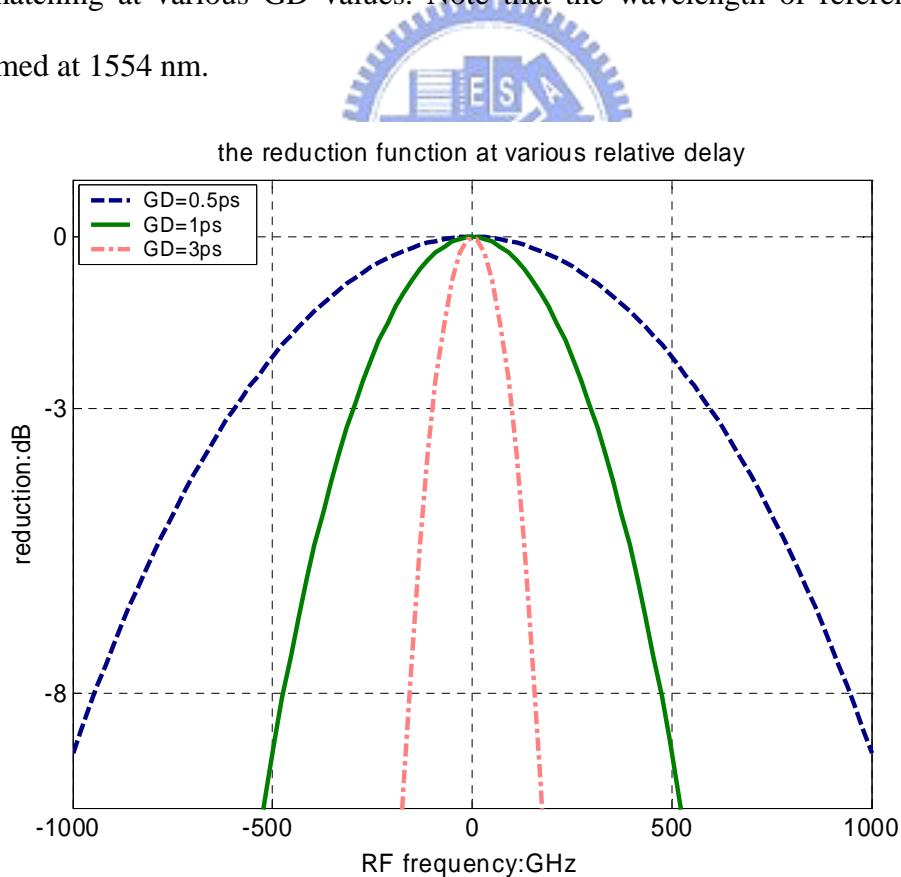


Fig 45 bandwidth reduction function

In figure 45, we know that the 3-dB bandwidth larger than 500 GHz is obtained in the case of $GD < 0.5\text{ps}$, which is not always satisfied. Thus to maximize the bandwidth, we need to minimize the GD.

But, GD is dependent on the dispersion properties of the HNLFF that we use and the arrangement of the reference and signal lights. To search the best arrangement for maximizing the bandwidth of optical RF spectrum analyzer, we can express GD with the propagation constant, β .

$$GD = \frac{L}{V} = L(1/V_S - 1/V_0)$$

$$V_{group} = \frac{\partial \omega}{\partial \beta} \quad , \quad \frac{1}{V_{group}} = \frac{\partial \beta}{\partial \omega}$$

So, we have: $GD = \frac{L}{V} = L \left(\left. \frac{\partial \beta}{\partial \omega} \right|_{\omega_S} - \left. \frac{\partial \beta}{\partial \omega} \right|_{\omega_0} \right) \dots \text{eq. (4-6)}$

Then with the Taylor series expansion of β :

$$\beta(\omega) = \beta_0 + \beta_1(\omega - \omega_{center}) + \frac{1}{2}\beta_2(\omega - \omega_{center})^2 + \frac{1}{6}\beta_3(\omega - \omega_{center})^3 + \dots \dots \text{eq. (4-7)}$$

, where $\beta_m = \left(\frac{d^m \beta}{d\omega^m} \right)_{\omega=\omega_{center}} \dots \text{eq. (4-8)}$

, and $\frac{\partial \beta}{\partial \omega}(\omega) = \beta_1 + \beta_2(\omega - \omega_{center}) + \frac{1}{2}\beta_3(\omega - \omega_{center})^2 + \dots \dots \text{eq. (4-9)}$

We can have the following representation of GD:

$$GD = L \left[\left(\beta_1 + \beta_2(\omega_S - \omega_{center}) + \frac{1}{2}\beta_3(\omega_S - \omega_{center})^2 + \dots \right) - \left(\beta_1 + \beta_2(\omega_0 - \omega_{center}) + \frac{1}{2}\beta_3(\omega_0 - \omega_{center})^2 + \dots \right) \right]$$

$$GD = L \left[\underbrace{\beta_2(\omega_S - \omega_0)}_{\text{linear term}} + \underbrace{\frac{1}{2}\beta_3 \left((\omega_S - \omega_{center})^2 - (\omega_0 - \omega_{center})^2 \right)}_{\text{higher order term}} + \dots \right] \dots \text{eq. (4-10)}$$

And, the following figure 46 shows the relation between the relative β_1 and the optical frequency of our HNLFF and that between the β_2 and the optical frequency. The

two dashed lines are translated from those in Fig 23 directly, and the solid line in first figure is a 2nd order poly-fit of its dashed line. And, the solid line in the second figure is derived from the 2nd order fitting function in the first figure.

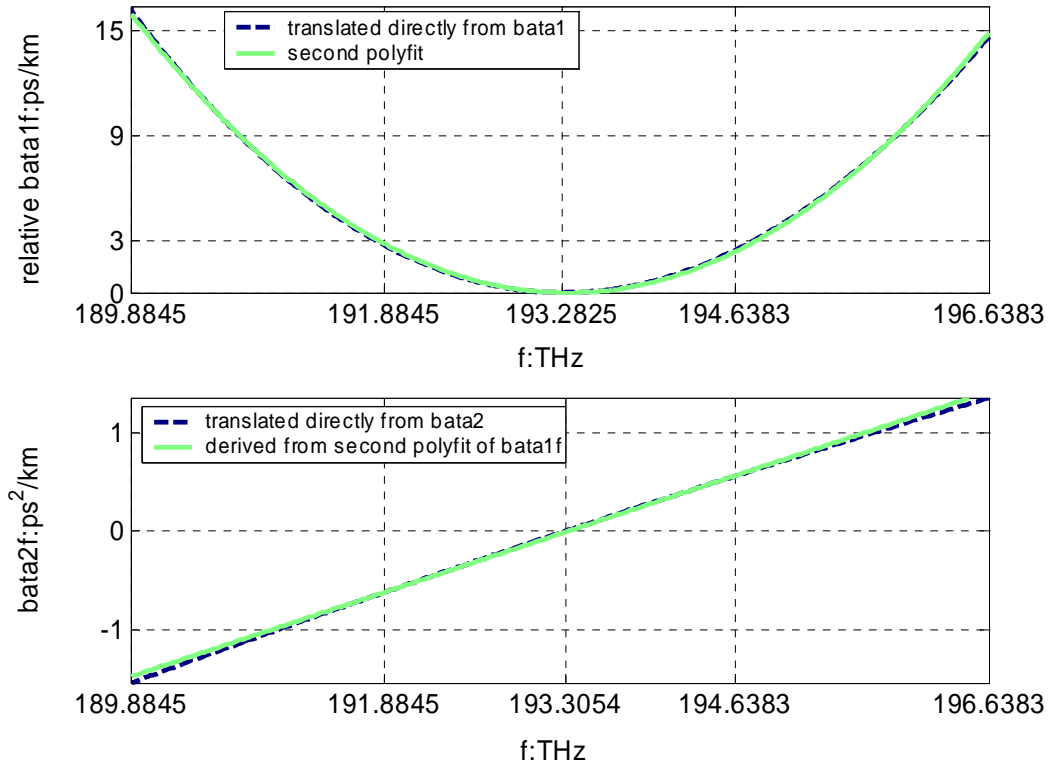


Fig 46 β_1 and β_2 of the Corning HNLF

From Fig 46 we know that:

1. The relation between GD and optical frequency, ω (or f) is a 2nd order polynomial function around λ_0 .
2. The relation between GD and optical frequency could be approximated as a linear function in the region far from λ_0 .

Thus the further discussion is divided into two parts—operated in the region far from λ_0 and around λ_0 :

Linear GD region

Neglect the higher order terms, the eq. (4-10) becomes:

$$GD = L\beta_2(\omega_s - \omega_0) \dots \text{eq. (4-11)}$$

Because GD is assumed to be linear to the optical frequency, we have a constant β_2 . And, the bandwidth is able to be estimated using the eq. (4-5) and eq. (4-11) with given β_2 as the following figure, which has well consistence with the experimental justification of Dorrer and Maywar [3].

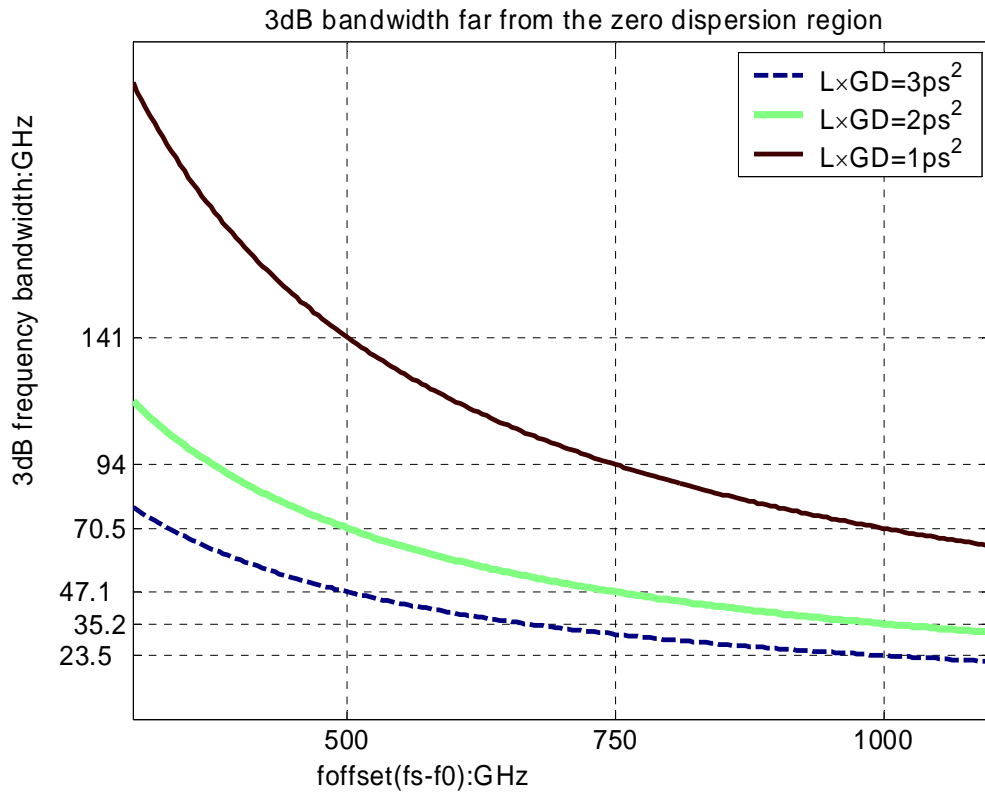


Fig 47 3dB bandwidth versus the separation between signal and reference laser at various L-GD production

The bandwidth is determined by the L-GD product and the separation between signal and reference laser, and is still very restricted. And, refer to the eq. (4-5) and

eq. (4-11), we know that the bandwidth is larger when the GD is smaller, but the minimum value of GD occurs at the condition $f_s = f_0$, which violates the requirement in the application of wide-bandwidth optical RF spectrum analyzer. Thus we don't operate in the linear GD region.

2nd order polynomial GD region

We will prove that the best and reasonable arrangement is to arrange the signal and reference laser around λ_0 symmetrically from as following derivation:

$$GD = L \left(\beta_2 (\omega_s - \omega_0) + \frac{1}{2} \beta_3 \left[(\omega_s - \omega_{center})^2 - (\omega_0 - \omega_{center})^2 \right] \right)$$

$$GD = L \left(\beta_2 (\omega_s - \omega_0) + \frac{1}{2} \beta_3 (\omega_s + \omega_0 - 2\omega_{center}) (\omega_s - \omega_0) \right)$$

Because we operate around the zeros dispersion wavelength, the $\beta_2 \sim 0$ and the

$\omega_{center} = \omega_{fiber-zero}$:

$$GD = \frac{L}{2} \beta_3 (\omega_s + \omega_0 - 2\omega_{fiber-zero}) (\omega_s - \omega_0)$$

$$GD = \frac{L}{2} \beta_3 \left((\omega_s - \omega_{fiber-zero}) - (\omega_{fiber-zero} - \omega_0) \right) (\omega_s - \omega_0) \dots \text{eq. (4-12)}$$

Thus the minimum value of GD is obtained at $\omega_s - \omega_{fiber-zero} = \omega_{fiber-zero} - \omega_0$, which means that the reference and signal laser is around λ_0 symmetrically.

4-1-2: The model considering the group delay inside the signal wave

In the previous discussion, we have known how to achieve the largest bandwidth of the optical RF spectrum analyzer, but we still have no idea about the bandwidth achievable in this arrangement.

Furthermore, the signal wave is not a chromatic wave but have a finite spectrum.

Thus the GD is no more a constant at every frequency components within the measurement span, and the phase mismatching inside the signal itself is needed to be considered. Therefore we have the following model considering the phase mismatching inside the signal itself and predict the bandwidth of the optical RF spectrum analyzer operated in the best arrangement. And, we also have some experimental results to justify this model.

Four-waves mixing model

The discussion in the previous section is based on the assumption that the signal is viewed as a chromatic wave and the four-waves mixing process is degraded to an interaction of the intensity of the source wave and the electric field of the reference wave. Therefore it only consider the phase-mismatching between the reference and signal lights.

But, the phase-mismatching between reference and signal lights is small in the best arrangement and the signal also has large bandwidth, so the previous model should be modified now.

Following figure explain the model that we consider now.

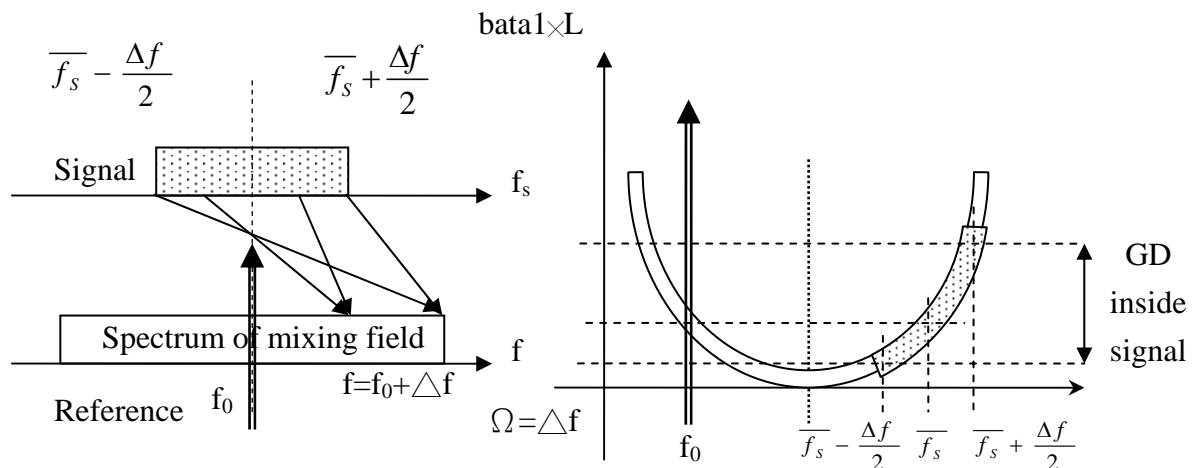


Fig 48 Sketch map of the model considering the phase mismatching inside signal

This model takes the target electric field that we measured around f_0 as the mixing of three original electric fields— $f_0 + f_s - f_s$. Furthermore, the spectrum of the reference light after HNLF at $(f_0 + \Delta f)$ is produced by the mixing of signal lights at $\bar{f}_s \pm \frac{\Delta f}{2}$ and reference light, so we can expect that the reduction due to phase mismatching is more serious in the edge of the spectrum that we measured. It is because that the GD inside the signal, GD_2 corresponding to the edge spectrum is larger.

In the figure 48, the thick lines represent the reference light before HNLF and the blocks with dots mean the signal with finite bandwidth. After the NLIFC that we expect, the reference light has an optical spectrum that is represented by the block without dots.

Because we use a lot of symbols in the previous description, we explain them with the following table.

Symbols	f	f_0	f_s	\bar{f}_s	Ω
Meaning	Span of measurement in optical frequency around f_0	Frequency of the reference light	Frequency span of the signal light	Central frequency of the signal light	Span of measurement in RF frequency
Range	$[f_0 - \Delta f, f_0 + \Delta f]$		$[\bar{f}_s - \frac{\Delta f}{2}, \bar{f}_s + \frac{\Delta f}{2}]$		$[-\Delta f, \Delta f]$

Table 10 some symbols used in this model

As the eq. (4-1): $E'(t) = A \exp[-i2\pi f_0 t] \bullet \exp[m \int_0^L I \left(t - \frac{x_1}{V_1} \right) \frac{dx_1}{L}]$. showing the effect of the phase mismatching between the intensity of the source field and the reference wave on the modulation process, we suggest that the effect of the phase

mismatching between the two waves around the $\overline{f_s}$ in the process forming $I(t)$ as:

$$I(t) = \int_0^L E\left(t + \frac{x_2}{2V_2}\right) E^*\left(t - \frac{x_2}{2V_2}\right) \frac{dx_2}{L} \dots \text{eq. (4-13)}$$

$$\text{, where } V_2 = \left(1/V_{f_s + \frac{\Delta f}{2}} - 1/V_{f_s - \frac{\Delta f}{2}}\right)^{-1} \dots \text{eq. (4-14)}$$

Thus the eq.(4-1) should be modified as:

$$E'(t) = A \exp[-i2\pi f_0 t] \bullet \exp\left[m \int_0^L \int_0^L E\left(t - \frac{x_2}{V_1} + \frac{x_2}{2V_2}\right) E^*\left(t - \frac{x_2}{V_1} - \frac{x_2}{2V_2}\right) \frac{dx_2}{L} \frac{dx_1}{L}\right].$$

...eq. (4-14)

, where V_1 and V_2 are corresponding to these two kinds of phase mismatching respectively.

Because we have arranged the source wave and the reference wave at the best condition, the V_1 are assumed to be infinite. (The phase mismatching between the intensity and reference wave is neglected.) Thus the eq. (4-14) can be rewritten as:

$$E'(t) = A \exp[-i2\pi f_0 t] \bullet \exp\left[m \int_0^L E\left(t + \frac{x_2}{2V_2}\right) E^*\left(t - \frac{x_2}{2V_2}\right) \frac{dx_2}{L}\right]. \dots \text{eq. (4-15)}$$

Before derivation of the power spectrum of $E'(t)$ from the eq. (4-15), there is one important condition needed to be considered:

Because $I(t)$ is real and $I(t) = \int_0^L E\left(t + \frac{x_2}{2V_2}\right) E^*\left(t - \frac{x_2}{2V_2}\right) \frac{dx_2}{L}$

$$\text{, } E\left(t + \frac{x_2}{2V_2}\right) E^*\left(t - \frac{x_2}{2V_2}\right) \text{ is also real.}$$

To satisfy the requirement, we have the condition that:

$$E\left(t + \frac{x_2}{2V_2}\right) = E\left(t - \frac{x_2}{2V_2}\right) \dots \text{eq. (4-16)}$$

Then let's calculate the power spectrum of $E'(t)$ starting from the eq. (4-15) and

eq. (4-16):

$$E'(t) = A \exp[-i2\pi f_0 t] \bullet \exp\left[m \int_0^L E\left(t - \frac{x_2}{2V_2}\right) E^*\left(t - \frac{x_2}{2V_2}\right) \frac{dx_2}{L}\right].$$

$$E'(t) = A \exp[-i2\pi f_0 t] \bullet \exp\left[m \int_0^L I\left(t - \frac{x_2}{2V_2}\right) \frac{dx_2}{L}\right]$$

$$E'(t) \cong A \exp[-i2\pi f_0 t] \bullet \left[1 + m \int_0^L I\left(t - \frac{x_2}{2V_2}\right) \frac{dx_2}{L}\right]$$

Let $t' = \frac{x_2}{2V_2}$, then $E'(t) \cong A \exp[-i2\pi f_0 t] \bullet \left[1 + m \int_0^{\frac{L}{2V_2}} I(t-t') \left(\frac{2V_2}{L}\right) dt'\right] \dots \text{eq. (4-17)}$

Thus $I'(f) = \left| \int E'(t) e^{i2\pi f t} dt \right|^2 = A^2 \left| \int \left[1 + m \int_0^{\frac{L}{2V_2}} I(t-t') \frac{2V_2}{L} dt'\right] e^{i2\pi(f-f_0)t} dt \right|^2$

$$I'(f) \propto \delta(f - f_0) + |m|^2 \left| F \left\{ \int_0^{\frac{L}{2V_2}} I(t-t') \frac{2V_2}{L} dt' \times e^{i2\pi(f-f_0)t} \right\} \right|^2$$

$$= \delta(f - f_0) + |m|^2 \left| F \left\{ \int_0^{\frac{L}{2V_2}} I(t-t') \frac{2V_2}{L} dt' \right\} \otimes \delta(f - f_0) \right|^2$$

$$= \delta(f - f_0) + |m|^2 \left| \left\{ I(f) \text{sinc}\left(\frac{L}{2V_2} f\right) e^{i\left(-\frac{L}{2 \times 2V} 2\pi f\right)} \right\} \otimes \delta(f - f_0) \right|^2$$

$$I'(f) \propto \delta(f - f_0) + |m|^2 \left| \left\{ I(f - f_0) \text{sinc}\left(\frac{L}{2V_2}(f - f_0)\right) e^{i\left(-\frac{L}{2 \times 2V} 2\pi(f - f_0)\right)} \right\} \right|^2$$

Thus we have:

$$I'(f) \propto \delta(f - f_0) + |m|^2 S(f - f_0) \text{sinc}^2\left(\frac{L}{2V_2}(f - f_0)\right) \dots \text{eq. (4-18)}$$

And, we can define the reduction function originated from the phase mismatching

between the two waves around the ω_0 in the process forming $I(t)$ at the best operation condition (neglect V_1):

$$R(f - f_0) = \text{sinc}^2\left(\frac{GD_2(f) \cdot (f - f_0)}{2}\right) \dots \text{eq. (4-19)}$$

$$\text{, where } GD_2 = \frac{L}{V_2} \dots \text{eq. (4-20)}$$

Note that GD_2 is a function of f . Furthermore, in the following simulation about the bandwidth based on this modified model, the determination of GD is referred to the solid curve in the first figure in Fig 46.

Simulation results

The following figures show the simulated bandwidth reduction based on this model corresponding to part of the experimental results that are shown later.

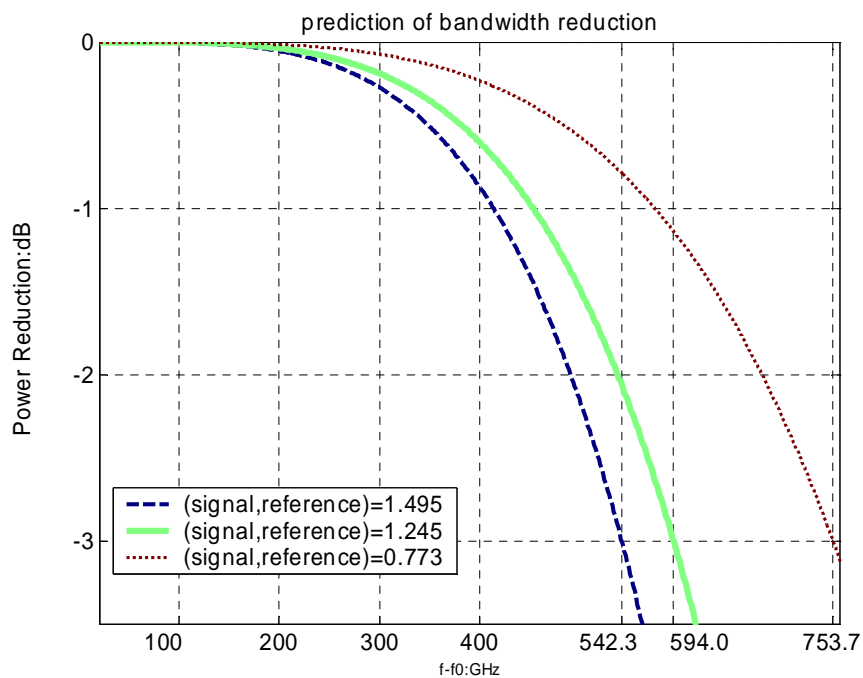


Fig 49 the simulated bandwidth reduction operated at best arrangement based on the modified model

In figure 49, we can find that the bandwidth is still decreased with the increasing of the separation of signal and reference light but is indeed increased by almost one order—the largest bandwidth is closed to 800GHz. We see it more specifically in the following figure that shows the relation between the available bandwidth and the separation between signal and reference light.

Although this simulation results agree with the result from experiment that we will show later, it doesn't involve the spectral extent and the signal overlapping, which reduce the useful bandwidth in practical measurement.

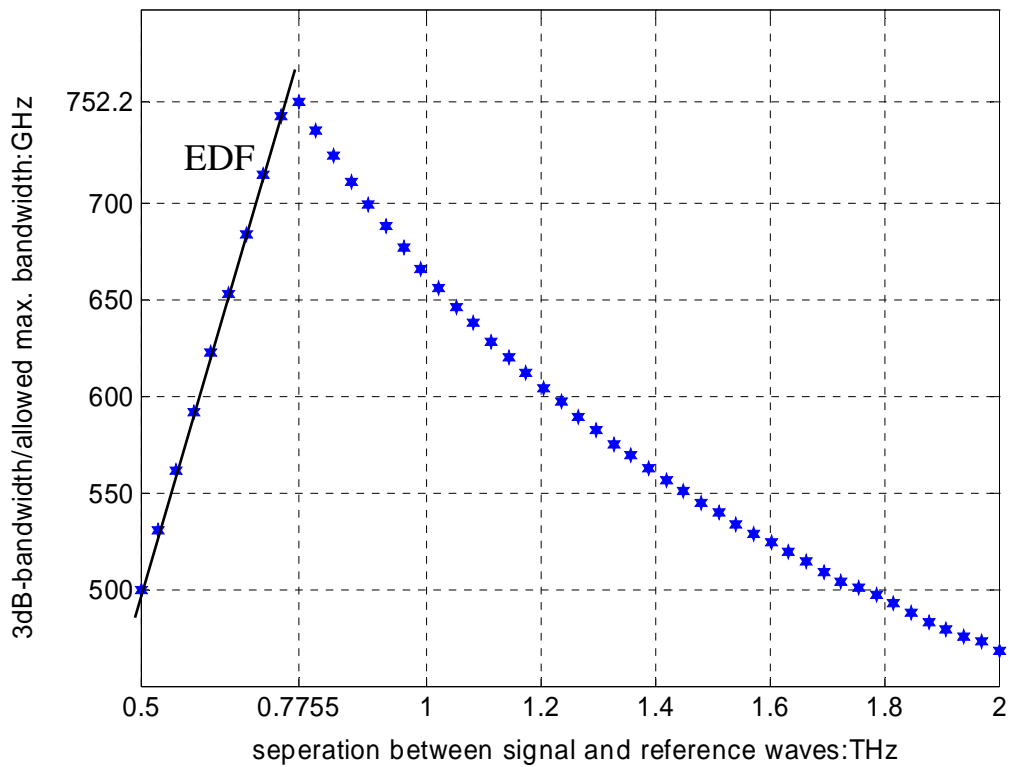


Fig 50 3dB-bandwidth versus the separation between signal and reference lights

Thus we consider the spectral extent and signal overlapping before justifying the previous simulated results with experiments.

Spectral extend and signal overlapping

In Fig 50, the points with separation smaller than 0.7755THz match the line with $\text{slop}=1$. It is because that we assume the bandwidth within the separation between signal and reference lights to avoid the overlapping between the measured RF spectrum and the signal wave. But, this assumption is still too ideal. In fact, the two fields will generate six new fields in four different frequencies (the nonlinear intensity to field conversion that we use is one of them), so we need to consider these useless fields when we estimate the available bandwidth for our optical RF spectrum analyzer.

The following figure explains the additional fields generated and resulting spectral extending after the high nonlinear fiber.

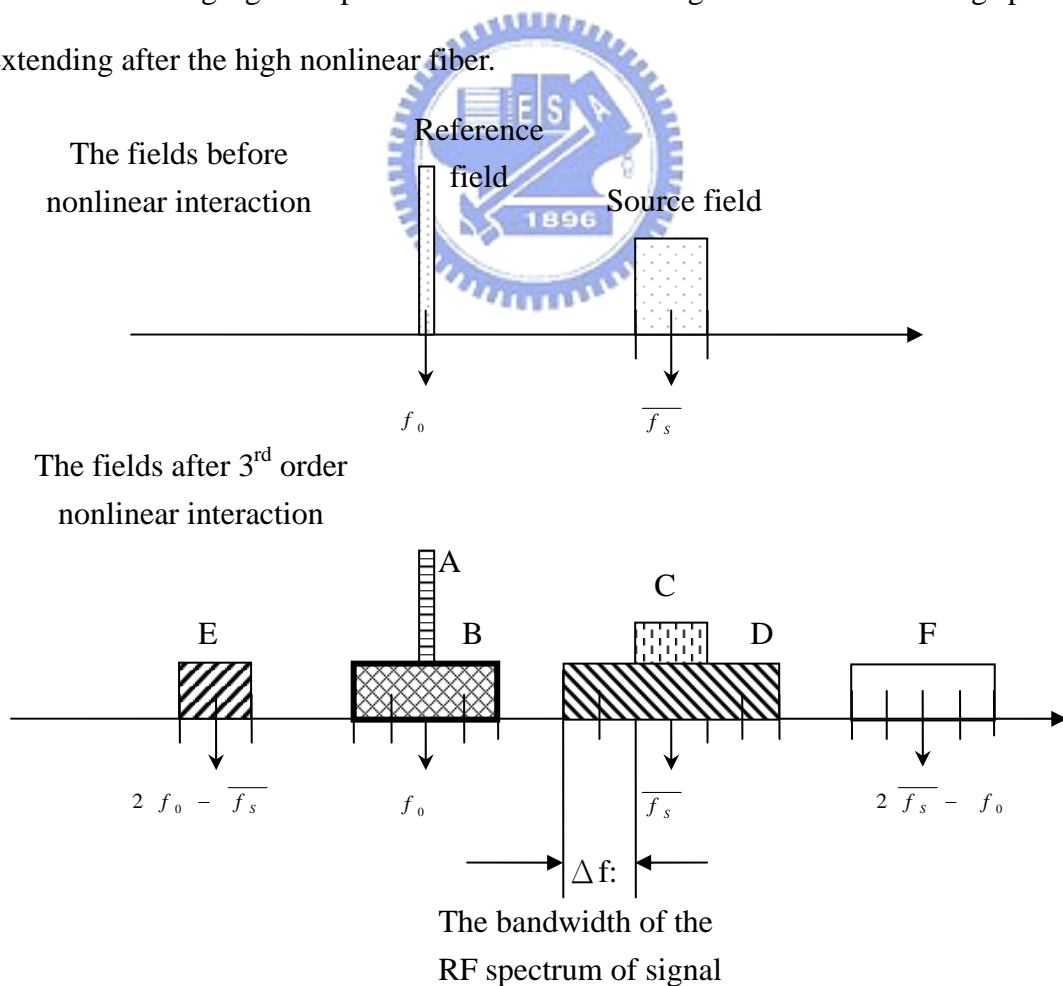


Fig 51 the explanation of additional fields generation and the spectral extending

And, we describe these fields in the following table.

Fields	Generation	Central frequency	Width	Edge
A	$f_0 + f_0 - f_0$	f_0	0	0
B	$f_0 + f_s - f_s$	f_0	$2\Delta f$	$f_0 \pm \Delta f$
C	$f_s + f_0 - f_0$	$\overline{f_s}$	Δf	$\overline{f_s} \pm \Delta f / 2$
D	$f_s + f_s - f_s$	$\overline{f_s}$	$3\Delta f$	$\overline{f_s} \pm 3/2\Delta f$
E	$f_0 + f_0 - f_s$	$2f_0 - \overline{f_s}$	Δf	$2f_0 - \overline{f_s} \pm \Delta f / 2$
F	$f_s + f_s - f_0$	$2\overline{f_s} - f_0$	$2\Delta f$	$2\overline{f_s} - f_0 \pm \Delta f$

Table 11 the six four-waves mixing fields

In the six fields, the field 'B' is the NLIFC filed that we want to measure, and the filed 'D' and 'E' will give restrictions on the bandwidth that we can utilize for avoidance of signal overlapping.

To prevent the filed B overlapping with the field D or E, we have to satisfy two conditions:

$$1. \overline{f_s} - \frac{3}{2}\Delta f > f_0 + \Delta f \Rightarrow |\overline{f_s} - f_0| > \frac{5}{2}\Delta f \Rightarrow \Delta f < \frac{2}{5}|\overline{f_s} - f_0| \dots \text{eq. (4-21)}$$

$$2. \overline{f_s} - \overline{f_s} + \Delta f / 2 < \overline{f_s} - \Delta f \Rightarrow |\overline{f_s} - f_0| > \frac{3}{2}\Delta f \Rightarrow \Delta f < \frac{2}{3}|\overline{f_s} - f_0| \dots \text{eq. (4-22)}$$

These two conditions make the bandwidth without signal overlapping smaller than the separation between the signal center frequency and that of reference wave.

And, it is obvious that the condition 1 is stronger than the condition 2.

Following figures are the simulated bandwidth reduction involving the condition-1 (eq. (4-21)) and condition-2 (eq. (4-22)).

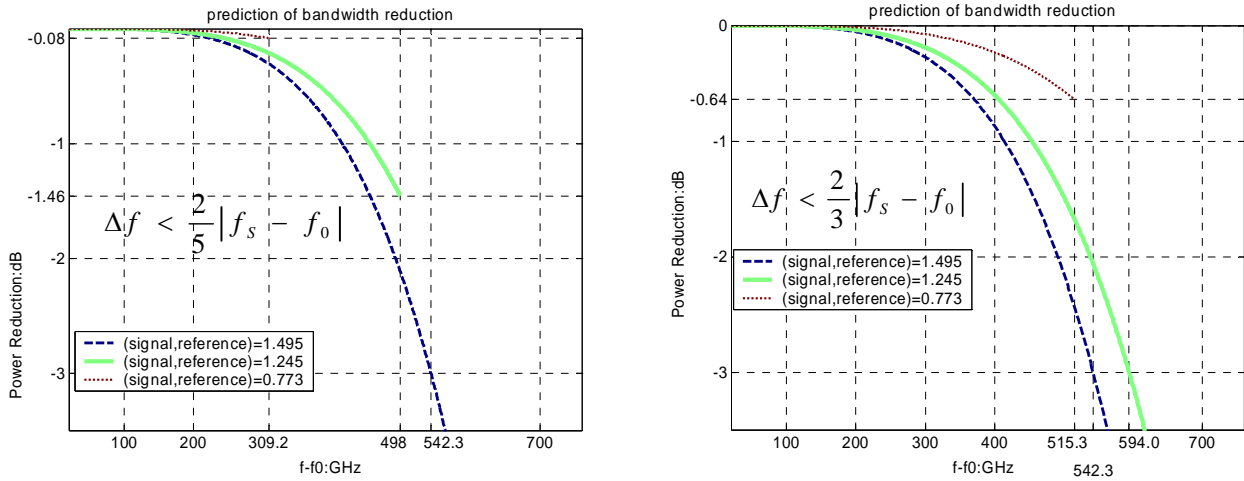


Fig 52 the simulated bandwidth reduction operated involving condition-1 and condition2

In the comparison between the Fig 49 and Fig 52, although the case of 0.773THz separation has largest bandwidth originally, it will suffer the signal overlapping when the signal bandwidth is larger than 309.2 GHz.

To have a more directly conclusion, let's see the following figure that summarizes the 3dB or maximum allowable bandwidth versus various the separations for the three different conditions.

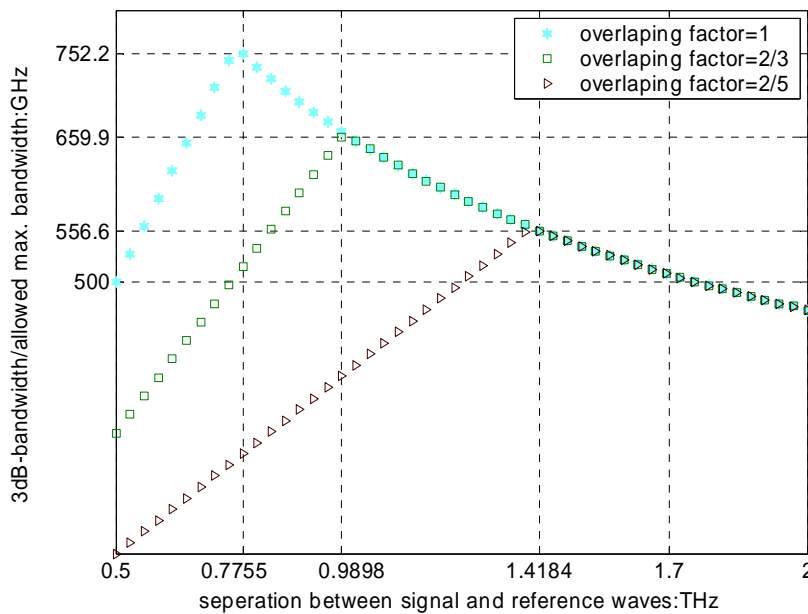


Fig 53 3dB-bandwidth versus the separation at various conditions

We can see that the maximum bandwidth is around 556.6 GHz in the case of

condition 2, in which field ‘B’ doesn’t overlap with field ‘D’ and field ‘E’.

Experimental results

Following we state the experiment that measure the allowable bandwidth of the optical RF spectrum analyzer. In this experiment, we utilize two CW lasers with a little difference in their wavelengths (or the optical frequencies) that results in a RF signal under test with tunable RF frequency to create the signal under test. For example, if the two CW lasers have a 10GHz difference in their optical frequency, we will have a 10GHz beating signal. Thus we can utilize it to measure the bandwidth of the optical RF spectrum analyzer.

Following figure shows the experiment setup. We adjust the wavelengths of the three tunable lasers satisfying the best arrangement condition and measure the bandwidth of the optical RF spectrum analyzer in various separations between signal and reference lights.

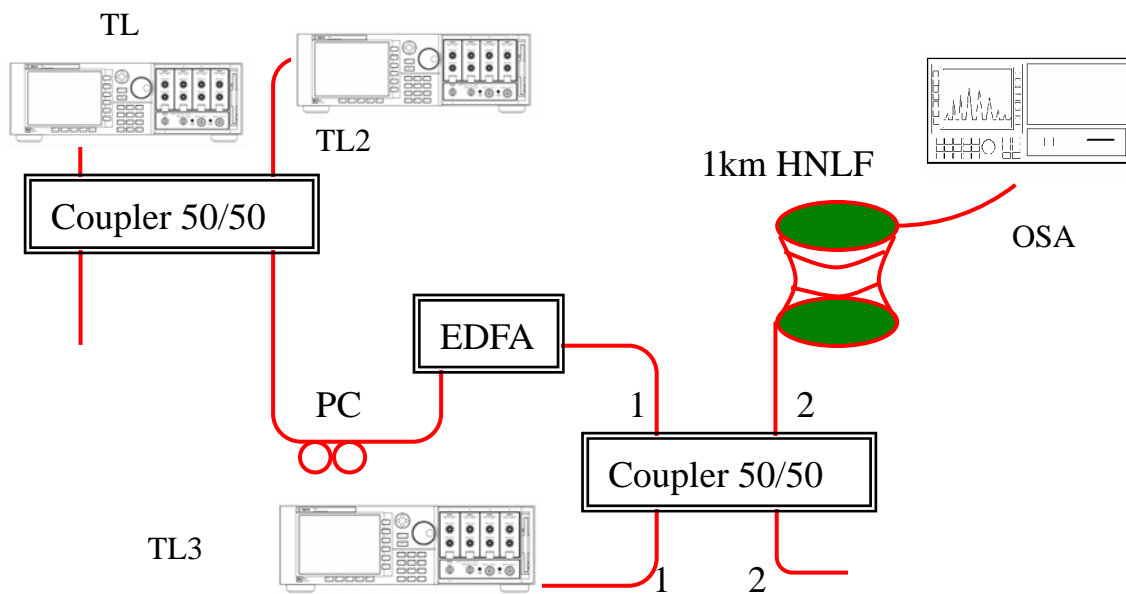


Fig 54 the experiment setup for measuring the bandwidth of the optical RF spectrum analyzer

And, following figures are the measured bandwidth reduction at three different separations. We can compare them with the previous simulated results.

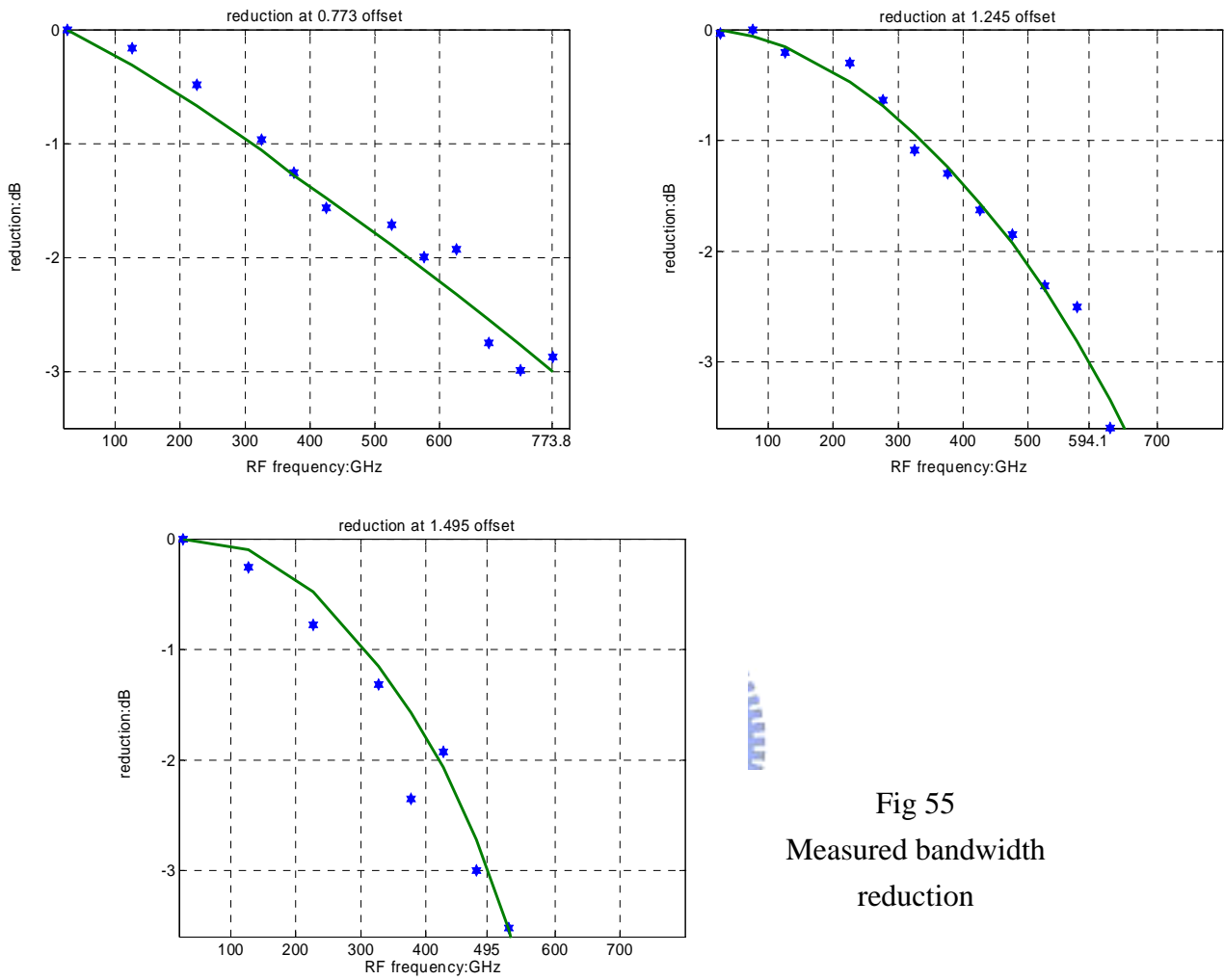


Fig 55
Measured bandwidth
reduction

And, the following figure shows the measured 3dB-bandwidth versus the separation between signal and reference lights.

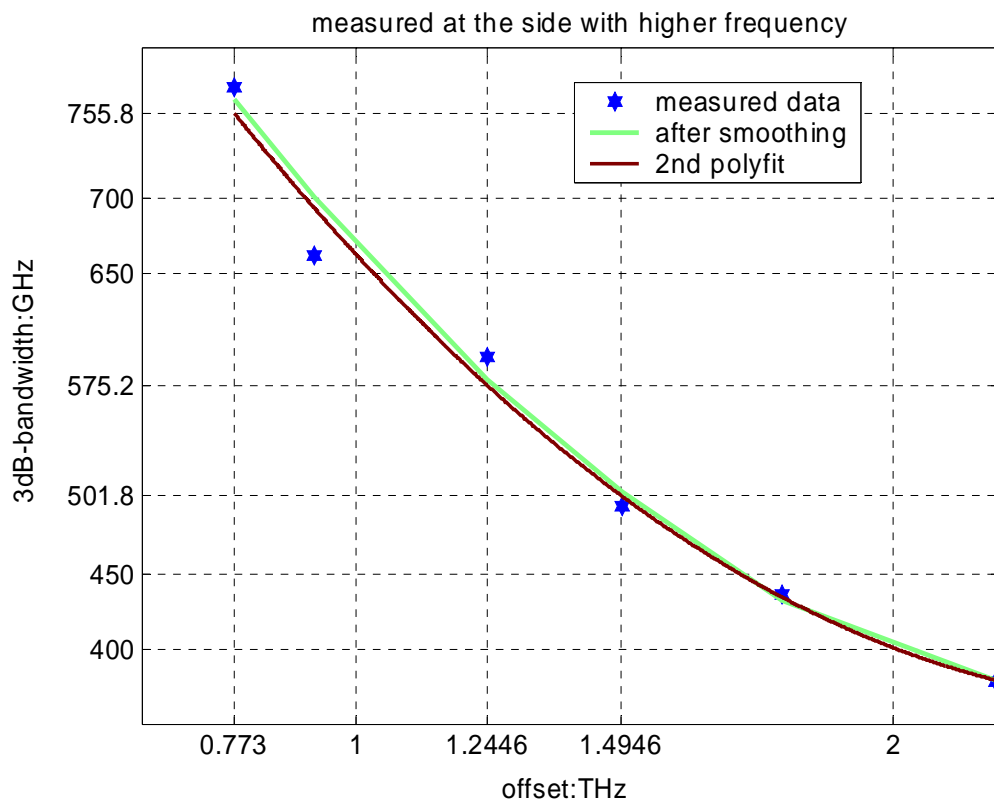


Fig 56 the measured 3dB-bandwidth versus the separation

We can compare this measured result with that from simulation (Fig 50), they are pretty similar especially in the smaller offset (the maximum 3dB bandwidth is around 750GHz), but note that the result is taken in the spectrum at higher frequency.

4-2 The resolution consideration and enhancement

Finally, we have to face the major imperfection of this approach for measuring the RF spectrum of a signal. Although the optical RF spectrum has a very largest bandwidth, its resolution performance is still too poor comparing with general RF spectrum analyzer. In the setup of Dr. Dorrer and ours, the measuring resolution is limited in the resolution of OSA, which has the resolution bandwidth around 1GHz. The resolution is not efficient for signal below 10GHz.

4-2-1: Enhancement with a mathematical deconvolution

Because the dominate restriction of the measuring resolution is the resolution of OSA measurement and we have know that the measurement process of OSA is a convolution operation, to enhance the resolution performance of this optical RF spectrum analyzer, the most directly method is to try to do the inverse operation—deconvolution.

Following is the simulation of resolution enhancement with deconvolution.

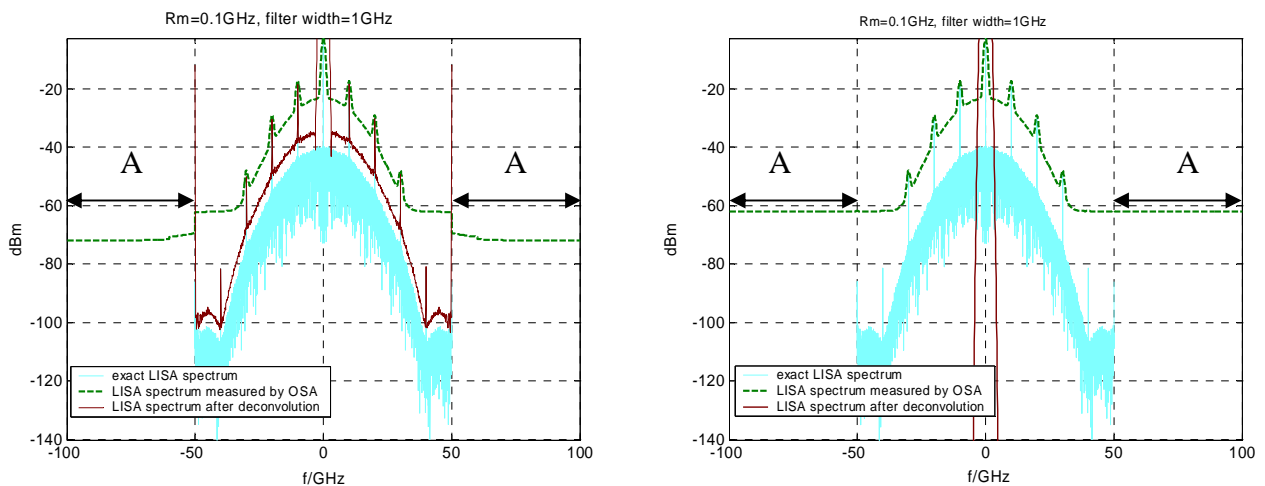


Fig 57 Simulated deconvolution result

The Fig 57 is the simulated result of deconvolution. It is obvious that the left figure can have a better resolution of measurement after the deconvolution, but the right one can not. Their difference is shown in region “A” and resulted from: in the left figure the OSA filter has a step in the edges of the filter, but that in right figure doesn’t have the step, so we can find the measured result of OSA is a continuous curve in right figure.

We can have following conclusions in this comparison:

1. This deconvolution process relies on the measured information in region “A”.
2. We don’t need the narrow bandwidth filter but need a filter with bandwidth equaling to the spectrum width.
3. The span of measurement is twice of the spectrum width of signal.

Following let’s see the simulated deconvolution result, if we use a filter with bandwidth equaling to the spectrum width of signal and cancel the forced step in the filter edge as following Fig 58.

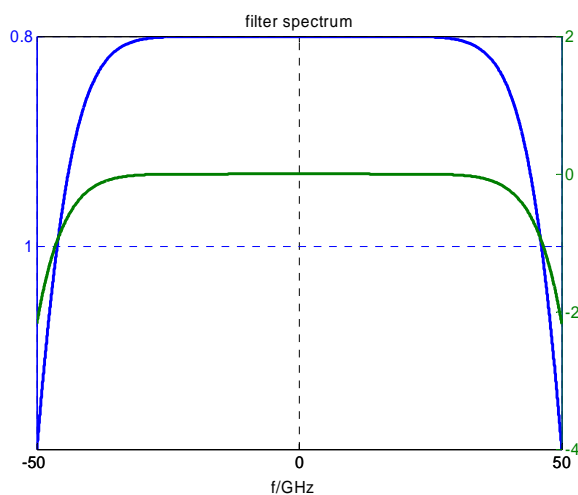


Fig 58 filter shape

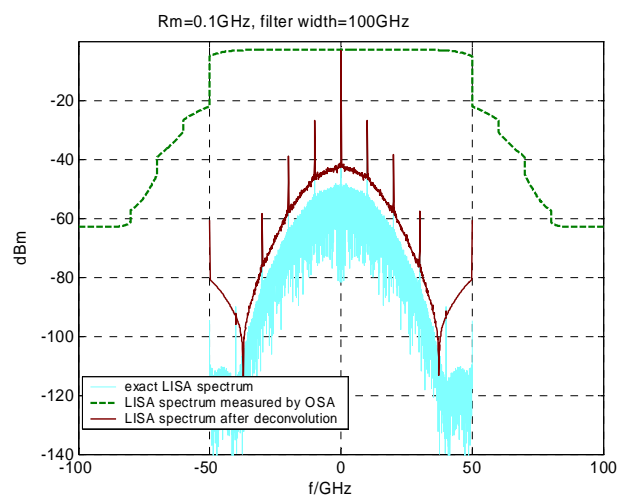


Fig 59 deconvolution result

We can see that the deconvolution indeed enhance the measuring resolution in this simulation, but the lack of wide-bandwidth OSA filter with steep edges and efficient dynamic range prevent us to put it into practice.

4-2-2: Enhancement with coherent heterodyne detection

A more practical approach for enhancing the resolution is to utilize the coherent heterodyne detection and scan the whole optical spectrum of reference light after HNLF step by step.

We can follow the ordinary coherent heterodyne technique that employs a suitable optical filter, fast photo detector and an electrical RF spectrum analyzer. This approach is explained in following diagram. The reference light after HNLF is passing through an optical filter with 3GHz width. This part of spectrum is combined with a local oscillator (LO) laser, and the separation between the center frequency the LO laser and that of the optical filter is 8GHz. And, we can measure this part of optical spectrum of reference light at around 8GHz in the electrical RF spectrum analyzer.

This approach can let us have much better measuring resolution, which is restricted on the spectrum of LO laser and the resolution of ESA, but it also relies an optical filter with sufficient dynamic range to have a correct heterodyne detection measurement.

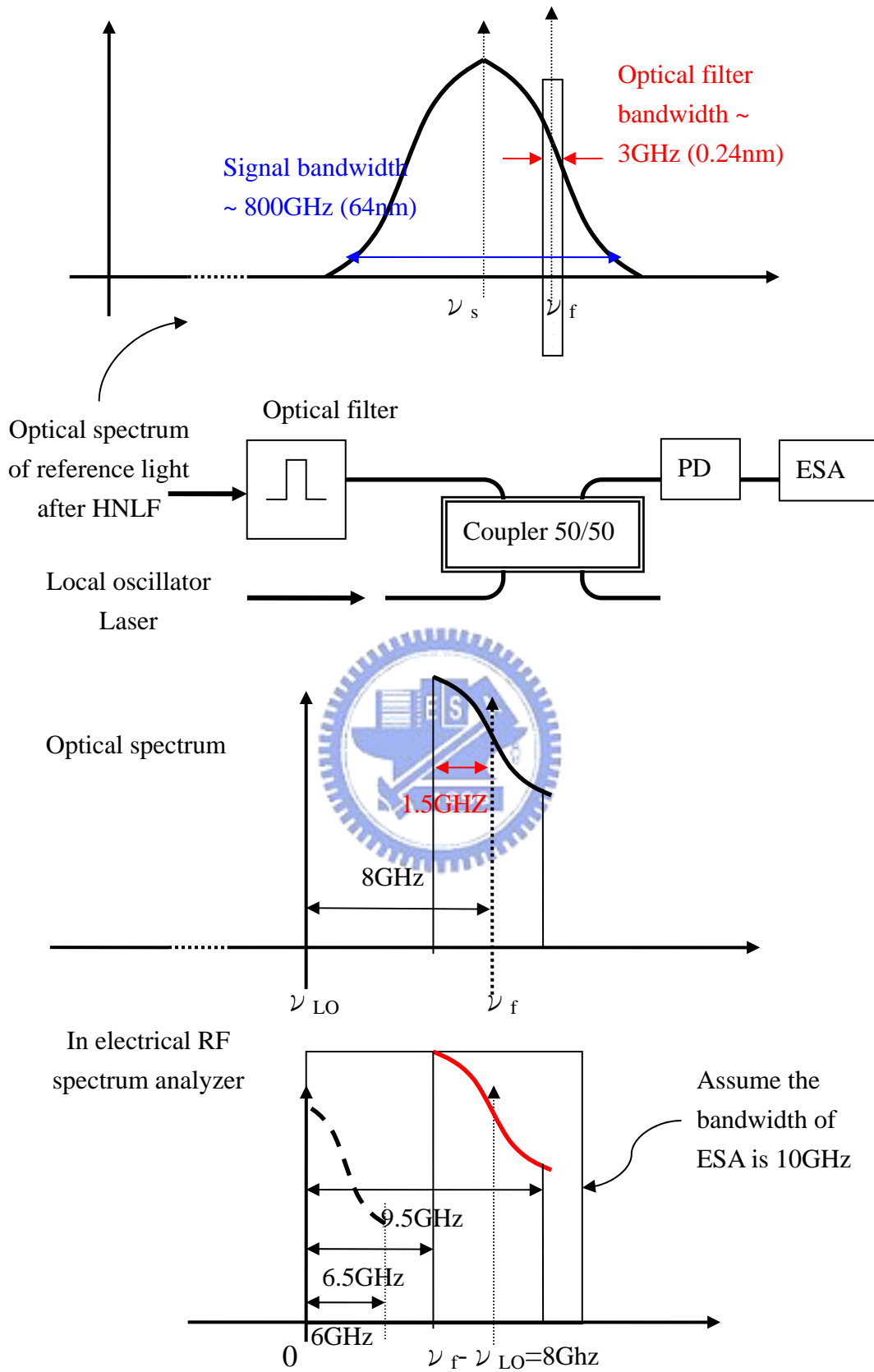


Fig 60 Explanation of the heterodyne approach

In 1994, NTT Transmission System laboratories proposed a novel optical spectrum analyzer based on coherent detection that doesn't require the image signal rejection. [9] It can help us to have a high resolution heterodyne detection without the complex arrangement and an optical filter with large dynamic range. And, the Agilent also provide a high-resolution optical spectrum analyzer—"Agilent 83453A high-resolution spectrometer" that has resolution better than 10MHz. [10]

Thus the bad measuring resolution of the optical RF spectrum analyzer can be overcome.



Chapter Five Conclusion

In this thesis, we perform an optical RF spectrum analyzer following the approach proposed by Dr. Dorrer and Dr. Maywar for measuring 10Gbps RZ signal and 40GHz sinusoidal signal and have some related discussions stated as below:

1. Theoretical discussion about the working principle of this optical RF spectrum.
2. Perform the simulated optical spectrum of reference light after HNLF. It is shown that the optical spectrum of reference light is very similar to the RF spectrum of signal under test, if the input signal power is not too large to deviate the key approximation.
3. This distortion originated from the deviation of the key approximation will not give us a more serious limitation in bandwidth in measuring higher frequency signal. This feature is also justified with simulation.
4. Through the discussion about the bandwidth performance of the optical RF spectrum, we know that the best arrangement is to set the signal light and the reference light at two sides of λ_0 of the HNLF symmetrically.
5. With a modified model, we can predict the bandwidth of the optical RF spectrum analyzer at some offset. And, the maximum bandwidth without considering spectral extending and signal overlapping is around 750GHz shown with experiment and simulation.
6. Several possible approaches for enhancing the measuring resolution are pointed out.

Finally, let's discuss the advantage, disadvantage, opportunity and improvement of this new all optical approach comparing with the conventional electrical RF spectrum analyzer as the end of this thesis. The discussion is stated in the following table.

Advantage	Disadvantage
<ol style="list-style-type: none"> 1. Ultra-wide bandwidth (~760GHz) 2. All optical approach 3. Simple approach (Just need a HNLF) 	<ol style="list-style-type: none"> 1. Bad measuring resolution 2. Suitable signal power
Opportunity	Improvement
<ol style="list-style-type: none"> 1. The bit rate of optical communication is increasing. 	<ol style="list-style-type: none"> 1. The most simple method is to replace the general OSA with other frequency resolving methods with higher resolution

Table 12 Features of the optical RF spectrum analyzer

From the Table 12, we can know that this all optical approach for measuring the RF spectrum of an optical signal is very attractive for high bit rate optical communication systems, because this approach has an amazing wide bandwidth and is a simple all optical approach without optical-to-electrical conversion. Furthermore, the requirement for high measuring resolution is not so urgent in higher bit rate signals.

Reference

1. C. Dorrer and D.N. Maywar, "800GHz RF Spectrum analyzer for Optical Signals", OFC2003 post deadline paper PD14
2. C. Dorrer and D.N. Maywar, "Ultra-high bandwidth RF spectrum analyzer for optical signals", Electronics Letters, Vol. 39, pp. 1004-1005 ,2003
3. C. Dorrer and D.N. Maywar, "RF Spectrum Analysis of Optical Signals Using Nonlinear Optics", J. Lightwave Technology, Vol. 22, pp. 266-274 ,2004
4. G.P. Agrawal, "Nonlinear fiber optics", Academic Press, 2001
5. Dennis Derickson, "Fiber Optics Test and Measurement", PH
6. Bostjan Batagelj, "Review of so far Proposed Fiber n2 Measurement Schemes", pp.103-106, ICTON 2002
7. M. Artiglia, E.Ciaramella and B. Sordo, "Using modulation instability to determine Kerr coefficient in optical fibers", Vol. 31, pp. 1012-1013, 1995
8. C. Mazzali, D.F. Grosz and H. L. Fragnito, Member, IEEE, "Simple Method for Measuring Dispersion and Nonlinear Coefficient Near the Zero-dispersion Wavelength of Optical Fibers", IEEE Photonics Technology Letters, Vol. 11, pp. 251-253, 1999
9. Seiji Yoshida, Yasuhiko Tada and Kiyoshi Nosu, "High resolution optical spectrum analysis by coherent detection with multi-electrode DBR-LD's as local oscillators", IMTC'94, pp. 230, 1994
10. Agilent Technologies, "Lightwave Test and Measurement 2002 Catalog", pp.81-83, 2002